Atmos. Meas. Tech. Discuss., 4, 5183–5274, 2011
www.atmos-meas-tech-discuss.net/4/5183/2011/
doi:10.5194/amtd-4-5183-2011

Atmospheric Measurement Techniques Discussions

The dynamic chamber method: trace gas exchange fluxes (NO, NO_2, O_3) between plants and the atmosphere in the laboratory and in the field

C. Breuninger[1], R. Oswald[1], J. Kesselmeier[1], and F. X. Meixner[1,2]

[1]Max Planck Institute for Chemistry, Biogeochemistry Department, P.O. Box 3060, 55020 Mainz, Germany
[2]Department of Physics, University of Zimbabwe, P.O. Box MP 167, Harare, Zimbabwe

Received: 14 June 2011 – Accepted: 22 July 2011 – Published: 15 August 2011

Correspondence to: C. Breuninger (c.breuninger@mpic.de)

Published by Copernicus Publications on behalf of the European Geosciences Union.

Abstract

We describe a dynamic chamber system to determine reactive trace gas exchange fluxes between plants and the atmosphere under laboratory and, with small modifications, also under field conditions. The system allows measurements of the flux density of the reactive NO-NO_2-O_3 triad and additionally of the non-reactive trace gases CO_2 and H_2O. The chambers are made of transparent and chemically inert wall material and do not disturb plant physiology. For NO_2 detection we used a highly NO_2 specific blue light converter coupled to chemiluminescence detection on the photolysis product, NO. Exchange flux densities derived from dynamic chamber measurements are based on very small concentration differences of NO_2 (NO, O_3) between inlet and outlet of the chamber. High accuracy and precision measurements are therefore required, and high instrument sensitivity (limit of detection) and the statistical significance of concentration differences are important for the determination of corresponding exchange flux densities, compensation point concentrations, and deposition velocities. The determination of NO_2 concentrations at sub-ppb levels (<1 ppb) requires a highly sensitive NO/NO_2 analyzer with a lower detection limit (3σ-definition) of 0.3 ppb or better. Deposition velocities and compensation point concentrations were determined by bi-variate weighted linear least-squares fitting regression analysis of the trace gas concentrations, measured at the inlet and outlet of the chamber. Performances of the dynamic chamber system and data analysis are demonstrated by studies of *Picea abies* L. (Norway Spruce) under field and laboratory conditions. Our laboratory data clearly show that highly significant compensation point concentrations can only be detected if the NO_2 concentration differences were statistically significant and the data were rigorously controlled for this criterion. The results of field experiments demonstrate the need to consider photo-chemical reactions of NO, NO_2, and O_3 inside the chamber for the correct determination of the exchange flux densities, deposition velocities, as well as compensation point concentrations. For spruce NO_2 deposition velocity ranged between 0.07 and 0.42 mm s^{-1} (per leaf area) and NO_2 compensation point

concentration ranged between 0.17 and 0.65 ppb. Under our field conditions NO_2 deposition velocities would have been overestimated up to 80 %, if NO_2 photolysis has not been considered. We also quantified the photolysis component for some previous NO_2 flux measurements. Neglecting photo-chemical reactions may have changed reported NO_2 compensation point concentration by 10 %. However, the effect on NO_2 deposition velocity was much more intense, ranged between 50 and several hundreds percent. Our findings may have consequences for the results from previous studies and ongoing discussion of NO_2 compensation point concentrations.

1 Introduction

Nitric oxide (NO), nitrogen dioxide (NO_2), often denoted as nitrogen oxides (NO_x), and ozone (O_3) are important compounds in atmospheric chemistry. NO_x has an important role in radical chemistry and in the chemical formation and destruction of tropospheric and stratospheric O_3 (Crutzen, 1979). Moreover, NO_x and O_3 are coupled by chemical reactions. NO is oxidized by O_3 to NO_2 and NO is regenerated by photolysis of NO_2 under daylight conditions. Typical NO_x mixing ratios in the atmosphere are a few tenth of ppb (remote sites) up to 1000 ppb (urban environments). Known sources of NO_x are fossil fuel combustion (energy and traffic), biomass burning, microbial activity in soils and lightning (Seinfeld and Pandis, 2006). Typical ambient non-urban NO_2 concentrations are 0.05 to 1 ppb (Lerdau et al., 2000). Mean annual mixing ratios of NO_2 are up to 20 ppb in urban or industrialized regions, or 5 ppb in regions of little industrial activity. During smog events the NO_2 concentration may exceed 1 ppm (Stulen et al., 1998).

NO_x is subject to a number of local photochemical removal processes, and long range transport through the atmosphere. In addition to gas-phase oxidation of NO_2, principally by the OH radical (forming HNO_3), NO_2 is removed from the atmosphere via uptake to plants. Lerdau et al. (2000) reported that depending on the leaf area indices of the relevant sites only 25 to max. 80 % of the emitted/produced NO_x may be exported to the atmosphere, when comparing observed canopy level NO_x concentrations and measured NO soil emission rates (see Jacob and Wofsy, 1990; Yienger and Levy, 1995; Wang et al., 1998). However, these results do not agree with leaf-level measurements regarding NO_2 emission from plants (besides plant uptake of NO_2) and indicating the existence of a so-called "plant compensation point" for NO_2. Corresponding compensation point concentrations of NO_2 between 0.3 and 3 ppb have been reported (Rondón et al., 1993; Thoene et al., 1996; Weber and Rennenberg, 1996a; Sparks et al., 2001; Geßler et al., 2000, 2002; Hereid and Monson, 2001) suggesting plants act as a NO_2 sink when ambient concentrations are exceeding, or as a source of NO_2, when ambient concentrations are below the NO_2 compensation point concentration. According to Lerdau et al. (2000), these results contradict the findings of Jacob and Wofsy (1990), who demonstrated that even at ambient NO_2 concentrations of 0.2 to 0.4 ppb a strong uptake by plants (primary rainforest) is required to align measured NO_2 concentrations in the canopy with the measured NO soil emission rates. Lerdau et al. (2000) emphasized the importance of finding an explanation for this discrepancy, particularly in remote regions far away from anthropogenic NO_x sources (e.g., primary rain and boreal forests under low NO_x regimes). Thus investigations of the contribution of NO_2 uptake by plants are required, particularly at NO_2 compensation point concentrations of (sub-) ppb levels. A recent study of five European tree species under laboratory conditions gives reason to assume a compensation point only at very low NO_2 values, if there is a compensation point at all (Chaparro-Suarez et al., 2011).

The commonly used technique for leaf-level exchange measurements of NO_2 is the dynamic chamber technique (a technique also used for many non-reactive (e.g. CO_2, H_2O, COS) and reactive trace gases (e.g. NO, O_3, VOCs, DMS, CS_2, HONO, HNO_3, CH_2O, HCOOH, CH_3COOH). An entire plant (or parts of a plant) is enclosed in a (transparent) chamber which is purged by (preferably ambient) air. Two measurements of NO_2 concentration are performed, namely (1) at the entrance of the chamber (= ambient NO_2 concentration) and (2) within the chamber. If the chamber is well mixed, the latter measurement can be replaced by that of the outlet NO_2 concentration. Alternatively, a set of two chambers, one enclosing the plant the other being empty, can be

AMTD
4, 5183–5274, 2011

used. To relate these two concentration measurements to the exchange (i.e. the uni- or bi-directional flux) of NO_2 between the (chamber) atmosphere and the enclosed plant (or parts of plant), the full mass balance of the dynamic chamber must be considered, i.e. NO_2 fluxes entering and leaving the chamber, as well as all other fluxes due to NO_2sinks and sources within the chamber's volume. Under typical field conditions (i.e. ambient air enters the dynamic chamber), not only NO_2, but also ambient NO and O_3 are purged through the chamber. The fast reaction between NO and O_3 is a "chemical" source of NO_2, while (under daylight conditions) photolysis of NO_2 ($\lambda \leq 420$ nm) is a "chemical" sink. Depending on ambient NO_2, NO, and O_3 concentrations and UV irradiation intensity, corresponding "gas phase fluxes" may reach the magnitude of the NO_2 flux from/to the enclosed plant(s) (Meixner et al., 1997; Pape et al., 2009). Consequently, simultaneous measurements of NO_2, NO, and O_3 concentrations at the outlet of the chamber are required. However, since there is substantial uptake of O_3 (and to a lesser extent NO) by the plants, NO_2, NO, and O_3 concentrations at the inlet of the chamber must also be measured. As a positive "by-product" of these additional concentration measurements, deposition velocities of O_3 (and NO) may be inferred by considering the dynamic chamber's mass balances of O_3 and NO.

In this paper we present results from a dynamic chamber system used previously for measurements of volatile organic compounds, formaldehyde, formic and acetic acid and sulfur compounds (e.g. Kesselmeier et al., 1993, 1996, 1998; Kuhn et al., 2000). The system allows exchange measurements of NO_2 (NO and O_3) under field conditions (uncontrolled) as well as studies under controlled conditions including (laboratory) fumigation experiments.

Because NO_2 compensation point concentrations were reported at (sub-)ppb levels, our laboratory NO_2 fumigation experiments were performed with 3- to 4-yr old Norway Spruce trees at 0.3–3.4 ppb. Such low ambient NO_2 concentrations can be expected under field conditions. Moreover, exchange fluxes derived from dynamic chamber measurements are based on generally (very) small differences of NO_2 (NO, O_3) concentrations between inlet and outlet of the chamber. Consequently, considerable attention

AMTD
4, 5183–5274, 2011

has been paid to the detection limits of corresponding analyzers, statistical significance of the concentration differences, as well as the statistical goodness of measurements have a substantial impact on the identification and quantification of statistically significant deposition velocities and compensation point concentrations. Furthermore, as the exchange of NO_2 is a complex interaction of transport, chemistry and plant physiology, we determined fluxes of NO, NO_2, O_3, CO_2, and H_2O in the field experiments.

2 Basic considerations

We consider a small branch of a tree (leaf area A_{leaf}), which is enclosed in a transparent plant chamber of volume V. The air within the plant chamber is well mixed by action of one (or more) fan(s). Ambient air (containing NO_2, NO, and O_3) enters the plant chamber at the inlet, flushes the chamber with the purging rate Q ($m^3\,s^{-1}$) and leaves the chamber at the outlet. Within the plant chamber trace gases of the NO-NO_2-O_3 triad may be (a) emitted and/or taken up from/by leaves, (b) deposited to the inner walls of the plant chamber, and (c) destroyed and/or generated by (fast) photo-chemical reactions. The mass balances of the NO-NO_2-O_3 triad of the dynamic plant chamber are derived in Appendix A.

2.1 Molar mass flux densities, deposition velocities, and compensation point concentrations

Equations (A7.1)–(A7.3) are formulated in terms of molar mass fluxes (in nmol s^{-1}). However, considering the exchange of reactive trace gases between the plant chamber's atmosphere and the enclosed leaves, the exchange flux density ($F_{\text{ex},i}$) of the molar mass (in nmol $m^{-2}\,s^{-1}$) is commonly used rather than the molar mass flux itself. In the case of plant chamber studies, the appropriate reference surface (reference area) is the surface area (A_{leaf}, in m^2) of the leaves. Therefore, the exchange flux density $F_{\text{ex},i}$ is defined as $F_{\text{ex},i} = \Phi_i/A_{\text{leaf}}$, and the corresponding balance equations will read

AMTD
4, 5183–5274, 2011

as follows:

$$F_{\mathrm{ex,NO_2}} = -\frac{Q}{A_{\mathrm{leaf}}}\left(m_{\mathrm{a,NO_2}} - m_{\mathrm{s,NO_2}} + \frac{V}{Q}\,k\,m_{\mathrm{s,NO}} m_{\mathrm{s,O_3}} - \frac{V}{Q}\,j(\mathrm{NO_2})\,m_{\mathrm{s,NO_2}}\right) \tag{1.1}$$

$$F_{\mathrm{ex,NO}} = -\frac{Q}{A_{\mathrm{leaf}}}\left(m_{\mathrm{a,NO}} - m_{\mathrm{s,NO}} - \frac{V}{Q}\,k\,m_{\mathrm{s,NO}} m_{\mathrm{s,O_3}} + \frac{V}{Q}\,j(\mathrm{NO_2})\,m_{\mathrm{s,NO_2}}\right) \tag{1.2}$$

$$F_{\mathrm{ex,O_3}} = -\frac{Q}{A_{\mathrm{leaf}}}\left(m_{\mathrm{a,O_3}} - m_{\mathrm{s,O_3}} - \frac{V}{Q}\,k\,m_{\mathrm{s,NO}} m_{\mathrm{s,O_3}} + \frac{V}{Q}\,j(\mathrm{NO_2})\,m_{\mathrm{s,NO_2}}\right) \tag{1.3}$$

In the case of defined laboratory experiments, where plants may be fumigated with only one of the three trace gases (i.e., gas-phase production and/or destruction of the trace gas can be ruled out), Eqs. (1.1)–(1.3) will reduce to the well-known form of

$$F^{*}_{\mathrm{ex},i} = -\frac{Q}{A_{\mathrm{leaf}}}\left(m_{\mathrm{a},i} - m_{\mathrm{s},i}\right) \quad i = \mathrm{NO_2, NO, O_3} \tag{1.4}$$

In the case of bi-directional exchange (see Eq. (A2)), the exchange between the plant chamber's atmosphere and the leaves can be directed to or away from the leaves. This exchange process can be subject to the so-called "compensation point concentration" ($m_{\mathrm{comp},i}$, in nmol m^{-3}). According to Conrad (1994), $m_{\mathrm{comp},i}$ is "that concentration at which the consumption rate reaches the same value as the production rate, so that the result of both processes is zero flux". The exchange flux density $F_{\mathrm{ex},i}$ is commonly parameterized (e.g. Hicks et al., 1987) by the so-called "deposition velocity" $v_{\mathrm{dep},i}$ (in m s^{-1} or mm s^{-1}) of trace gas i and its compensation point concentration, $m_{\mathrm{comp},i}$:

$$F_{\mathrm{ex,NO_2}} = -v_{\mathrm{dep,NO_2}}\left(m_{\mathrm{s,NO_2}} - m_{\mathrm{comp,NO_2}}\right) \tag{2.1}$$

$$F_{\mathrm{ex,NO}} = -v_{\mathrm{dep,NO}}\left(m_{\mathrm{s,NO}} - m_{\mathrm{comp,NO}}\right) \tag{2.2}$$

$$F_{\mathrm{ex,O_3}} = -v_{\mathrm{dep,O_3}}\left(m_{\mathrm{s,O_3}} - m_{\mathrm{comp,O_3}}\right) \tag{2.3}$$

AMTD
4, 5183–5274, 2011

The dynamic chamber method

C. Breuninger et al.

Note, that (by convention) $F_{ex,i}$ is directed "downward" to the leaves, if $m_{s,i} > m_{comp,i}$, $F_{ex,i}$ is zero, if $m_{s,i} = m_{comp,i}$, and $F_{ex,i}$ is directed "upward" from the leaves, if $m_{s,i} < m_{comp,i}$.

Given, that the quantities Q, A_{leaf}, k, and $j(NO_2)$ are a priori known and/or simultaneously measured with $m_{s,i}$ and $m_{a,i}$, then, the desired quantities, $v_{dep,i}$ and $m_{comp,i}$, are commonly determined from the linear relationship between $F_{ex,i}$ and $m_{s,i}$, where $v_{dep,i}$ is the slope and $m_{comp,i}$ is the intersect of $F_{ex,i}$ with the $m_{s,i}$-axis (see Rondón and Granat, 1994; Thoene et al., 1996; Weber and Rennenberg, 1996a; Sparks et al., 2001; Hereid and Monson, 2001; Geßler et al., 2002).

However, since $F_{ex,i}$ (see Eqs. (1.1)–(1.3)) contains the term $Q/A_{leaf}\,(m_{a,i} - m_{s,i})$, the calculation of any form of linear regression between $F_{ex,i}$ and $m_{s,i}$ is mathematically sensu stricto not appropriate, because the dependent variable $F_{ex,i}$ contains the independent variable ($m_{s,i}$). This problem can be resolved by returning to the originally measured quantities, $m_{a,i}$ and $m_{s,i}$. If we combine Eqs. (1.1)–(1.3) and Eqs. (2.1)–(2.3) and resolve these equations for m_{s,NO_2}, $m_{s,NO}$, and m_{s,O_3}, we yield three linear relationships between the measured variables m_{s,NO_2} and m_{a,NO_2}, $m_{s,NO}$ and $m_{a,NO}$, and m_{s,O_3} and m_{a,O_3}:

$$m_{s,NO_2} = n_1 + b_1 \cdot m_{a,NO_2} \tag{3.1}$$

$$m_{s,NO} = n_2 + b_2 \cdot m_{a,NO} \tag{3.2}$$

$$m_{s,O_3} = n_3 + b_3 \cdot m_{a,O_3} \tag{3.3}$$

using the definitions:

$$n_1 = \frac{\bar{A}_{leaf} v_{dep,NO_2} m_{comp,NO_2} + V\bar{k}\bar{m}_{s,NO}\bar{m}_{s,O_3}}{\bar{Q} + \bar{A}_{leaf} v_{dep,NO_2} + V\bar{j}(NO_2)}; \quad b_1 = \frac{\bar{Q}}{\bar{Q} + \bar{A}_{leaf} v_{dep,NO_2} + V\bar{j}(NO_2)} \tag{4.1}$$

$$n_2 = \frac{\bar{A}_{leaf} v_{dep,O_3} m_{comp,O_3} + V\bar{j}(NO_2)\,\bar{m}_{s,NO_2}}{\bar{Q} + \bar{A}_{leaf} v_{dep,O_3} + V\bar{k}\bar{m}_{s,O_3}}; \quad b_2 = \frac{\bar{Q}}{\bar{Q} + \bar{A}_{leaf} v_{dep,NO} + V\bar{k}\bar{m}_{s,O_3}} \tag{4.2}$$

$$n_3 = \frac{\bar{A}_{\text{leaf}} v_{\text{dep},O_3} m_{\text{comp},O_3} + V \bar{j}(NO_2)\, \bar{m}_{s,NO_2}}{\bar{Q} + \bar{A}_{\text{leaf}} v_{\text{dep},O_3} + V \bar{k}\, \bar{m}_{s,NO}}; \quad b_3 = \frac{\bar{Q}}{\bar{Q} + \bar{A}_{\text{leaf}} v_{\text{dep},O_3} + V \bar{k}\, \bar{m}_{s,NO}} \tag{4.3}$$

The quantities n_i and b_i may be evaluated (graphically) as the intercept and the slope of the plot of measured $m_{s,i}$ versus measured $m_{a,i}$. Application of different forms of linear regression analysis delivers n_i and b_i and bi-variate weighted linear least-squares fitting (which considers uncertainties of both, $m_{s,i}$ and $m_{a,i}$) provides also their standard errors $s_{n,i}$ and $s_{b,i}$ (see Sect. 3.4.6).

The linear relationships between $F_{ex,i}$ and $m_{s,i}$ are still maintained. This can be shown by resolving Eqs. (3.1)–(3.3) for $m_{a,i}$ and making use of Eqs. (1.1)–(1.3):

$$F_{ex,NO_2} = \frac{\bar{Q}}{\bar{A}_{\text{leaf}}} \left(\frac{n_1}{b_1} - \frac{V}{\bar{Q}} \bar{k}\, \bar{m}_{s,NO} \bar{m}_{s,O_3} \right) + \frac{\bar{Q}}{\bar{A}_{\text{leaf}}} \left(1 - \frac{1}{b_1} + \frac{V}{\bar{Q}} \bar{j}(NO_2) \right) \cdot m_{s,NO_2} \tag{5.1}$$

$$F_{ex,NO} = \frac{\bar{Q}}{\bar{A}_{\text{leaf}}} \left(\frac{n_2}{b_2} - \frac{V}{\bar{Q}} \bar{j}(NO_2)\, \bar{m}_{s,NO_2} \right) + \frac{\bar{Q}}{\bar{A}_{\text{leaf}}} \left(1 - \frac{1}{b_2} + \frac{V}{\bar{Q}} \bar{k}\, \bar{m}_{s,O_3} \right) \cdot m_{s,NO} \tag{5.2}$$

$$F_{ex,O_3} = \frac{\bar{Q}}{\bar{A}_{\text{leaf}}} \left(\frac{n_3}{b_3} - \frac{V}{\bar{Q}} \bar{j}(NO_2)\, \bar{m}_{s,NO_2} \right) + \frac{\bar{Q}}{\bar{A}_{\text{leaf}}} \left(1 - \frac{1}{b_3} + \frac{V}{\bar{Q}} \bar{k}\, \bar{m}_{s,NO} \right) \cdot m_{s,O_3} \tag{5.3}$$

Finally, the desired deposition velocities ($v_{dep,i}$) of the NO-NO_2-O_3 triad result from Eqs. (4.1)–(4.3), resolving for $v_{dep,i}$,

$$v_{dep,NO_2} = \frac{\bar{Q}}{\bar{A}_{\text{leaf}}} \left(\frac{1}{b_1} - 1 - \frac{V}{\bar{Q}} \bar{j}(NO_2) \right) \tag{6.1}$$

$$v_{dep,NO} = \frac{\bar{Q}}{\bar{A}_{\text{leaf}}} \left(\frac{1}{b_2} - 1 - \frac{V}{\bar{Q}} \bar{k}\, \bar{m}_{s,O_3} \right) \tag{6.2}$$

$$v_{dep,O_3} = \frac{\bar{Q}}{\bar{A}_{\text{leaf}}} \left(\frac{1}{b_3} - 1 - \frac{V}{\bar{Q}} \bar{k}\, \bar{m}_{s,NO} \right) \tag{6.3}$$

AMTD
4, 5183–5274, 2011

The dynamic chamber method

C. Breuninger et al.

and the desired compensation point concentrations ($m_{\mathrm{comp},i}$) of the NO-NO_2-O_3 triad result from combining Eqs. (4.1)–(4.3) and Eqs. (6.1)–(6.3):

$$m_{\mathrm{comp,NO_2}} = \frac{n_1 - b_1 \frac{V}{\bar{Q}} \bar{k} \bar{m}_{\mathrm{s,NO}} \bar{m}_{\mathrm{s,O_3}}}{1 - b_1 - b_1 \frac{V}{\bar{Q}} \bar{j}(\mathrm{NO_2})} \tag{7.1}$$

$$m_{\mathrm{comp,NO}} = \frac{n_2 - b_2 \frac{V}{\bar{Q}} \bar{j}(\mathrm{NO_2}) \bar{m}_{\mathrm{s,NO_2}}}{1 - b_2 - b_2 \frac{V}{\bar{Q}} \bar{k} \bar{m}_{\mathrm{s,O_3}}} \tag{7.2}$$

$$m_{\mathrm{comp,O_3}} = \frac{n_3 - b_3 \frac{V}{\bar{Q}} \bar{j}(\mathrm{NO_2}) \bar{m}_{\mathrm{s,NO_2}}}{1 - b_3 - b_3 \frac{V}{\bar{Q}} \bar{k} \bar{m}_{\mathrm{s,NO}}} \tag{7.3}$$

The quantities n_1, n_2, n_3 and b_1, b_2, b_3 cannot be determined (graphically or numerically) from single pairs of $m_{\mathrm{a},i}$ and $m_{\mathrm{s},i}$, but from a (statistically sufficient) set of measured $m_{\mathrm{a},i}$ and $m_{\mathrm{s},i}$ (i.e. data sets classified for defined conditions of irradiation, temperature, humidity, concentrations, respectively). Therefore, n_1, n_2, n_3 and b_1, b_2, b_3 represent mean values for these data sets. Consequently, the quantities Q, A_{leaf}, $j(\mathrm{NO_2})$, k, $m_{\mathrm{s,NO_2}}$, $m_{\mathrm{s,NO}}$,and $m_{\mathrm{s,O_3}}$ in Eqs. (5.1)–(5.3), (6.1)–(6.3), and (7.1)–(7.3) must be averaged over the same (time) period (the same data set) of $m_{\mathrm{a},i}$ and $m_{\mathrm{s},i}$ measurements from which the quantities n_i and b_i were derived.

2.2 Constraints of precision

Exchange flux densities $F_{\mathrm{ex},i}$ are determined from molar concentrations of the NO-NO_2-O_3 triad, both ambient measurements ($m_{\mathrm{a},i}$) as well as those in the plant chamber ($m_{\mathrm{s},i}$) (see Eqs. (1.1)–(1.3)). These are all measured with one set of analyzers. The calculation procedure for exchange flux densities, deposition velocities as well as compensation point concentrations is based on linear regression analysis of $m_{\mathrm{a},i}$ and $m_{\mathrm{s},i}$, which are (a) both error-prone, and (b) not very different from each other, i.e.

AMTD
4, 5183–5274, 2011
The dynamic chamber method
C. Breuninger et al.

their difference is usually (very) small. The uncertainties of these differences depend mainly on the precision of the analyzers; leading to large uncertainties in the derived quantities $F_{\mathrm{ex},i}$, $v_{\mathrm{dep},i}$, and $m_{\mathrm{comp},i}$.

For the sake of simplicity we assume well defined laboratory conditions. Here, the trace gas exchange flux densities $F_{\mathrm{ex},i}$ are described by Eq. (1.4), which implying that (a) only pre-scribed concentrations of trace gas i ($= m_{\mathrm{a},i}$) enter the dynamic plant chamber, (b) the enclosed leaves are only exposed to corresponding $m_{\mathrm{s},i}$, (c) purging rate Q and leaf area A_{leaf} are known and unchanging, and (d) sample concentrations of the other trace gases ($m_{\mathrm{s},j\neq i}$), photolysis rate $j(\mathrm{NO_2})$ as well as wall-sorptions of trace gas i are negligible. After evaluation of the linear relationship between $m_{\mathrm{a},i}$ and $m_{\mathrm{s},i}$, corresponding exchange flux densities $F^*_{\mathrm{ex},i}$, deposition velocities $v^*_{\mathrm{dep},i}$, and compensation point concentrations $m^*_{\mathrm{comp},i}$ are given by

$$F^*_{\mathrm{ex,NO_2}} = \frac{\bar{Q}}{\bar{A}_{\mathrm{leaf}} b_1}\left(n_1 + (b_1 - 1)\cdot m_{\mathrm{s,NO_2}}\right) \tag{8.1.1}$$

$$F^*_{\mathrm{ex,NO}} = \frac{\bar{Q}}{\bar{A}_{\mathrm{leaf}} b_2}\left(n_2 + (b_2 - 1)\cdot m_{\mathrm{s,NO}}\right) \tag{8.1.2}$$

$$F^*_{\mathrm{ex,O_3}} = \frac{\bar{Q}}{\bar{A}_{\mathrm{leaf}} b_3}\left(n_3 + (b_3 - 1)\cdot m_{\mathrm{s,O_3}}\right) \tag{8.1.3}$$

$$v^*_{\mathrm{dep,NO_2}} = \frac{\bar{Q}}{\bar{A}_{\mathrm{leaf}}}\,\frac{1 - b_1}{b_1} \tag{8.2.1}$$

$$v^*_{\mathrm{dep,NO}} = \frac{\bar{Q}}{\bar{A}_{\mathrm{leaf}}}\,\frac{1 - b_2}{b_2} \tag{8.2.2}$$

$$v^*_{\mathrm{dep,O_3}} = \frac{\bar{Q}}{\bar{A}_{\mathrm{leaf}}}\,\frac{1 - b_3}{b_3} \tag{8.2.3}$$

AMTD

4, 5183–5274, 2011

The dynamic chamber method

C. Breuninger et al.

$$m^*_{\mathrm{comp,NO_2}} = \frac{n_1}{1-b_1} \tag{8.3.1}$$

$$m^*_{\mathrm{comp,NO}} = \frac{n_2}{1-b_2} \tag{8.3.2}$$

$$m^*_{\mathrm{comp,O_3}} = \frac{n_3}{1-b_3} \tag{8.3.3}$$

Regarding only NO_2, a schematic representation (using simulated data) of how the quantities defined by Eqs. (8.1.1), (8.2.1), and (8.3.1) are determined from genuine measurements of $m_{\mathrm{a,NO_2}}$ and $m_{\mathrm{s,NO_2}}$ is given in Fig. 1a. Since the "1:1"-line is equivalent to $m_{\mathrm{a,NO_2}} = m_{\mathrm{s,NO_2}}$ (i.e. $F_{\mathrm{ex,NO_2}} = 0$, see Eq. (1.4)), the intersect of the linear regression line and the "1:1"-line is the NO_2 compensation point concentration, $m_{\mathrm{comp,NO_2}}$. Here, the difficulties associated with an experimental proof of a (highly) significant $m_{\mathrm{comp,NO_2}}$ becomes obvious. The lower $m_{\mathrm{comp,NO_2}}$ will be, the more the intersect shifts down the "1:1"-line, closer and closer to the limit of detection of the NO_2 concentration measurements (LOD($m_{\mathrm{a,NO_2}}$), LOD($m_{\mathrm{s,NO_2}}$); 3σ-definition). This dilemma becomes even more obvious, if we consider the schematic representation of Eq. (1.4) in Fig. 1b, where LOD($F_{\mathrm{ex,NO_2}}$) has been calculated from corresponding $s_{\mathrm{m\_s,NO_2}}$ and $s_{\mathrm{m\_a,NO_2}}$ by Gaussian error propagation. Here, $m_{\mathrm{comp,NO_2}}$ ($F_{\mathrm{ex,NO_2}} = 0$) is the intersect of the $m_{\mathrm{s,NO_2}}$-axis with the best-fit line of $F_{\mathrm{ex,NO_2}}$ vs. $m_{\mathrm{s,NO_2}}$ (which is mathematically not correct, see above). For high NO_2 compensation point concentrations (as in Fig. 1), $m_{\mathrm{comp,NO_2}}$ can still be evaluated by interpolation from significant data pairs (i.e. data pairs, where > LOD($m_{\mathrm{NO_2}}$), $\geq +$LOD($F_{\mathrm{ex,NO_2}}$), or $\leq -$LOD($F_{\mathrm{ex,NO_2}}$), respectively). If $m_{\mathrm{comp,NO_2}}$ falls below LOD($m_{\mathrm{s,NO_2}}$) and F_0 is consequently below $+$LOD($F_{\mathrm{ex,NO_2}}$), $m_{\mathrm{comp,NO_2}}$ may only be determined by extrapolation from significant data pairs.

According to Eqs. (8.1.1), (8.2.1), and (8.3.1), the errors of $F_{\mathrm{ex,NO_2}}$, $v_{\mathrm{depNO_2}}$, and $m_{\mathrm{comp,NO_2}}$ are entirely due to the errors of n_1 and b_1, which are in turn entirely due to the goodness of the linear relationship between $m_{\mathrm{a,NO_2}}$ and $m_{\mathrm{s,NO_2}}$, as well as to the errors of $m_{\mathrm{a,NO_2}}$ and $m_{\mathrm{s,NO_2}}$ ($s_{\mathrm{m\_a,NO_2}}$ and $s_{\mathrm{m\_s,NO_2}}$, see Sect. 3.4.7). This leads

AMTD
4, 5183–5274, 2011

to the simple conclusion, that determinations of F_{ex,NO_2}, v_{depNO_2}, and m_{comp,NO_2} are more precise, the higher the regression coefficient $R^2(m_{s,NO_2}, m_{a,NO_2})$ and lower the standard errors s_{m_s,NO_2} and s_{m_a,NO_2} are.

Only one NO_2 analyzer is used for the measurements of both concentrations, m_{a,NO_2} and m_{s,NO_2}. As shown below (Sect. 3.2), the standard error s_{m_a,NO_2} (s_{m_s,NO_2}) was found to be a weak exponential function of m_{a,NO_2} (m_{s,NO_2}), starting with a fixed value $s_{m,LOD(NO_2)}$ at $m_{a,NO_2} = m_{s,NO_2} = 0$. To demonstrate, how the goodness ($R^2(m_{s,NO_2}, m_{a,NO_2})$) of the linear relationship between m_{a,NO_2} and m_{s,NO_2} and how the magnitude of s_{m_a,NO_2} and s_{m_s,NO_2} impact the NO_2 exchange measurements, we consider (a) the determination of the minimum possible, but still highly significant NO_2 compensation point concentration (m_{comp,NO_2}), and (b) the precision of the NO_2 exchange flux density (F_{ex,NO_2}). For that we simulated data sets of m_{a,NO_2} and m_{s,NO_2} within the range $\mathrm{LOD}(m_{s,NO_2}) \leq m_{s,NO_2} \leq 615\,\mathrm{nmol\,m^{-3}}$ (15 ppb) for prescribed NO_2 deposition velocities ($0.1 \leq v_{dep,NO_2} \leq 0.8\,\mathrm{mm\,s^{-1}}$, per leaf area) and for pre-scribed $R^2(m_{s,NO_2}, m_{a,NO_2})$ between 0.999 and 0.6. The latter was achieved by random number application to the m_{a,NO_2} data. Standard errors s_{m_s,NO_2} and s_{m_a,NO_2} were calculated from m_{a,NO_2} and m_{s,NO_2} (see Eq. (9.1), Sect. 3.2), while the standard error of F_{ex,NO_2} (s_{F_ex,NO_2}) was calculated from s_{m_s,NO_2}, s_{m_a,NO_2}, and $r(m_{s,NO_2}, m_{a,NO_2}) = [R^2(m_{s,NO_2}, m_{a,NO_2})]^{1/2}$ by application of the general form of Gaussian error propagation (see Sect. 3.4.7).

Application of bi-variate linear regression analysis to this simulated data set delivers the quantities n_1 and b_1 as well their standard errors $s_{n,1}$ and $s_{b,1}$ (which depend on s_{m_s,NO_2}, s_{m_a,NO_2}, and $R^2(m_{s,NO_2}, m_{a,NO_2})$). Application of the general form of Gaussian error propagation (see Sect. 3.4.7) to Eq. (8.3.1) delivers the standard error of the NO_2 compensation point concentration (s_{m_comp,NO_2}). The "detectable existence" of m_{comp,NO_2} (i.e. testing the hypothesis $m_{comp,NO_2} \neq 0$) has been statistically secured by application of the t-test to the values of m_{comp,NO_2}, s_{m_comp,NO_2} and N (number of (m_{s,NO_2}, m_{a,NO_2}) data pairs). In Fig. 2, the minimum detectable NO_2 compensation point concentration, i.e. the lowest, but still highly significant m_{comp,NO_2}

AMTD
4, 5183–5274, 2011

(P ≥ 0.999) is shown for a pre-scribed range of NO_2 deposition velocities as function of the regression coefficient $R^2(m_{s,NO_2}, m_{a,NO_2})$ and for three different values of LOD(m_{s,NO_2}), namely 0.4, 4.5 and 44.6 nmol m^{-3} (0.01, 0.1, 1.0 ppb). These three values represent a certain "history" of NO/NO_2 chemiluminescence analyzers: LOD(m_{s,NO_2}) = 44.6 nmol m^{-3} (1 ppb) represents the state-of-art of commercial NO_2 analyzers of 1985–1995, LOD(m_{s,NO_2}) = 4.5 nmol m^{-3} (0.1 ppb) the best performance between 1995–2005's, while LOD(m_{s,NO_2}) = 0.4 nmol m^{-3} (0.01 ppb) is characteristic for the most advanced NO/NO_2analyzers which have been recently applied over the remote Southern Atlantic Ocean (Hosaynali Beygi et al., 2011). For typical ranges of laboratory measurements, i.e. $0.9 \le R^2 \le 0.99$, minimum detectable NO_2 compensation point concentrations range between 17.5–99u4 nmol m^{-3} (0.39–2.23 ppb), if NO_2 analyzers with LOD(m_{s,NO_2}) = 44.6 nmol m^{-3} (1.0 ppb) have been used. Best performance of present-day NO_2 analyzers allow minimum detectable m_{comp,NO_2} between 3.6 and 21.3 nmol m^{-3} (0.08–0.48 ppb). Very low minimum detectable m_{comp,NO_2}(0.8–4.0 nmol m^{-3} or 0.02–0.09 ppb) may be reached if the most advanced state of NO_2 analyzers is considered. It should be noted that, due to the potential goodness of the measurements, the minimum detectable m_{comp,NO_2} could be lower than the actual LOD(m_{s,NO_2}), but statistically still highly significant.

The impact of s_{m_s,NO_2}, s_{m_a,NO_2}, and $R^2(m_{s,NO_2}, m_{a,NO_2})$ on the precision of the NO_2 exchange flux density (= $s_{F\_ex,NO_2}/F_{ex,NO_2}$) is demonstrated in Fig. 3. For the sake of clarity, another data set has been simulated (random number application), namely for pre-scribed NO_2 deposition velocities ($0.3 \le v_{dep,NO_2} \le 0.6$ mm s^{-1}, per leaf area), a pre-scribed NO_2 compensation point concentration (m_{comp,NO_2} = 67 nmol m^{-3} (1.5 ppb)), and for $0.99 \le R^2 \le 0.9$. Also shown in Fig. 3 is the precision of m_{s,NO_2} (= $s_{m\_s,NO_2}/m_{s,NO_2}$; right axis) for the "history" of LOD(m_{s,NO_2}) values, namely LOD(m_{s,NO_2}) = 44.6, 4.5, and 0.4 nmol m^{-3} (1.0, 0.1, 0.01 ppb). Before 1995 (LOD(m_{NO_2}) = 1 ppb), a precision of m_{s,NO_2} better than 10 % could hardly be achieved in the lower ppb-range. Best performing present-day NO_2 chemiluminescence analyzers (LOD(m_{NO_2}) = 0.1 ppb) exceed the 10 % level of m_{s,NO_2} precision not before m_{s,NO_2} falls below 14.8 nmol m^{-3} (0.33 ppb), while another order of magnitude can be reached with most advanced NO_2 analyzers ($s_{m\_s,NO_2}/m_{s,NO_2} >$ 10 % not before $m_{s,NO_2} < 1.5$ nmol m^{-3} (0.03 ppb)). The "history" of NO_2 analyzers is also mirrored in the precision of F_{ex,NO_2} (reddish, bluish, and greenish areas in Fig. 3). In any case, the precision of F_{ex,NO_2} (= $s_{F\_ex,NO_2}/F_{ex,NO_2}$) reaches infinity at $m_{s,NO_2} = m_{comp,NO_2}$, since there the NO_2 exchange flux density equals zero. Otherwise, the precision of F_{ex,NO_2} rapidly falls (very) well below the 10 % level. This is a consequence of the fact, that m_{a,NO_2} and m_{s,NO_2} are the decisive quantities for the determination of F_{ex,NO_2}. Since m_{a,NO_2} and m_{s,NO_2} are highly correlated, the standard error of F_{ex,NO_2} is proportional to $[s^2_{m\_a,NO_2} + s^2_{m\_s,NO_2}]^{1/2}$–$2\, s_{m\_a,NO_2} s_{m\_s,NO_2}\, [R^2(m_{s,NO_2},\, m_{a,NO_2})]^{1/2}$, rather than proportional to $[s^2_{m\_a,NO_2} + s^2_{m\_s,NO_2}]^{1/2}$ alone (see Sect. 3.4.7). In other words, the error of F_{ex,NO_2} benefits from the compensation of the errors of m_{a,NO_2} and m_{s,NO_2}.

Finally, it should be emphasized, that the estimates of this sub-section are made on the basis of Eqs. (8.1.1), (8.2.1), and (8.3.1) for (best) defined laboratory conditions. Under field conditions, however, the equations for the determination of F_{ex,NO_2}, v_{depNO_2}, and m_{comp,NO_2} will contain also average quantities of $m_{s,NO}$, m_{s,O_3}, $j(NO_2)$, and k (cf. Eqs. (5.1), (6.1), (7.1)). It follows, that their variability (standard errors) leads to larger standard errors of n_1 and b_1 and diminish $R^2(m_{s,NO_2},\, m_{a,NO_2})$. Consequently, corresponding minimum detectable NO_2 compensation point concentrations will certainly be higher and precisions of F_{ex,NO_2} will be lower than those given in Fig. 2 and 3.

2.3 Constraints of design

In addition to the demand for precise and highly sensitive measurements of NO_2 concentration, surface exchange flux measurements of NO_2 (NO, O_3) in a dynamic leaf

AMTD
4, 5183–5274, 2011

chamber system require that:

1. The environment in the chamber should as closely as possible represent the surrounding (ambient) environment.

2. Enclosing the plant (part of plants) by the chamber should not affect the plant itself, neither through mechanical stress nor due to changed environmental conditions. Changes in concentrations of relevant trace gases should be small in order to prevent affecting plant metabolism and stomata regulation.

3. Primary plant-physiological processes, such as CO_2 surface exchange fluxes (assimilation) and H_2O surface exchange fluxes (transpiration) should be closely followed, measured and finally related to the NO_2 (NO, O_3) surface exchange.

4. Losses of NO_2 (NO, O_3) on chamber materials must be negligible (if not: must be quantified).

5. The chamber system should be applicable for laboratory and field measurements without substantial modifications.

6. Simultaneous measurements of surface exchange fluxes of NO_2, O_3, NO, CO_2, and H_2O should be feasible.

7. Differences of NO_2 (NO, O_3) concentrations between inlet and outlet of the dynamic chamber, which are expected to be small, must be resolved with statistical significance.

Furthermore, fumigation experiments to study the NO_2 surface exchange in the laboratory (NO_2 exchange under controlled conditions) demand the generation of very low (ppb- and sub-ppb levels) and temporally stable NO_2 concentrations in order to identify statistically significant NO_2 compensation point concentrations. These low NO_2 concentrations have to be reproducible and verifiable.

AMTD
4, 5183–5274, 2011

3 Material and methods

3.1 Trace gas analyzers

NO and NO_2 concentrations were measured by a gas-phase chemiluminescence NO analyzer (Model 42C, Thermo Electron Corporation, USA). In a low pressure reaction chamber, the NO of the air sample reacts with ozone (provided by the analyzer) forming electronically excited NO_2 molecules. Decaying to the ground state, the excited NO_2 molecule emits a photon (chemiluminescence) and the total light intensity in the reaction chamber, detected by a photomultiplier, is proportional to the NO concentration. NO_2 in the air sample is also measured by the NO analyzer after conversion of NO_2 to NO. In most commercial NO/NO_2 analyzers a molybdenum converter is applied (heated to 300–400 °C), where NO_2 is catalytically reduced to NO at the converter's surface. However, previous studies demonstrated that molybdenum converters are non-specific for NO_2 because other oxidized nitrogen compounds of ambient air, like gaseous nitrous acid (HONO), nitric acid (HNO_3), the nitrate radical (NO_3), dinitrogen pentoxide (N_2O_5), peroxyacetyl nitrate (PAN) and other organic nitrates were found to be also converted to NO, which leads to systematic and considerable overestimation of the measured NO_2 values (Winer et al., 1974; Matthews et al., 1977; Grosjean and Harrison, 1985; Gehrig and Baumann, 1993; Steinbacher et al., 2007). During some studies hydrated, crystalline ferrous sulfate ($FeSO_4$) for the surface reduction of NO_2 to NO were used. However, $FeSO_4$ converter also overestimates the mixing ratio of NO and NO_2 (Ridley et al., 1988). Significant interferences of *n*-propyl nitrate, nitrous acid (HNO_2) and PAN were reported (Kelly et al., 1980; Cox et al., 1983; Fehsenfeld et al., 1987). As a consequence Fehsenfeld et al. (1987) did not recommend $FeSO_4$ converter for measuring NO_2. Another frequently used analyzer to measure NO_2 is the Luminox detector (LMA-3, Scintrex/Unisearch Inc.). Its measurement principle is based on the chemiluminescent reaction of NO_2 with luminol in aqueous solution (Maeda et al., 1980; Wendel et al., 1983; Schiff et al., 1986). The luminol technique is noted for interferences by ambient O_3 and PAN, and exhibits non-linear response at low NO_2

AMTD
4, 5183–5274, 2011

concentrations. The interferences due to O_3 and PAN are significant especially at low NO_2 concentrations (Kelly et al., 1990). Table 1 shows an overview about commonly used NO_2 converters and their reported interferences. No interferences or any artifacts were reported for photolytic converters, where NO_2 is photolysed by ultraviolet light <420 nm (Fehsenfeld et al., 1990) or were negligible, respectively (Ryerson et al., 2000). Consequently, we used a highly NO_2 specific blue light converter (BLC) which photodissociates NO_2 into NO at a wavelength of approximately 395 nm (manufactured by Droplet Measurement Technologies Inc., Colorado, USA). To obtain a better accuracy and precision of the NO_2 (and NO) measurements at sub-ppb concentrations, the NO/NO_2analyzer has always been operated with pure oxygen (instead with the oxygen of ambient air) for the internal generation of ozone, necessary for the reaction with NO in the low pressure reaction chamber.

Measurements of CO_2 and H_2O concentrations were performed by infrared dual channel gas analyzer for difference measurements between the outlet of an empty reference chamber and the sample gas (LI-7000, LiCor, Lincoln, NE, USA). An additional gas analyzer (LI-6262, LiCor, Lincoln, NE, USA) monitored the absolute CO_2 and H_2O concentrations to deliver a base signal for the LI-700 operating in differential mode. O_3 concentration was detected using an UV-absorption analyzer (Model 49C, Thermo Electron Corporation, USA). All measured parameters are listed in Table 2.

3.2 Calibrations, limits of detection, standard errors, and precision of trace gas concentration measurements

For the calibration of the NO/NO_2 analyzer (field conditions), a NO standard (5.09 ± 0.1 ppm, Air Liquide, Germany) was applied. The standard was diluted by synthetic air, which had been additionally cleaned with activated charcoal and Purafil (Purafil, Inc., USA) to remove any potential NO and NO_2 contaminations. For the dilution of the NO standard a gas phase titration unit was applied (GPT, 146C Dynamic Gas Calibrator, Thermo Electron Corporation, USA). In the GPT, NO_2 calibration gas is produced by titration (see Reaction (R1)) of the diluted NO standard with O_3 (generated by a UV lamp in the GPT). The BLC's efficiency was determined by the ratio of measured NO_2 and the known value of NO_2 obtained by titration of NO. The O_3 analyzer was calibrated by the GPT-generated O_3, where the exact O_3 concentration is known from the gas phase titration of the NO standard. For the calibration of the CO_2/H_2O analyzer three gaseous CO_2 standards were used (355.4 ppm, 401.1 ppm, 453.8 ppm, Air Liquid, Germany); the H_2O signal has been calibrated by a dew point generator (LI-610, LiCor, Lincoln, NE, USA). To maintain high quality concentration measurements even under long-term field conditions, it was necessary to control and to service the system frequently. In the field, calibrations were performed once a week to ensure stability of the analyzers (quantifying potential drifts), while in the laboratory calibrations were performed just before the start of the experiment.

The determination of the limit of detection (LOD) is particularly important for the exchange measurements of NO and NO_2, as (very) low concentrations have been encountered under both, laboratory and field conditions. According to MacDougall and Crummett (1980) the "limit of detection" is the lowest concentration level that can be determined to be statistically different from a measurement of "zero" concentration. Here we define LOD(m_{NO_2}), LOD(m_{NO}), and LOD(m_{O_3}) as three times that standard deviation ($s_{m\_NO_2,0}$, $s_{m\_NO,0}$, $s_{m\_O_3,0}$), which has been obtained through a statistically significant number (laboratory: 360, field: 160–360) of zero-air measurements. In Table 2 the LOD(m_i) of the instruments are summarized. The conversion efficiency of the BLC for NO_2 was around 25 % during laboratory measurements and 32–36.5 % under field conditions.

Besides the determination and rigorous control of the LOD's, the quantification of the analyzers' reproducibility (precision) is still more necessary, as exchange fluxes of the NO-NO_2-O_3 triad are evaluated from very small differences of concentrations measured at the inlet and the outlet of the dynamic plant chamber. We define the precision of the analyzers as the ratio of the standard errors $s_{m,i}$ and the corresponding concentrations m_i (i = NO, NO_2, O_3). The standard errors of NO and NO_2 measurements

AMTD
4, 5183–5274, 2011

were found to be a (weak) function of the NO and NO_2 concentrations themselves:

$$s_{m,NO_2} = s_{m\_NO_2,0} \cdot \exp(B_{NO_2} \cdot m_{NO_2}) \quad (9.1)$$

$$s_{m,NO} = s_{m\_NO,0} \cdot \exp(B_{NO} \cdot m_{NO}) \quad (9.2)$$

where $s_{m\_NO_2,0}$ and $s_{m\_NO,0}$ are the standard errors at $m_{NO_2} = 0$ and $m_{NO} = 0$, B_{NO_2} and B_{NO} (in nmol^{-1} m^3) have been derived from calibration exercises.

3.3 Dynamic chamber system

3.3.1 Design and construction

The open (flow through), dynamic chamber system was a further development of the systems operated in previous studies (Schäfer et al., 1992; Kesselmeier et al., 1996; Kuhn et al., 2002). The system was designed for measurements of trace gas exchange in the field with minimal effects on the gases. The system has been demonstrated to work under field conditions. The design of the chambers is illustrated in Fig. 4 and details of the used materials and parts are listed in Table 3. The chambers had an inner diameter of 40 cm. The height of the chambers could be varied by extending the frame and could be adjusted for the plant specimen. The initial height was 45 cm and we used extensions of 15 cm at field measurements. The chamber frame and the lid were made of PVC and acrylic glass.

The inner walls consisted of a thin transparent Teflon film (FEP). Previous investigations of the spectral transmissivity of the FEP film have shown that photosynthetically active radiation (PAR) nearly completely transmits this film: in the spectral range of PAR (400–700 nm) transmissivity is about 95 %. In the range of $\lambda \leq 400$ nm, the transmissivity of the FEP film is about 90 % (Schäfer et al., 1992; Pape et al., 2009). A consequence of the horizontal installation of the chamber during field measurement is that transmission of the acrylic glass parts of the chamber plays only a minor role. Furthermore, the Teflon film was reported to show no interferences with trace gases tested such as organic acids (Schäfer et al., 1992; Kesselmeier et al., 1997), monoterpenes and isoprene (Kesselmeier et al., 1996, 1997; Kuhn et al., 2000), and reduced sulfur compounds (Kesselmeier et al., 1993).

The FEP film was fixed with elastic silicone straps around the outer side of the frame. The inner side of the lid was covered by the Teflon film as well. The lid was fixed to the chamber with four clamps. Several holes in the lid allowed the installation of tubes, mixing fans and the intake system of purging air. The purging air flow through the chamber was established in the field by a blowing axial inlet fan which was controlled by an air mass flow sensor installed outside the chamber frame. In the laboratory we used pressurized air for flushing the chamber. For a continuous turbulent mixing of the air inside the chamber a Teflon propeller driven by a magnetically coupled motor attached outside and two Teflon coated mixing fans were used. This design ensured that the air pumped through the chamber only came into contact with parts made of Teflon (PFA or PTFE). For the measurements several chambers were combined (Fig. 5). As in former studies on the NO_2 exchange with different plants, an extra empty ("reference") chamber was also applied. The empty chamber was used to detect basic contamination in the system, adsorption/desorption, as well as to investigate gas-phase chemical reactions within the chamber volume and at the wall surface. A central V25 microprocessor unit (PASCAL based code) controlled the power supply for the mass flow sensors, purging and mixing fans, and signal recording by a PC card. Each chamber could be controlled independently. Furthermore, the V25 operated a number of environmental sensors for air and needle temperature, photosynthetically active radiation (PAR) and relative humidity, and recorded their signals.

3.3.2 Implementation of concentration and flux density measurements

Exchange flux densities of the NO-NO_2-O_3 triad as well as of CO_2 and H_2O are determined from the difference of molar concentrations measured at the inlet and outlet of the dynamic chambers. Ideally, a total of 10 analyzers per dynamic chamber would guarantee simultaneous concentration measurements at all these positions. However, full simultaneity is usually prohibited, both for reasons of cost, and because operation of two trace gas analyzers with an agreement (in their absolute accuracy) much less of the expected difference between inlet and outlet concentration is currently not feasible. Therefore, only one set of analyzers was used operating in a mode of continuous switching between the inlet and outlet position(s) of the (different) dynamic chamber(s). For gas piping the tubes from the different positions at the chambers were combined to one insulated and heated (above ambient temperature) bundle to prevent water vapor condensation. To ensure similar conditions for all lines, all tubes were set to the same length (in this field study 37 m). The sampling air flow was maintained by Teflon membrane pumps with an air flow of 8–10 $L\,min^{-1}$. To avoid contamination of tubes and analyzers a PTFE particulate filter (pore size 2 µm) was installed in front of the intake line. Switching between the different intake lines was maintained by several 3-way PFA solenoid valves. The necessary quantity of valves depends on the number of dynamic chambers in operation. The sample line connected the valve block to the analyzers. Even when an individual intake line was not switched to the analyzers, the air flow through it was kept constant. A second V25 unit was used to control the solenoid valves and the cycle times and recorded the data of the trace gas analyzers. Measurement cycle times and switching (during field experiments) is shown in Fig. 12a. The shown cycling time of 4 min is a result of optimization between fast switching and the analyzers' and system's capabilities: the most important issues in this respect are the analyzers' (moving) averaging times of 30 s and the temporal response of the analyzers to switching concentrations.

Air temperature and needle surface temperatures inside the chambers were continuously recorded by Teflon covered thermocouples (0.005", Chromega^{TM}-Constantan, Omega, UK). PAR was detected outside the chamber with a LiCor quantum sensor (model LI-190SA, LiCor, Lincoln, NE, USA). Relative humidity was measured with a combined temperature and relative humidity probe (Model MP100A, Rotronic, Switzerland).

AMTD
4, 5183–5274, 2011

3.3.3 Laboratory set-up

For laboratory experiments the plant chambers were installed inside a thermostatted cabinet (Heraeus, Germany), which was kept under controlled temperature and humidity conditions (day: 25 °C, 60 %; night: 20 °C, 50 %) with a light/dark regime of 12/12 h. In addition to the cabinet irradiation (Osram Powerstar HQI-BT 400 W/D) we used a set of light emitting diodes with a spectral bandwidth of 400–700 nm. The total measured PAR in the middle of the chamber was about 450 µmol photons $m^{-2}\,s^{-1}$. The plant chambers were continuously flushed with purified air, obtained by passing compressed air through a gas purification system consisting of several columns in series, filled with silica gel (2–5 mm, Merck, Germany), molecular sieve (0.3 nm perlform, Merck, Germany), charcoal (0.3 mm LS-Labor Service, Germany), and glass wool (Merck, Germany). The purified air was then led through a glass tank filled with demineralized water to humidify the air. Different NO_2 concentrations (between 0.3 and 4 ppb) were generated by mixing NO_2 from a pressurized standard cylinder ($m_{\mathrm{std,NO_2}} = 41\,151 \pm 2049$ nmol m^{-3} (1.004 ± 0.050 ppm) NO_2 in N_2; Air Liquide, Germany) into the purified air stream. Mixing was performed by adjustment of two mass flow controllers (MKS Instruments, USA), one to keep the flow of NO_2 standard gas ($Q_{\mathrm{std,NO_2}}$), the other the flow of the purified air stream (Q_{dil}) constant. The blended NO_2 concentration ($m_{\mathrm{blend,NO_2}}$) and its standard error ($s_{\mathrm{m\_blend,NO_2}}$) are given by

$$m_{\mathrm{blend,NO_2}} = \frac{\left(m_{\mathrm{std,NO_2}} Q_{\mathrm{std,NO_2}} + m_{\mathrm{dil,NO_2}} Q_{\mathrm{dil}}\right)}{\left(Q_{\mathrm{std,NO_2}} + Q_{\mathrm{dil}}\right)} \tag{10.1}$$

$$s_{\mathrm{m\_blend,NO_2}} = \pm \frac{\left(m_{\mathrm{blend,NO_2}}\right)^2}{\mathrm{m}_{\mathrm{std,NO_2}}\, Q_{\mathrm{std,NO_2}}} \sqrt{\left(\frac{s_{\mathrm{Q\_std,NO_2}} Q_{\mathrm{dil}}}{Q_{\mathrm{std,NO_2}}}\right)^2 + \left(s_{\mathrm{Q,dil}}\right)^2} \tag{10.2}$$

Discussion Paper | Discussion Paper | Discussion Paper | Discussion Paper |
AMTD
4, 5183–5274, 2011

where $s_{\text{m\_blend,NO}_2}$ results of Gaussian error propagation applied to Eq. (10.1); concentrations (and standard errors) of $m_{\text{std,NO}_2}$, $m_{\text{blend,NO}_2}$, and $m_{\text{dil,NO}_2}$ are in nmol m^{-3}, flow rates (and standard errors) of in $Q_{\text{std,NO}_2}$ and Q_{dil} are in m^3 s^{-1}. For calculation of $s_{\text{m\_blend,NO}_2}$ it is assumed, that $m_{\text{std,NO}_2}$ is constant (during the time of the laboratory experiment) and m_{dil} is zero.

The NO_2 mixture was directed into the dynamic plant chambers (without using the blowing axial inlet fan as for our field studies). For the laboratory measurements one plant chamber and one empty chamber with a volume (V) of 57 L were used. Each chamber was flushed at a constant flow (Q) of 14 L min^{-1}, controlled by mass flow controllers (MKS Instruments, USA), resulting in an exchange of the entire chamber's volume every 4 min. For two minutes each, air samples were directed to the analyzers from three different intake lines (purging NO_2 mixture (upstream of the chambers), outlet of empty and plant chambers). All analyzers were placed inside a cabinet (GKPv 6522, Liebherr, Germany) thermostatted at 25 °C to minimize variations of the analyzers' signals caused by temperature fluctuations.

3.3.4 Field site description and set-up

The field experiment was conducted within the project EGER (ExchanGE processes in mountainous Regions). The second intensive observation period (IOP-2) of EGER took place in summer 2008 (1 June–15 July) in the "Fichtelgebirge" (northeast Bavaria, Germany), a mountainous region, covered mainly by forests and arable land (including meadows), and lakes. The research site "Weidenbrunnen" (50°08′31″ N, 11°52′01″ E; 774 m a.s.l.) is part of a spruce forest ecosystem, which resulted from intensive reforestation in the last century. The plant cover is dominated by Norway Spruce (*Picea abies* L.). The stand-age was 56 yr (according to Alsheimer 1997) and the mean canopy height was 23 m (Serafimovich et al., 2008). The tree density of the stand was 1007/ha (Alsheimer 1997), with a leaf area index (LAI) of 5.2 (Thomas and Foken, 2007).

For the field measurements we used two dynamic chambers to determine exchange flux densities of two spruce branches of two different trees. In addition, one empty chamber was operated nearby the plant chambers. The chambers were installed at a height of 13 m above ground (at a 32 m tall tower). The ambient air inlet was mounted at 16 m height. The chambers had a volume (V) of 75 L, and a constant flow (Q) of 60 L min^{-1} maintained a continuous and complete air exchange in 75 s. For best performance, all analyzers were placed inside an air-conditioned container on the forest ground close to the tower. All insulated and heated (see above) intake lines were running from the individual positions of the chambers to the container and were of equal length (about 37 m). The four intake lines (ambient air; outlets of plant chamber 1, plant chamber 2, and empty chamber) were sampled consecutively for four minutes each. The measurement cycle was as follows: (1) ambient air, (2) plant chamber 1, (3) reference chamber, and (4) plant chamber 2 (see Fig. 12a).

3.3.5 Plant material

Laboratory experiments were performed with 3- to 4-yr old Norway Spruce trees (*Picea abies* L.) grown in pots in a commercial soil mixture. All specimens originated from the EGER field site and were dug out half a year before the measurements started. For the laboratory studies the above-ground parts of the whole tree were enclosed in the chamber. A typical young tree had a leaf area (A_{leaf}) of 0.44 m^2 in total. For the field experiments branches of adult Norway Spruces were investigated. The front part of an intact branch with older needles and new shoots, still attached to the tree, was enclosed to around 40 cm length in the chamber. Two plant chambers on different trees were used for the field studies. At the end of the studies the enclosed leaf area was measured to be 0.36 m^2 (tree 1) and 0.37 m^2 (tree 2) with a dry weight of 66 g (tree 1) and 78 g (tree 2). For determination of leaf area and dry weight the leaves of the enclosed branches were harvested at the end of experiments. Leaves were scanned by a calibrated scanner system (DeskSCAN II, Hawlett-Packard, USA; area determining software SIZE, Müller, Germany). Dry leaf weight was obtained after drying for

AMTD
4, 5183–5274, 2011

two days at 70 °C in an oven (Heraeus, Germany). During the long term field measurements spruces were producing new needles, therefore we estimated the leaf area during measurement time by linear interpolation. The needles of spruce have stomata on the entire needle surface, therefore the area of the whole surface was used. For needle surface area calculation the single surface area was multiplied by factor 2.74 according to Riederer et al. (1988). All exchange measurements started one day after enclosure in order to allow an acclimatization of the branch or plant.

3.3.6 Monitoring of plant-physiological processes

Working with chambers and enclosed plants (parts of plants) necessitates control of the plant living conditions. Chamber operation and design must not disturb plant metabolism. For example an insufficient purging air flow would affect the gas exchange of the plant. An increase of water vapor concentration and a drop of the CO_2 level would trigger a nonphysiological stomatal behavior. Thus, the simultaneous measurement of CO_2 mixing ratios and surface exchange fluxes (assimilation), H_2O surface exchange fluxes (transpiration) and determination of stomatal conductance were performed to provide an indication of the plant condition. For long term field measurements further comparing measurements with non enclosed plants (or part of the plants) would be advantageous to indicate the potential effects of enclosures. Within this context, measurements of the photosynthetic capacity in response to temperature, radiation, CO_2 mixing ratio and relative humidity or analysis of the nutrient composition of enclosed and control plants are of great help.

3.4 Quality assurance and error analysis

3.4.1 Corrections for concentration changes in long tubing

Long intake lines (mostly necessary for field experiments) may impact the trace gas concentrations (Beier and Schneewind, 1991). Trace gases may ad- or absorb on the inner walls of the tubing, and/or react with each other according Reactions (R1) and (R2) (see Appendix A). Therefore, we used opaque tubing to completely prevent photolysis of NO_2. Hence, Reaction (R1) ($NO + O_3$) was the most important reaction to consider. For a known residence time, temperature and pressure in the tubes, the mixing ratios of NO, NO_2 and O_3 can be corrected according to Beier and Schneewind (1991). To proceed, the residence time of the individual trace gas in the tubing as well as the characteristic chemical reaction time (τ_i; $i = \mathrm{NO}, \mathrm{O_3}$) must be known. The latter is calculated by $\tau_{\mathrm{NO}} = (k\,N_{\mathrm{O_3}})^{-1}$ and $\tau_{\mathrm{O_3}} = (k\,N_{\mathrm{NO}})^{-1}$, respectively ($N_{\mathrm{O_3}}$ and N_{NO} in molecules cm^{-3}, $k_{\mathrm{R1}} = k = 1.4 \times 10^{-12} \exp(-1310/T)$ in cm^3 molecules^{-1} s^{-1}; see Atkinson et al., 2004).

3.4.2 Temporal response of analyzers

Tests were carried out to check the response of analyzers to changes of concentrations when switching between intake lines with low concentration of the respective trace gas (NO, NO_2, O_3) to another intake line with high trace gas concentration (after stabilization), and back to the intake line of low concentration.

3.4.3 Temperature dependence of analyzers

The signals of analyzers are sensitive to the surrounding temperature. These effects are of particular importance for field studies where it is more difficult to keep temperatures constant. Thus a series of tests were performed to determine the temperature dependence of all trace gas analyzers. The tests were done inside the conditioning cabinet (Heraeus, Germany) under different temperature conditions (temperature range: 18–46 °C). For each analyzer a calibration was carried out at each temperature level. We considered the correction of the analyzers' signals necessary if the observed drift with temperature exceeded the maximum signal noise measured with zero air. We did not perform a correction when the drift was below 1 % for the entire temperature range or the analyzer's noise was greater than the temperature drift.

AMTD
4, 5183–5274, 2011

3.4.4 Dynamic chamber: internal mixing, exchange rate of chamber volume, wall absorption, and transmissivity

Effective turbulent mixing and fast exchange of the plant chamber's volume are essential for the determination of exchange flux densities of reactive as well as non-reactive trace gases (cf. Meixner, 1994; Meixner et al., 1997). Particularly, the derivation of accurate NO_2 and O_3 leaf conductances from NO_2 and O_3 deposition velocities obtained by dynamic chamber measurements critically depends from the effectiveness of internal mixing and the chamber volume's exchange rate (cf. Pape et al., 2009). Fast internal mixing of the chamber's volume was assured by operation of three fans (see Fig. 4) inside the chamber. A similar procedure was chosen by Pape et al. (2009), who quantified complete mixing of the chamber volume in less than 2 s. The exchange rate of the chamber's volume is primarily determined by the volume V and the purging rate Q. However, due to delay effects of the sampling lines and due to the limited response times of the analyzers after switching between the different intakes, it is not possible to directly observe the trace gas' mixing in the plant chamber. Therefore, the time needed to equilibrate trace gas concentrations in an empty plant chamber was determined by measurements of a fast-response helium detector (Pico leak detector, MKS Instrument Inc., USA). A helium pulse was released into the purging stream of the chamber and the needed time for equilibration was determined.

Sorption effects (ad-, ab-, desorption) to and from the inner wall materials of the dynamic chamber should not modify the concentrations of (reactive) trace gases. Using the laboratory set-up, we investigated potential sorption effects to the inner walls of an empty chamber by fumigating it consecutively with different NO, NO_2 and O_3 concentrations. There were no desorption effects observed. Wall absorption was quantified in form of "blank" deposition velocities, where $v_{\text{dep\_wall},i} = Q\ (m_{a,i} - m_{s,i})/(A_{\text{wall}} m_{s,i})$ ($i = NO_2$, NO, O_3).

In the field, the transmissivity of the FEP film (the dynamic chamber's wall) for PAR and the NO_2 photolysis rate $j(NO_2)$ was monitored by continuous and simultaneous

AMTD
4, 5183–5274, 2011

measurements of corresponding radiation fluxes inside and outside the chamber. PAR was measured with a LiCor quantum sensor (model LI-190SA, LiCor, Lincoln, NE, USA) and $j(NO_2)$ was determined as an omni-directional actinic UV radiation flux using a $j(NO_2)$-sensor (filter radiometer, Meteorologie Consult GmbH, Königstein, Germany).

3.4.5 Significance of concentration differences

In the laboratory, the exchange flux density is directly proportional to $\Delta m_i = (m_{a,i} - m_{s,i})$, the difference of trace gas concentrations at the inlet and the outlet of the dynamic chamber (see Eq. (1.4)). Even under field conditions, the major component of the exchange flux density $F_{ex,i}$ is $Q/A_{leaf}\ \Delta m_i$. Keeping in mind, that (a) the sign of Δm_i determines direction of the exchange flux density, and (b) the errors of $m_{a,i}$ and $m_{s,i}$ are decisively controlling the error of Δm_i, (and consequently that of $F_{ex,i}$), it is obvious to control the significance of Δm. The corresponding statistical test requires the number of individual measurements, the averages and standard errors of $m_{s,i}$ and $m_{a,i}$. These were provided and calculated from the individual concentration measurements during one measurement cycle (laboratory: 30 min, field: 4 min). Prior to this, we identified outliers in the data sets by application of the Nalimov-test, a variant of Grubbs' test. The significance of differentiation between the two averages of $m_{s,i}$ and $m_{a,i}$ was statistically secured by application of the t-test. Δm with statistical significance below 99 % ($\alpha < 0.99$) were correspondingly flagged and not included in subsequent calculations.

3.4.6 Regression analysis

Since the concentrations $m_{a,i}$ and $m_{s,i}$ are measured with identical analyzers (see above), corresponding standard errors $s_{ms,i}$ and $s_{ma,i}$ are of the same order of magnitude. Therefore, bi-variate weighted linear least-squares fitting (which considers uncertainties of both, $m_{s,i}$ and $m_{a,i}$) is preferred to any standard forms of linear regression analysis (which consider, at best, uncertainties in the y-values, but no uncertainties in the x-values). The preferred algorithm delivers corresponding values of intersect (n_i)

and slope (b_i) and other statistical quantities, like the standard errors of n_i and b_i ($s_{n,i}$, $s_{b,i}$), as well as correlation and regression coefficients, $r(m_{s,i}, m_{a,i})$ and $R^2(m_{s,i}, m_{a,i})$. York et al. (2004) presented the original set of equations for bi-variate weighted linear least-squares fitting regression analysis, where the slope b_i has to be solved iteratively (see Appendix B). We made use of a Microsoft Excel spreadsheet for the iterative calculation, which has been provided by Cantrell (2008) as a Supplement of his paper (http://www.atmos-chem-phys.net/8/5477/2008/acp-8-5477-2008-supplement.zip).

3.4.7 Standard errors of exchange flux densities, deposition velocities, and compensation point concentrations

Standard errors of exchange flux densities $F_{ex,i}$, deposition velocities $v_{dep,i}$, and compensation point concentrations $m_{comp,i}$ of the NO-NO_2-O_3 triad may be derived by applying standard Gaussian error propagation. The standard errors of all variables on the right hand side of Eqs. (1.1)–(1.3), (6.1)–(6.3), and (7.1)–(7.3) must be known, and all variables of each individual equation should be independent of each other. However, the latter is not the case for (at least) $m_{s,i}$ and $m_{a,i}$ (see Eqs. (1.1)–(1.3)). Therefore, application of the generalized form of the Gaussian error propagation is preferred, which considers the mutual dependence of each pair variables (Taylor, 1982; Phillips et al., 2002). The general formulation of the standard error s_y of a quantity $y = f(x_1, x_2, x_3, \ldots, x_n)$ reads as follows:

$$s_y^2 = \sum_{i=1}^{n} \left(\frac{\partial y}{\partial x_i} \cdot s_{x,i} \right)^2 + 2 \cdot \sum_{i=1}^{n-1} \sum_{j=i+1}^{n} \frac{\partial y}{\partial x_i} \cdot \frac{\partial y}{\partial x_j} \cdot s_{x,i} \cdot s_{x,j} \cdot r\left(x_i; x_j\right) \quad (11)$$

where $r\ (x_i;\ x_j)$ are the correlation coefficients between each pairs of all x_i and x_j.

The individual variables x_i for the quantities $y = F_{exNO_2}$, F_{exNO}, F_{exO_3}, v_{dep,NO_2}, $v_{dep,NO}$, v_{dep,O_3}, m_{comp,NO_2}, $m_{comp,NO}$, and m_{comp,O_3} are defined by Eqs. (1.1)–(1.3), (6.1)–(6.3), and (7.1)–(7.3). These are listed in Appendix C as well as all the corresponding derivatives necessary to calculate the standard errors of these quantities according

Discussion Paper | Discussion Paper | Discussion Paper | Discussion Paper |

AMTD

4, 5183–5274, 2011

The dynamic chamber method

C. Breuninger et al.

to Eq. (11).

3.4.8 Significance of the compensation point concentrations

The bi-variate weighted linear least-squares regression analysis of $m_{a,i}$ and $m_{s,i}$ delivers the intercept n_i, the slope b_i, and their standard errors $s_{n,i}$ and $s_{b,i}$. According to Eqs. (7.1)–(7.3), each of the compensation point concentrations $m_{comp,i}$ of the NO-NO_2-O_3 triad can be considered as a random variable, represented by the average of $m_{comp,i}$ and the standard error $s_{m,comp,i}$. The decision whether or not a compensation point concentration exists is equivalent to the test of the hypothesis whether or not the average of $m_{comp,i}$ is highly significantly ($\alpha = 0.999$), significantly ($\alpha = 0.99$), or likely ($\alpha = 0.95$) different from $m^*_{comp,i} = 0$.

For that, it is assumed that each of the test quantities T_i

$$T_i = \left(\bar{m}_{comp,i} - m^*_{comp,i}\right) \cdot \frac{\sqrt{N}}{s_{m,comp,i}} \quad i = NO_2, NO, O_3 \tag{12}$$

matches the t-distribution with $N-1$ degrees of freedom. Depending on α, the hypothesis $m_{comp,i} = m^*_{comp,i}$ must be rejected, if

$$\left|\bar{m}_{comp,i} - m^*_{comp,i}\right| \geq \frac{s_{m,comp,i}}{\sqrt{N}} \cdot t_{\alpha;N-1}; \quad \left(\text{i.e. } \frac{t_{\alpha;N-1}}{T_i} \leq 1\right) \tag{13}$$

where $t_{\alpha;N-1}$ are the values of the t-distribution $(N-1)$ for $\alpha = 0.999$, 0.99, 0.95, respectively.

4 Results

4.1 Analyzers and system performance

The results for the test of temperature dependence of all analyzers (see Sect. 3.4.3) are listed in Table 4. Between 18 and 46 °C the efficiency of the BLC drifted from

AMTD
4, 5183–5274, 2011

37.0 % to 47.4 % over the whole temperature range. This means that for an initial concentration of 10 ppb NO_2 a drift of 2.2 ppb over the whole temperature range would be observed, which is equivalent to 3.6 nmol m^{-3}/K (0.08 ppb/K). For NO the signal drift was 2.8 nmol m^{-3}/K (0.07 ppb/K). The data of the CO_2 and O_3 analyzers did not need to be corrected because the signal drift was below 1 % for the entire temperature range, in contrast to the NO and NO_2 values. For the mathematical correction the slope of the regression line of the temperature tests (trace gas concentration versus temperature) was used.

On the basis of the results of calibration procedures it was found, that the standard error of the O_3 concentration measurements could be considered as constant (±13.3 nmol m^{-3} or ±0.32 ppb) for the observed range of O_3 concentrations (719–2866 nmol m^{-3} or 19–77 ppb). The standard errors of NO_2 and NO concentration measurements are described by Eqs. (9.1) and (9.2); the parameters $s_{\mathrm{m\_NO_2},0}$, and $s_{\mathrm{m\_NO},0}$ are given in Table 2 (3σ-definition: $\mathrm{LOD}(m_i) = 3\, s_{\mathrm{m},i,0}$), and $B_{\mathrm{NO2}} = 3.42 \times 10^{-4}$ nmol^{-1} m^3 (1.40×10^{-2} ppb^{-1}), and $B_{\mathrm{NO}} = 7.88 \times 10^{-4}$ nmol^{-1} m^3 (3.23×10^{-2} ppb^{-1}).

In Fig. 6, the precision ($s_{\mathrm{m},i}/m_i$) of the concentration measurements is exemplified for NO_2 during laboratory (red curve) and field experiments (green curve). The precision of $m_{\mathrm{NO_2}}$ was only approx. 35 % during laboratory experiments at $\mathrm{LOD}(m_{\mathrm{NO_2}}) = 1.04$ ppb (46.4 nmol m^{-3}). After considerable improvement of the NO/NO_2 analyzer precision at 1 ppb improved to nearly 10 % in the field (however, precision was still 35 % at $\mathrm{LOD}(m_{\mathrm{NO_2}}) = 0.31$ ppb (13.8 nmol m^{-3})). For further comparison, we consider that concentration m_i, where corresponding precision curves fall short of the 10 %-precision lines. These concentrations were 161.9 nmol m^{-3} (3.63 ppb; laboratory conditions), 45.9 nmol m^{-3} (1.03 ppb; field conditions), and they would be 14.7 nmol m^{-3} (0.33 ppb) and 1.3 nmol m^{-3} (0.03 ppb), if analyzers could be applied with $\mathrm{LOD}(m_{\mathrm{NO_2}}) = 0.1$ and 0.01 ppb, respectively. For the NO and O_3 analyzers applied under field conditions, corresponding NO and O_3 concentrations (<10 % precision)

AMTD
4, 5183–5274, 2011

were 15.2 nmol m^{-3} (0.34 ppb; LOD(m_{NO}) = 0.10 ppb) and 144.5 nmol m^{-3} (3.24 ppb; LOD(m_{O_3}) = 0.98 ppb), respectively.

The performance of the dynamic chamber system depends critically on the temporal delay of concentrations (measured by only one set of analyzers) which are caused by switching between different intake lines of considerable length and by chemical reactions inside corresponding tubing (see Sect. 3.4.1). The tubing residence time for the 36.5 m long tubes of the field experiment was ≤4.1 s under ambient temperature and pressure conditions, calculated from sample flow (1.42–1.67 m^3 s^{-1} or 8.5–10 L min^{-1}), the length of the tubes, and the tubes' inner diameter (0.00435 m). Since a considerable high flow through the intake filters and the long, thin tubes caused a distinct pressure drop (approx. 490 hPa), the actual residence time was consequently shorter (1.9 s). The characteristic chemical time scale (τ_{chem}; e-fold time) for the NO + O_3 reaction (see Reaction (R1)) was within 20<τ_{chem} <120 s during the entire field experiment. Since τ_{chem} was always much longer than the tubing's residence time, any effects of the NO + O_3 reaction on measured concentrations could be neglected (as well as for the NO_2 + $h\nu$ Reaction (R2), since opaque tubes have been used). However, the flow rate between the valve block (see Fig. 5) and the analyzers is about 1/10 of the tubing purge flow; therefore, the "response time" of the entire system for a sudden change of concentrations was tested. Results are shown in Fig. 7 for NO_2 (step change from 41 to 861 nmol m^{-3}). Immediately after switching some typical pressure effects (valves) could be observed, but a temporally stable concentration was reached after 90 s. For the return switch a quite similar effect were observed, and "response times" of NO, O_3, CO_2, and H_2O were comparable (data not shown). Based on these tests, the first 90 s of each concentration measurement were skipped from further data processing.

4.2 NO_2 blending for fumigation experiments

For laboratory NO_2 fumigation experiments very low (ppb- and sub-ppb levels) and temporally stable NO_2 concentrations have to be made available. That is essentially

AMTD
4, 5183–5274, 2011

necessary to significantly identify any NO_2 compensation point whose concentrations are expected at these low concentration levels. Blended NO_2 concentrations (m_{blend,NO_2}) of 13.4, 26.8, 44.6, 80.3, and 151.7 nmol m^{-3} (0.3, 0.6, 1.0, 1.8, 3.4 ppb) were provided by diluting an NO_2 standard into purified air (see Sect. 3.3.3). A typical course of these concentrations are shown in Fig. 8, where the vertical dashed lines indicate times where blending was changed to obtain the next NO_2 concentration. A stable signal of the new NO_2 concentration level was reached after max. 60 min. Fluctuation of the blended NO_2 concentration was between 8.0 and 16.1 nmol m^{-3} (0.18–0.36 ppb). These fluctuations do not depend on the analyzers' temperature (see Sect. 4.1). During laboratory measurements, the temperature variation of the instrument was only ±0.5 °C, which would be equivalent to a change of m_{blend,NO_2} = 44.6 nmol m^{-3} (1 ppb) of less than 1 %. The measured fluctuations could be also due to the precision of m_{blend,NO_2} which depends on the precision of the applied mass flow controllers. According to the manufacturer, the precision of the mass flow controllers is ±0.8 % of full scale. Using this information, the precision of m_{blend,NO_2} has been calculated through Eqs. (10.1) and (10.2) and is also shown in Fig. 6. Uncertainty of the mass flow controllers may have added <20 % to the observed variation of measured the blended NO_2 concentration.

4.3 Characterization of the dynamic plant chamber

4.3.1 Radiation and NO_2 photolysis rate

Transmissivity of PAR through the chamber walls (FEP film) is a fundamental requirement if the plant is not to be affected by the chamber itself. Moreover, the calculation of the exchange flux density $F_{ex,i}$ (see Eqs. (1.1)–(1.3)) has to consider the NO_2 + $h\nu$ reaction. For this, the photolysis rate $j(NO_2)$ inside the chamber volume has to be known. Therefore the transmissivity was controlled by simultaneous measurements inside and outside the chamber. While PAR was 10 % lower inside the chamber than outside, $j(NO_2)$ was 30 % lower inside the chamber (Fig. 9). Therefore, 70 % of ambient

AMTD
4, 5183–5274, 2011

$j(NO_2)$ was used for the calculations of $F_{ex,i}$, $v_{dep,i}$, $m_{comp,i}$ and their standard errors.

4.3.2 Sorption effects and chamber volume exchange time

An empty dynamic chamber has been exposed to various concentrations of NO_2, NO, and O_3 and "blank flux densities" have determined according to Eq. (1.4). "Blank flux densities" for NO, NO_2, and O_3 are listed in Table 5. They were always negative (i.e. no desorption from the chamber's inner surfaces) and revealed very low values. Expressed in corresponding "wall deposition velocities" -2.12×10^{-3} (NO), -2.92×10^{-3} (NO_2), and $-1.94 \times 10^{-3}\,mm\,s^{-1}$ (O_3) were found. These values were two orders of magnitude lower than $v_{dep,i}$ observed under laboratory as well as under field conditions. Comparing incoming and outgoing concentrations of the NO-NO_2-O_3 triad, a maximum of 2 % of the trace gases may have been absorbed by the inner surfaces of the plant chamber. Therefore, with regard to the mass balance of the dynamic plant chamber, neglecting of any mass fluxes to the walls of the chamber ($\Phi_{wall,i}$) (see Appendix A) is justified.

The chamber volume exchange time was determined from an experiment, where a short pulse of (chemically inert) helium has been added to the purging flow of the dynamic chamber (see Sect. 3.4.4). Results are shown in Fig. 10. For the time of complete exchange (i.e., a constant level of He is observed), we used the time interval to reach 98 % of the final He concentration (t_{98}). Due to the limited temporal resolution of the He detector (5 s), t_{98} might have been between 80 and 85 s. This result was similar to the time (79 s) calculated from chamber volume ($V = 79$ L) and purging rate ($Q = 60\,L\,min^{-1}$).

AMTD
4, 5183–5274, 2011

4.4 Demonstration of exchange flux density measurements

4.4.1 NO_2 exchange flux density: Laboratory results

Here, we confine ourselves to the results of "daytime" experiments, i.e. fumigation of the 3- to 4-yr old Norway Spruce trees with $13 < m_{a,NO_2} < 152\,\text{nmol}\,\text{m}^{-3}$ (0.3–3.4 ppb), controlled temperature (25 °C), relative humidity (60 %), and PAR (450 µmol photons $\text{m}^{-2}\,\text{s}^{-1}$, for 12 h) conditions. During experiment no significant difference of m_{O_3} or m_{NO} between reference and plant chamber could be detected, and the amount of $j(NO_2)$ inside the chamber was negligible with respect to any measurable effects due to Reaction (R2). As shown in Sect. 4.1, the performance of the NO_2 analyzer was definitely sub-optimal (LOD(m_{NO_2}) = 1.04 ppb; 3σ-definition). Therefore, we based our evaluations of F_{ex,NO_2}, v_{dep,NO_2}, and m_{comp,NO_2} on a 2σ NO_2 detection limit (28.5 nmol m^{-3} or 0.6 ppb) for the observed concentrations (m_{a,NO_2}, m_{s,NO_2}). A total of 51 pairs of m_{a,NO_2} and m_{s,NO_2} have been obtained during the fumigation experiments. 17 data pairs passed the LOD(m_{NO_2}) criterion, where another three of them had to be rejected due to the significance criterion for $\Delta m_{NO_2} = (m_{a,NO_2} - m_{s,NO_2})$. Fourteen data pairs of m_{a,NO_2} and m_{s,NO_2} have been subjected to a bi-variate weighted regression analysis (see Sect. 3.4.6), which resulted in $R^2 = 0.9706$, $n_1 = 1.7 \pm 2.63\,\text{nmol}\,\text{m}^{-3}$, $b_1 = 0.71 \pm 0.035$, $v_{dep,NO_2} = 0.22 \pm 0.013\,\text{mm}\,\text{s}^{-1}$, and $m_{comp,NO_2} = 5.9 \pm 9.13\,\text{nmol}\,\text{m}^{-3}$. The significance probability of $m_{comp,NO_2} \neq 0$ is 96.87 % ("likely"). NO_2 exchange flux densities (F_{ex,NO_2}) and their standard errors have been calculated according to Eq. (11) and are shown in Fig. 11. Figure 11a displays results of F_{ex,NO_2} where the 2σ-LOD(m_{NO_2})-definition, Fig. 11b where the 1σ-LOD(m_{NO_2})-definition has been applied. Furthermore, in both panels F_{ex,NO_2} data were separated for the significance of Δm_{NO_2} (significant: blue circles, non-significant: reddish diamonds); the (F_{ex,NO_2};m_{s,NO_2})-regression lines have been calculated according to Eq. (8.1.1) for all F_{ex,NO_2} data (pink line), and for those F_{ex,NO_2} data, where Δm_{NO_2} is significant (blue line). Corresponding NO_2 compensation point

AMTD
4, 5183–5274, 2011

The dynamic chamber method

C. Breuninger et al.

concentrations m_{comp,NO_2} were calculated according Eq. (8.3.1) and are represented by red filled circles (significant Δm_{NO_2}) and pink hollow circles (all data). Details of statistical evaluation are listed in Table 6. The most striking result is, that (regardless of which linear least-square fitting algorithm and which LOD(m_{NO_2})-definition is applied) the values of m_{comp,NO_2} are always highly significant, if all F_{ex,NO_2} data were used. Applying the simple linear least-square fitting algorithm (without considering s_{m_a,NO_2} nor s_{m_s,NO_2})m_{comp,NO_2} remains highly significant, even if only those F_{ex,NO_2} data are considered where Δm_{NO_2} is significant. However, applying linear least-square fitting algorithms which consider either s_{m_s,NO_2}, or s_{m_a,NO_2} and s_{m_s,NO_2}, the existence of m_{comp,NO_2} becomes "unlikely" ("likely"). With the exception of applying the 2σ NO_2 detection limit to all F_{ex,NO_2} data, the impact of different statistical treatments on the evaluation of NO_2 deposition velocities is small ($0.19 \leq v_{dep,NO_2} \leq 0.22\,mm\,s^{-1}$).

4.4.2 NO-NO_2-O_3 exchange flux densities: Field results

In Fig. 12, typical time series of trace gas mixing ratios are shown, measured at two different spruce branches during the EGER field campaign. The observed mixing ratio changes were due to switching between the different intakes. After switching, concentrations showed the delay effects mentioned above (see Sect. 4.1). Due to this, the first 90 s after valve switching were skipped from subsequent data processing (these first 90 s interval indicated as grey shaded vertical bars in Fig. 12). Values for CO_2 and H_2O were measured as the difference between empty chamber and each switched intake. The temporal variation of CO_2 and H_2O concentrations of the plant chambers versus ambient air or empty chamber represented the physiological activity of the plants, since the CO_2 exchange flux density represents the photosynthetic CO_2 assimilation and the H_2O flux density the transpiration of the enclosed plant parts.

During the field experiment nearly 3000 pairs of $m_{a,i}$ and $m_{s,i}$ have been obtained. Applying the LOD(m_i) (3σ-definition) and the significance criterion for $\Delta m_i = (m_{a,i} - m_{s,i})$, around 60 % of the NO_2 data pairs remained. In Table 7 the details of the data

AMTD
4, 5183–5274, 2011

pairs selection for both trees are listed for NO, NO_2 and O_3. Classification according to measurements during day and night demonstrated, that during night fewer data pairs were distinguishable from each other, especially those of NO. Between the spruce branches in both sampling chambers no differences were noticeable.

After classification of all individual concentration data into different categories of leaf conductance (approx. identical to different categories of radiation conditions), bi-variate weighted regression analysis between classified pairs of $m_{a,i}$ and $m_{s,i}$ was performed (see Sect. 3.4.6). The data pairs were additionally screened for singular concentration peaks of NO, NO_2 and O_3, which mainly occurred due to advection of automobile exhaust gases from a busy country road (2000 cars/h) in a distance of about 1–2 km from the site. The problem of advection at this field site is well known, and has been documented through profile measurements of in- and above canopy concentrations, as well as through eddy covariance flux measurements of NO-NO_2-O_3 performed simultaneously to our dynamic chamber measurements (Plake et al., 2009). For the analysis of dynamic chamber derived O_3 flux densities, we assumed $m_{comp,O_3} = 0$ ($n_3 = 0$), since emissions of O_3 from plants are not known so far.

For the present study, we restrict our results to one spruce branch (chamber 1) and one category with high PAR radiation (mean PAR = 355 µmol photons m^{-2} s^{-1}). The analysis for NO_2 resulted in $R^2(m_{a,NO_2}, m_{s,NO_2}) = 0.9480$, $n_1 = 6.5 \pm 1.59$ nmol m^{-3}, $b_1 = 0.79 \pm 0.016$, $v_{dep,NO_2} = 0.18 \pm 0.034$ mm s^{-1}, and $m_{comp,NO_2} = -9.5 \pm 14.75$ nmol m^{-3}. The probability of $m_{comp,NO_2} \neq 0$ is 99.99 % ("highly significant"); however, a negative NO_2 compensation point concentration is physically meaningless. For O_3 the analysis resulted in $R^2(m_{a,O_3}, m_{s,O_3}) = 0.9847$, $b_3 = 0.80 \pm 0.005$, and $v_{dep,O_3} = 0.32 \pm 0.018$ mm s^{-1}. In Fig. 13a (14a), results of bi-variate weighted regression analysis between m_{a,NO_2} and m_{sNO_2} (m_{a,O_3} and m_{sO_3}) are shown, while in Fig. 13b (14b) those of F_{ex,NO_2} (F_{ex,O_3}) versus m_{sNO_2} (m_{sO_3}). In Fig. 13a and b, data can be individually identified for their significance of Δm_{NO_2} by corresponding color coding. For O_3, there is no corresponding color coding, since all Δm_{O_3} were

AMTD
4, 5183–5274, 2011

significant (see Table 7). Linear relationships between F_{ex,NO_2} and m_{sNO_2} were calculated by Eq. (5.1) for data pairs owing significant Δm_{NO_2} and for all data pairs. In Table 8 all results of statistical analysis of F_{ex,NO_2} and $F_{ex,O3}$ data are listed. Results of bi-variate weighted regression analysis for NO are shown in Fig. 15. A large part of m_{NO} was lower than LOD(m_{NO}) (grey diamonds) or corresponding data pairs were non-significant with respect to $\Delta m_{NO} = (m_{a,NO} - m_{s,NO})$ (reddish diamonds). The regression coefficient $R^2(m_{a,NO}, m_{s,NO})$ was only 0.5355. Therefore, consecutive analyses are biased: probabilities of significant $m_{comp,NO}$ and $v_{dep,NO}$ becomes unlikely (51.7 and 22.4 %, respectively). Hence, there were no further evaluations for $F_{ex,NO}$, $v_{dep,NO}$, and $m_{comp,NO}$.

5 Discussion

5.1 Effects on enclosed plants

Enclosing plants or parts of plants in a dynamic chamber requires the control of plant conditions in order to be sure that observations and data are not created under artificial conditions and consequently transferable to the normal environment. It is important to make sure that the plant is not affected by the chamber, especially for long-term studies. Consequently, we checked the status of the plants after field experiment. We could not identify visual differences between enclosed and not enclosed plant material. Moreover, no differences in physiological performance were detectable. Furthermore, analyses of the composition of nutrients of needles were without findings. Detailed results of these analyses will be given in a consecutive publication.

In most chamber studies plant conditions were monitored just by measuring the CO_2 and H_2O exchange of the plant(s) and these values were used to calculate corresponding leaf conductances (e.g., Thoene et al., 1996; Sparks et al., 2001; Geßler et al., 2002). These measurements allow quantification of the actual photosynthesis and transpiration rates of the enclosed plants. However, to check for a potential

AMTD
4, 5183–5274, 2011

effect of the enclosure on the plant control measurements (e.g. photosynthesis and transpiration rates, nutrient content) on enclosed and comparable non-enclosed parts of the plant are necessary. Some elemental analyses of the needles were previously done by Rennenberg et al. (1998), but rather to secure a sufficient initial nutrient supply of the plants than to control effects of the chamber on the nutrient conditions during the experiments.

5.2 Overview of previous NO_2 exchange flux measurements using dynamic plant chambers

Table 9 shows a list of past dynamic chamber studies that have focused on NO_2 exchange between different plant species and the atmosphere. Most of these measurements were made with NO_2 converters which were not specific for NO_2 detection. Some authors used heated molybdenum converters (Thoene et al., 1991, 1996; Teklemariam and Sparks, 2006; Raivonen et al., 2009), heated ferrous sulphate converters (Rondón et al., 1993, Rondón and Granat, 1994), or a detector based on chemiluminescence on liquid surfaces (Hanson et al., 1989; Hereid and Monson, 2001; Sparks et al., 2001). All these converters overestimate NO_2 concentrations because of interferences with other (oxidized) nitrogen compounds (see Sect. 3.1). Only the application of photolytic converter guarantees the interference-free determination of low NO_2 concentrations.

During most of the field studies filtered air was used for purging the dynamic chambers. In most cases, this air was free of O_3 and NO_x, and known NO_2 concentrations were delivered to the dynamic chamber by diluting standard mixtures of NO_2 from a cylinder (Geßler et al., 2000, 2002; Sparks et al., 2001; Hereid and Monson, 2001). Some studies additionally controlled the CO_2 and water vapor concentrations of the purging air, the irradiance and temperature conditions inside the chamber (Hereid and Monson, 2001; Sparks et al., 2001). Filtered and/or synthetic air (i.e. home-made H_2O and CO_2 concentrations, free of non target reactive trace gases) hardly represents ambient air. Therefore, a potential influence on the physiological behavior of the plant

AMTD
4, 5183–5274, 2011

cannot entirely be excluded.

For field measurements of the NO-NO_2-O_3 triad under ambient conditions, fast gas phase reactions inside the chambers must be considered. Therefore, NO, NO_2, and O_3 concentrations have to be measured simultaneously, even if only one of the trace gases is of interest (Pape et al., 2009). All previous field studies described corrections of the calculated exchange flux densities not in detail. Rondón et al. (1993) specified some corrections for measured NO concentrations only, although O_3 and UV radiation were present in their dynamic chamber. In those cases where measurements of exchange flux densities were performed applying a simultaneously operated empty chamber (as "reference" chamber), corresponding flux densities were calculated from the concentration differences Δm_{NO_2} between the outlet of the plant and empty chambers, respectively. This allowed a certain correction for chamber specific wall absorption and/or desorption processes (Geßler et al., 2000, 2002; Raivonen et al., 2009). However, this procedure may not rule out adverse effects of fast gas-phase reactions on the evaluated flux densities, deposition velocities, and compensation point concentrations (see below).

5.3 Precision, data quality, and photochemical reactions

5.3.1 Precision and data quality

As shown in Sect. 4.1, the precision of NO_2 concentration measurements of our NO_2 analyzer improves from 35 % (at its limits of detection) rapidly to <10 % at 162 nmol m^{-3} (3.63 ppb; laboratory) and 46 nmol m^{-3} (1.03 ppb; field). In Sect. 2.1 we presented the expected precision of the NO_2 exchange flux density for NO_2 concentrations up to 200 nmol m^{-3}, for pre-scribed $m_{comp,NO_2} = 67$ nmol m^{-3} (1.5 ppb), pre-scribed NO_2 deposition velocities (0.3–0.6 mm s^{-1}), and typical $R^2(m_{a,NO_2}, m_{s,NO_2})$ ranging from 0.99 to 0.9 (see Fig. 3). Since F_{ex,NO_2} approaches zero at $m_{s,NO_2} = m_{comp,NO_2}$, the exchange flux density's precision ($\sigma_{Fex,NO_2}/F_{ex,NO_2}$) will become indefinite there. Consequently,

AMTD
4, 5183–5274, 2011

the uncertainty of F_{ex,NO_2} will become as higher as closer m_{s,NO_2} approaches m_{comp,NO_2} (from either side). Analogously to the results shown in Fig. 3, we determined which NO_2 concentration difference, $\pm|m_{s,NO_2} m_{comp,NO_2}|$, will be necessary to keep the NO_2 exchange flux density's precision for our NO_2 analyzer under 10 %. For laboratory conditions ($\text{LOD}(m_{NO_2}) = 45\,\text{nmol m}^{-3}$ or 1.01 ppb), this difference was $\pm 13.8\,\text{nmol m}^{-3}$ or ± 0.31 ppb ($v_{dep,NO_2} = 0.6\,\text{mm s}^{-1}$; $R^2(m_{a,NO_2}, m_{s,NO_2}) = 0.99$), and $\pm 91\,\text{nmol m}^{-3}$ or ± 2.05 ppb ($v_{dep,NO_2} = 0.3\,\text{mm s}^{-1}$; $R^2(m_{a,NO_2}, m_{s,NO_2}) = 0.9$). During the EGER field experiment ($\text{LOD}(m_{NO_2}) = 13.8\,\text{nmol m}^{-3}$ or 0.31 ppb) corresponding values were ± 4.5 and $\pm 8.5\,\text{nmol m}^{-3}$ (0.1 and ± 0.19 ppb), respectively. A serious consequence of these calculations is, that, for a given detection limit, there is a well defined limit of m_{comp,NO_2} where the NO_2 compensation point concentration can be inferred from flux density data ($\sigma_{Fex,NO_2}/F_{ex,NO_2} \leq 10\,\%$) by interpolation of data measured on both sides of m_{comp,NO_2}. Below that limit, due to the obvious conflict of the requested $|m_{s,NO_2} m_{comp,NO_2}|$ and $\text{LOD}(m_{NO_2})$, m_{comp,NO_2} can only be inferred from flux density data at $m_{s,NO_2} > m_{comp,NO_2}$ by extrapolation, owing the risk of (much) higher uncertainties. These limits were for our NO_2 analyzer 33.5 and 133.8 nmol m^{-3} (0.75 and 3.0 ppb; laboratory) and 13.4 and 44.6 nmol m^{-3} (0.3 and 1.0 ppb; field) for the above mentioned combinations of v_{dep,NO_2} and $R^2(m_{a,NO_2}, m_{s,NO_2})$.

In previous studies the NO_2 sensitivity (a proxy for precision) of corresponding NO_x or NO_2 analyzers has been specified through their detection limit only (see Table 9). Neubert et al. (1993) and Geßler et al. (2000), who used analyzers equipped with photolytic NO_2 converters mentioned a $\text{LOD}(m_{NO_2})$ of $4.5\,\text{nmol m}^{-3}$ (0.1 ppb); however, the corresponding definition of LOD (1σ, 2σ or 3σ of $\sigma_{NO_2,0}$) is not reported. Based on the manufacturer's data of the analyzers and on our experience, we assume that the reported values correspond to the 1σ-definition ($P = 0.68$). This assumption is in agreement with the values of Rondón and Granat (1994), who have used the same NO_2 analyzer model, namely with $\text{LOD}(m_{NO_2}) = 8.9\,\text{nmol m}^{-3}$ (0.2 ppb; 2σ definition). Using the same LOD-definition (2σ), Rondón and Granat (1994) reported a four times lower LOD

AMTD
4, 5183–5274, 2011

for NO of 2.2 nmol m^{-3} (0.05 ppb). Weber and Rennenberg (1996a; 1996b) using also a photolytic NO_2 converter, have not reported any specifications about their instrument's sensitivity; therefore, we assumed that, based on the manufacturer's information about the applied NO/NO_2 analyzer, the LOD for NO was 33.5 nmol m^{-3} (0.075 ppb; 3σ-definition). According to Rondón and Granat (1994), and based on our experience the corresponding LOD for NO_2 can be assumed to have not been better than 10 nmol m^{-3} (0.225 ppb; 3 × LOD(m_{NO})). Using the results of our simulation of the minimum detectable NO_2 compensation point concentration (see Sect. 2.2), we can state that NO_2 compensation point concentrations ≥ 44.6 nmol m^{-3} (≥1 ppb) can be detected with high significance, if NO_2 analyzers with LOD(m_{NO_2}) ≈ 13.4 nmol m^{-3} (0.3 ppb) were used (as Weber and Rennenberg, 1996a and Geßler et al., 2002) and $R^2(m_{a,NO_2}, m_{s,NO_2})$ was in a typical range (0.9–0.99) of laboratory measurements. Using NO_2 analyzers with LOD(m_{NO_2}) ≈ 44.6 nmol m^{-3} (≈1 ppb; e.g. analyzers with molybdenum converters) the significant detection of m_{comp,NO_2} > 44.6 nmol m^{-3} (1 ppb) would already be difficult, if the v_{dep,NO_2} is very small (<0.3 mm s^{-1}). For example, Thoene et al. (1996) reported m_{comp,NO_2} = 73.1 nmol m^{-3} (1.64 ppb) which has most likely be detected with high significance, because they reported v_{dep,NO_2} = 0.8 mm s^{-1}. On the other hand, the detection of m_{comp,NO_2} = 13.4–31.2 nmol m^{-3} (0.3–0.7 ppb; Rondón et al., 1993) at v_{dep,NO_2} = 0.8 mm s^{-1} seems now, from a statistical point of view, to be unlikely.

The data quality of exchange flux densities requires the control of quantifiable parameters of the measurement technique. To these belong the results of regular calibrations of the applied analyzers, their detection limits and those parameters which quantify the dependence of the analyzers' signals from other external factors like the ambient temperature. Our studies showed that the temperature dependence of the applied chemiluminescence NO/NO_2 analyzer can not be neglected (0.08 ppb/K). Hence, constant ambient temperature is definitely necessary to operate the analyzers at the requested level of precision. For our laboratory experiments we solved this problem with a commercial thermostat housing for the analyzers. During field experiments this may be not always feasible. There, we used an air conditioning system for the entire instruments' shelter (container). Since the still remaining fluctuations of temperature were large enough to affect the precision of the NO/NO_2 analyzer, we corrected the analyzer's signals (see Sect. 4.1) It should be stated, that all mentioned previous studies on NO_2 exchange flux densities have even not mentioned this problem.

Laboratory measurements at very low concentrations demand low and stable blended NO_2 concentrations for fumigation of the plants. During our experiments we observed substantial fluctuations of the blended NO_2 concentration which entered the dynamic plant chamber. These fluctuations were due to the blending procedure (and the limited sensitivity of the NO/NO_2 analyzer). As shown in Fig. 6 (blue line), the noise of NO_2 concentrations caused by the blending procedure itself will substantially affect the precision of the NO_2 concentration measurements (and consequently those of NO_2 flux density), particularly if the detection limit of future NO_2analyzers will be improved to be better than 10 nmol m^{-3} (0.25 ppb). Then, the improved precision of the NO_2 concentration measurements will fall short of the noise of the blended NO_2 concentration at the inlet of the dynamic chamber (see Fig. 6) and the improvement of the blending procedure (e.g. by application of more precise flow controllers) will become necessary.

5.3.2 Significance of concentration differences

The error of NO_2 exchange flux density measurements by the dynamic chamber method mainly depends on the error of trace gas concentration differences, Δm_i, between the inlet and the outlet of the dynamic plant chamber. In contrast to laboratory conditions, NO_2 concentrations in the field were relative high and rarely conflicted LOD(m_{NO_2}). However, during field measurements about 30 to 40 % of daytime Δm_{NO_2} data were found to be not significantly different from each other (Table 7) and had to be rejected from further analysis. This rather high percentage of rejected data was mostly due to the temporal variation of ambient NO_2 concentration (m_{a,NO_2}) during the 4 min measurement interval, rather than due to the precision or to LOD(m_{NO_2}). Ambient NO_2

AMTD
4, 5183–5274, 2011

mixing ratio can rapidly change due to the spatially and temporally varying sources within area surrounding the site of measurements (nearby country roads). In our laboratory studies the percentage of non-significant Δm_{NO_2} "daytime" data was 37 % for $m_{a,NO_2} < 44.6\,\mathrm{nmol\,m^{-3}}$ (1 ppb) and vanished for $m_{a,NO_2} \geq 71.4\,\mathrm{nmol\,m^{-3}}$ (1.6 ppb).

In some of the previous studies means or data sets were compared for significant differences by analysis of variance (e.g. Weber and Rennenberg, 1996a, b; Hereid and Monson, 2001; Sparks et al., 2001). However, actual numbers on significant Δm_{NO_2} were not reported. We like to emphasize, that (1) our approach to apply a significance test on the measured concentrations directly is rather novel, and (2) the control of the significance of Δm_{NO_2} is one of the fundamental quality control criteria for highly significant NO_2 exchange flux densities, NO_2 deposition velocities, and above all the detection of highly significant NO_2 compensation point concentrations. When using data without significance control of Δm_{NO_2}, NO_2 compensation point concentrations will be overestimated (see below) and therefore be (highly) significant but not true.

5.3.3 Photo-chemical reactions in the dynamic plant chamber: impact on net exchange flux densities, deposition velocities, and compensation point concentrations

In the previous studies mentioned above, the impact of photo-chemical reactions was for the most part not considered, neither for the calculation of v_{dep,NO_2} nor for that of m_{comp,NO_2}. Not all components of the NO-NO_2-O_3 triad were always measured. Furthermore, most field studies have not used ambient air as purging air. Instead, ambient air was filtered to remove reactive trace gases, particularly O_3 and NO_x. Afterwards, the desired NO_2 concentration was blended (e.g., Geßler et al., 2000). Use of filtered air, free of NO and O_3, allows Reaction (R1) to be neglected, but photolysis of NO_2 (R2) will still occur, as soon as appreciable amounts of $j(NO_2)$ are present in the plant chamber. Consideration of photo-chemical reactions, like the NO_2 loss by Reaction (R2) and the formation of NO_2 by Reaction (R1) were mentioned by Neubert et al. (1993), the production and destruction of NO by Rondón et al. (1993).

With the framework of equations developed in Sects. 2.1 and 2.2, we provide a straightforward tool to examine the impact of photo-chemical reactions on the determination of exchange flux densities, deposition velocities, and compensation point concentrations. While actual $F_{ex,i}$, $v_{dep,i}$, and $m_{comp,i}$ are described by Eqs. (5.1)–5.3), (6.1)–(6.3), and (7.1)–(7.3), the quantities $F^*_{ex,i}$, $v^*_{dep,i}$, and $m^*_{comp,i}$ are given by Eqs. (8.1.1)–(8.1.3), (8.2.1)–(8.2.3), and (8.3.1)–(8.3.3). The latter are the quantities, which would have been observed if no photo-chemical reactions had taken place (e.g. for NO_2 during our laboratory experiments, see Sect. 4.4.1). According to Eqs. (1.4), (8.1.1), (8.2.1), and (8.3.1), the exchange flux densities $F^*_{ex,i}$ are identical to the so-called "chamber flux densities", $F_{cham,i} = -Q/A_{leaf}\,(m_{a,i} - m_{s,i})$.

In previous experiments, where photo-chemical reactions have not been considered, the actual exchange flux densities $F_{ex,i}$ have been substituted by $F_{cham,i}$ alone. During some of the more recent experiments photo-chemical reactions were either (partially) excluded by corresponding set-ups or were taken into consideration by application of the "empty chamber (reference chamber) approach" (Rondón et al., 1993; Geßler et al., 2000, 2001; Hereid and Monson, 2001; Sparks et al., 2001; Raivonen et al., 2009). However, photo-chemical reactions within the latter chamber will be definitely different from those in the dynamic plant chamber, simply for the fact, that neither $j(NO_2)$, nor m_{s,NO_2}, $m_{s,NO}$, or m_{s,O_3} are identical in both chambers. In order to examine potential under/overestimation of simple "chamber flux densities" $F_{cham,i}$, by neglecting NO-NO_2-O_3 gas-phase production and destruction fluxes, we combine the mentioned equations to obtain:

$$F_{ex,NO_2} = F_{cham,NO_2} - \frac{V}{\bar{A}_{leaf}}\left(\bar{k}\,\bar{m}_{s,NO}\bar{m}_{s,O3} - \bar{j}(NO_2)\,\bar{m}_{s,NO_2}\right) \tag{14.1}$$

$$F_{ex,NO} = F_{cham,NO} - \frac{V}{\bar{A}_{leaf}}\left(\bar{j}(NO_2)\,\bar{m}_{s,NO_2} - \bar{k}\,\bar{m}_{s,NO}\bar{m}_{s,O_3}\right) \tag{14.2}$$

AMTD
4, 5183–5274, 2011

The dynamic chamber method

C. Breuninger et al.

$$F_{\mathrm{ex,O_3}} = F_{\mathrm{cham,O_3}} - \frac{V}{\bar{A}_{\mathrm{leaf}}}\left(\bar{j}(\mathrm{NO_2})\bar{m}_{\mathrm{s,NO_2}} - \bar{k}\,\bar{m}_{\mathrm{s,NO}}\bar{m}_{\mathrm{s,O_3}}\right) \tag{14.3}$$

Whether actual exchange flux densities $F_{\mathrm{ex},i}$ are higher, equal or lower than corresponding $F_{\mathrm{cham},i}$ depends whether the difference of the corresponding gas-phase destruction and production fluxes (second term, right hand side of Eqs. (14.1)–(14.3)) is positive, negative and different from zero.

If we differentiate our calculated exchange flux densities $F_{\mathrm{ex},i}$ of the field experiment into the chamber flux densities $F_{\mathrm{cham},i}$ and the gas-phase flux densities $F_{\mathrm{gas},i}$, which comprised the gas-phase production and destruction of NO-NO_2-O_3, we can identify the fraction of $F_{\mathrm{gas},i}$, of each $F_{\mathrm{ex},i}$. For the selected leaf conductance category (see Sect. 4.4.2), the percentage of $F_{\mathrm{gas},i}$ is displayed in Fig. 16 for NO, NO_2 and O_3. The fraction of $F_{gas,O3}$at the exchange flux density of O_3 is very small (±1 %); therefore, it can be neglected. For the NO_2 exchange flux density the fraction of $F_{\mathrm{gas,NO_2}}$ becomes much more important. The median contribution of $F_{\mathrm{gas,NO_2}}$ to $F_{\mathrm{ex,NO_2}}$ was just +8 %, but in particular cases it could be +22 % or −12 %, respectively. Quite clear becomes the impact of the gas-phase reactions for the NO exchange flux density. Here, $F_{\mathrm{gas,NO}}$ amounted +42 % (median value), but ranging from +85 % to −170 %. That means, that under certain conditions $F_{\mathrm{ex,NO}}$ can change its sign, if $F_{\mathrm{gas,NO}}$ will not be considered: the estimated NO emission will convert to a NO deposition (or vice versa).

Similar relations can be developed for deposition velocities $v_{\mathrm{dep},i}$ by combining Eqs. (6.1)–(6.3) with Eqs. (8.2.1)–(8.2.3):

$$v_{\mathrm{dep,NO_2}} = v^{\mathrm{cham}}_{\mathrm{dep,NO_2}} - \frac{V}{\bar{A}_{\mathrm{leaf}}}\bar{j}(\mathrm{NO_2}) \tag{15.1}$$

$$v_{\mathrm{dep,NO}} = v^{\mathrm{cham}}_{\mathrm{dep,NO}} - \frac{V}{\bar{A}_{\mathrm{leaf}}}\bar{k}\,\bar{m}_{\mathrm{s,O_3}} \tag{15.2}$$

$$v_{\mathrm{dep,O_3}} = v^{\mathrm{cham}}_{\mathrm{dep,O_3}} - \frac{V}{\bar{A}_{\mathrm{leaf}}}\bar{k}\,\bar{m}_{\mathrm{s,NO}} \tag{15.3}$$

AMTD
4, 5183–5274, 2011

The dynamic chamber method

C. Breuninger et al.

where the quantities with the superscript "*cham*" are those which be derived from using "chamber flux densities" $F_{\mathrm{cham},i}$ instead of actual exchange flux densities $F_{\mathrm{ex},i}$. The actual deposition velocities $v_{\mathrm{dep},i}$ are in any case lower than $v_{\mathrm{dep},i}^{\mathrm{cham}}$ with the exception $m_{\mathrm{s,O_3}} = 0$, $m_{\mathrm{s,NO}} = 0$, and $j(\mathrm{NO_2}) = 0$ (i.e. during nighttime). To examine how much the gas-phase reactions will affect $v_{\mathrm{dep},i}$, we split our calculated deposition velocity $v_{\mathrm{dep},i}$ for the field data into $v_{\mathrm{dep},i}^{\mathrm{cham}}$ and the complementary part caused by gas-phase reactions. The contribution of photolysis (see Eq. 15.1) to $v_{\mathrm{dep,NO_2}}$ was 80 %, that of Reaction (R1) on $v_{\mathrm{dep,O_3}}$ only 3 %. Corresponding estimates on $v_{\mathrm{dep,NO}}$ were not performed, since NO deposition velocities were not significant during the EGER field experiment. For their experimental conditions, Neubert et al. (1993) identified an error of about 20 % for their $v_{\mathrm{dep,NO_2}}$ determination, if they would neglect photolysis of NO_2. However, our results should be compared to those of previous studies with caution: in most of the previous studies it is not clear whether the photolysis of NO_2 was correctly taken into account. Nevertheless, we tried to estimate the potential impact of NO_2photolysis on these, previously reported $v_{\mathrm{dep,NO_2}}$. For that, the quantities A_{leaf}, V, $j(\mathrm{NO_2})$, and $v_{\mathrm{dep,NO_2}}$ have to be a priori known or they must be derived from other (accompanying) data. Most of the authors have not reported any data of A_{leaf}. So, we estimated the unknown A_{leaf} on the basis of available information about chamber design and our experience concerning the ratio between length of branch and needle area. Moreover, most authors did not specify the used chamber wall material nor its transmissivity for the wavelength range of $j(\mathrm{NO_2})$. Therefore, we estimated the transmissivity on basis of available material information. Thoene et al. (1991, 1996) and Geßler et al. (2002) used borosilicate glass (Schott Glaswerke, Mainz, Germany). Combining the manufacturer's specification (http://www.schott.com/tubing) and our experience with different wall materials (including glass) we estimated the $j(\mathrm{NO_2})$ transmissivity of borosilicate glass to 60 %. For FEP-Teflon film, used by Rondón et al. (1993), we estimated 70 % transmissivity (related to our Teflon film). If NO_2 photolysis would not have been considered at all, Thoene et al., (1991, 1996) and Rondón et al. (1993) would have potentially overestimated their $v_{\mathrm{dep,NO_2}}$ values by 17–81 %, and Geßler et al. (2002) by up to 100 %

(according to Eq. (15.1), depending on prevailing radiation conditions). However, since these authors have applied an empty ("reference") chamber (see Sect. 5.2), the impact on NO_2 photolysis on their reported v_{dep,NO_2} values might be smaller if the underlying assumption is correct that the effect of NO_2 photolysis is identical in the plant and in the empty chamber. The results of field measurements by Sparks et al. (2001) and Hereid and Monson (2001) most likely have not been affected by NO_2 photolysis because they used a leaf chamber system with red light-emitting diodes which produce no appreciable radiation in the wavelength range of $j(NO_2)$.

The corresponding relations for the compensation point concentrations $m_{comp,i}$ are obtained by combining Eqs. (7.1)–(7.3) with (8.3.1)–(8.3.3):

$$m_{comp,NO_2} = m_{comp,NO_2}^{cham} \cdot \frac{1 - b_1 \left[1 + \frac{V}{n_1 \bar{Q}} \bar{k}\, \bar{m}_{s,NO} \bar{m}_{s,O_3} (1 - b_1)\right]}{1 - b_1 \left(1 + \frac{V}{\bar{Q}} \bar{j}(NO_2)\right)} \tag{16.1}$$

$$m_{comp,NO} = m_{comp,NO}^{cham} \cdot \frac{1 - b_2 \left[1 + \frac{V}{n_2 \bar{Q}} \bar{j}(NO_2)\, \bar{m}_{s,NO_2} (1 - b_2)\right]}{1 - b_2 \left(1 + \frac{V}{\bar{Q}} \bar{k}\, \bar{m}_{s,O_3}\right)} \tag{16.2}$$

$$m_{comp,O_3} = m_{comp,O_3}^{cham} \cdot \frac{1 - b_3 \left[1 + \frac{V}{n_3 \bar{Q}} \bar{j}(NO_2)\, \bar{m}_{s,NO_2} (1 - b_3)\right]}{1 - b_3 \left(1 + \frac{V}{\bar{Q}} \bar{k}\, \bar{m}_{s,NO}\right)} \tag{16.3}$$

Here, the value of the fraction (right hand side of Eqs. (16.1)–(16.3)) determines whether the actual compensation point concentrations $m_{comp,i}$ are higher, equal, or lower than $m_{comp,i}^{cham}$.

For our experimental conditions, m_{comp,NO_2} would be overestimated by 10 %, if the gas-phase reactions would not have been considered (i.e. assuming $m_{comp,NO_2} = m_{comp,NO_2}^{cham}$). For the compensation point concentration of O_3 the overestimation would

AMTD
4, 5183–5274, 2011

be only 1 %. The m_{comp,NO_2} values reported in previous studies (Thoene et al., 1991, 1996; Rondón et al., 1993, Geßler et al., 2002) would be overestimated between 3 and 17 %, if the photolysis of NO_2 was not considered.

When the value of the fractions on the right hand side of Eqs. (16.1)–(16.3) are examined for being greater, equal, or lower than unity, the following relations are obtained:

$$m_{comp,NO_2} > (=,<) m^{cham}_{comp,NO_2}, \quad \text{if} \quad m^{cham}_{comp,NO_2} > (=,<) \frac{\bar{k}\,\bar{m}_{s,NO}\bar{m}_{s,O_3}}{\bar{j}(NO_2)} \tag{17.1}$$

$$m_{comp,NO} > (=,<) m^{cham}_{comp,NO}, \quad \text{if} \quad m^{cham}_{comp,NO} > (=,<) \frac{\bar{j}(NO_2)\,\bar{m}_{s,NO_2}}{\bar{k}\bar{m}_{s,O3}} \tag{17.2}$$

$$m_{comp,O_3} > (=,<) m^{cham}_{comp,O_3}, \quad \text{if} \quad m^{cham}_{comp,O_3} > (=,<) \frac{\bar{j}(NO_2)\,\bar{m}_{s,NO_2}}{\bar{k}\,\bar{m}_{s,NO}} \tag{17.3}$$

The relevance of these relations consists in their potential for simply checking, whether or not the correct evaluation of compensation point concentrations has to consider photo-chemical reactions. Having evaluated measured concentrations $m_{a,i}$ and $m_{s,i}$ by bi-variate weighted linear regression (which delivers n_i and b_i), the quantities $m^{cham}_{comp,i}$ are determined. Using the simultaneously measured averages of k, $j(NO_2)$, m_{s,NO_2}, $m_{s,NO}$, and m_{s,O_3}, the right hand fractions of relations Eqs. (17.1)–(17.3) can be calculated, which provide the necessary quantities to test whether or not $m^{cham}_{comp,i}$ have to be corrected for photo-chemical reactions in the dynamic plant chamber (by Eqs. (16.1)–(16.3)).

5.4 Bi-variate weighted linear regression

The determination of deposition velocities $v_{dep,i}$, as well as compensation point concentrations $m_{comp,i}$ is based on linear regression of the measured concentration of trace gas i in ambient air and within the dynamic plant chamber. Therefore, it was necessary to consider errors of both variables in the determination of $v_{dep,i}$ and $m_{comp,i}$. For our laboratory results (see Sect. 4.4.1) we have shown the effect of applying simple linear regression (no errors considered at all), linear regression (y-errors considered), and bi-variate weighted linear regression (y- and x-errors considered) on the significance of derived v_{dep,NO_2} and m_{comp,NO_2} data (see Table 6). Generally speaking, applying a simple linear least-square fitting algorithm, the probability of $m_{comp,i} \neq 0$ can be highly significant, while applying the bi-variate weighted linear least-square fitting algorithm the probability for the existence of $m_{comp,i}$ could easily become "likely" or even "unlikely". In a few cases previous authors have applied the bi-variate algorithm (e.g. Geßler et al., 2000, 2002). Finally, it should be stated that in all previous studies values of v_{dep,NO_2} and m_{comp,NO_2} have been derived from linear relationships between F_{ex,NO_2} and m_{s,NO_2} which is mathematically not correct, since the dependent variable F_{ex,NO_2} contains the independent variable m_{s,NO_2} (see Sect. 2.1).

6 Conclusions

In this paper we presented a dynamic chamber system for surface exchange flux measurements of reactive and non-reactive trace gases on plants under field and laboratory conditions. We conclude our findings as follows:

1. One of the most important characteristics of our dynamic chamber system is the minimal disturbance of plant physiology and growth. Changes in concentrations of relevant trace gases should be small in order to be comparable to the outer environment. Furthermore, small changes prevent enclosure induced artifacts on plant metabolism and stomata regulation. Reliable investigations should not only focus on a few interesting trace gases but always include CO_2 and water vapor exchange because of plant physiological feedback regulations.

2. According to our "blank" measurements, the wall material of our plant chamber

AMTD
4, 5183–5274, 2011

can be considered as chemically inert. We emphasize, that mass fluxes to the walls of the chamber can basically not be neglected and must be considered in the mass flux balance of the dynamic plant chamber, if there are any appreciable effects of ad- or desorption.

3. The performance of the dynamic chamber system must be controlled and, if necessary, suitable parameterized correction algorithms applied to maintain/improve the precision of NO_2 concentration and exchange flux density measurements. The sensitivity of the NO/NO_2 analyzer to changes in ambient temperature is one of these key parameters. The drift in our analyzer was 0.07 ppb/K (NO) and 0.08 ppb/K (NO_2). The precision of the NO_2 exchange flux densities is almost entirely determined by the precision of the NO_2 concentration measurements, which in turn depends on the sensitivity (limit of detection) of the NO_2 analyzer. At best a flux density precision of ≤10 % may be reached, as long as NO_2 concentrations in the plant chamber differ by 0.1 ppb from the expected NO_2 compensation point concentration.

4. Determination of NO_2 concentrations at sub-ppb level and of NO_2 exchange flux densities at the thousandths (hundredths) of nmol m^{-2} s^{-1} level definitely require (a) a NO_2 specific converter (photolytic converter) and (b) a highly sensitive NO/NO_2 analyzer (lower detection limit (3σ) of at least 13 nmol m^{-3} (0.3 ppb), preferably 4.5 nmol m^{-3} (0.1 ppb)).

5. The significance of concentration differences Δm_i (between trace gas concentrations measured at the inlet and the outlet of the dynamic chamber) is the fundamental quality criterion for the determination of high quality exchange flux densities and deposition velocities, but particularly for the detection of (highly) significant compensation point concentrations. Especially under field measurements, the percentage of non-significant Δm_i can be rather high due to the temporal variation of ambient concentrations during the measurement interval.

6. Laboratory measurements for the identification of NO_2 compensation point concentrations under controlled conditions require low, reproducible, and verifiable NO_2 concentration for NO_2 fumigation experiments. The precision of corresponding NO_2 concentration measurements is not only limited by the noise of the NO/NO_2 analyzer, but also by the noise of the NO_2 blending procedure. Application of future NO/NO_2 analyzers (lower detection limit $(3\sigma) <$ 2.2 nmol m^{-3} (<0.05 ppb) will be useless, unless the uncertainty of the NO_2 blending for fumigation experiments is improved significantly.

7. Photo-chemical reactions in the dynamic plant chamber's volume must be considered (or be excluded by corresponding set-ups). Otherwise, particularly the exchange of the NO-NO_2-O_3 triad with the plants could be seriously over- or underestimated. This is particularly important for the determination of the NO_2 deposition velocity. Under our experimental conditions in the field, the overestimation of the NO_2 deposition velocity had reached about 80 % if photolysis of NO_2 has been neglected. Excluding the chemical reaction of NO with O_3 by corresponding experimental design (e.g. using NO and O_3 free purging air), effects of NO_2 photolysis would still be present, as long as there is appreciable illumination of the plants. This is unavoidable because for plant physiological studies the presence of photosynthetically active radiation is essential. The only way out would be to use a chamber wall material where the transmissivity for PAR is high, and in the wavelength range of $j(NO_2)$ negligible. For laboratory studies, the application of light-emitting diodes which do not emit in the wavelength range of $j(NO_2)$ is promising.

8. Use of an empty ("reference") chamber for considering (compensating) photochemical reactions implies that NO_2-photolysis, and the concentrations of NO_2, NO, and O_3 in the empty and in the plant chambers are identical; however, this is not the case.

AMTD
4, 5183–5274, 2011

9. In a mathematical stricter sense, deposition velocities and compensation point concentrations should be derived from linear relationships between the originally measured quantities, namely the NO, NO_2, and O_3 concentrations at the inlet and the outlet of the dynamic chamber. A straight-forward and thorough statistical treatment of measured data will result in high-quality and reliable data of exchange flux densities, deposition velocities, and compensation point concentrations, if solid characterization and quantification of trace gas concentration errors as well as errors of all other quantities (necessary for calculation of the exchange flux densities) is achieved and general Gaussian error propagation as well as bi-variate weighted linear least-squares fitting regression analysis is applied.

10. It is recommended, that results from previous studies on NO_2 exchange flux densities, NO_2 deposition velocities, and NO_2 compensation point concentrations which have been obtained by dynamic plant chambers should be handled with care owing to neglecting (at least) the effects of NO_2 photolysis in the plant chamber's volume and insufficient characterization of the specifity and precision of the NO_2 analyzers. A re-evaluation would be helpful.

Appendix A

Mass balance of the NO-NO_2-O_3 triad of a dynamic plant chamber

Considering the molar mass flux of the trace gas i (i = NO_2, NO, O_3), i.e. the derivative of molar mass M_i with respect to time ($\partial M_i/\partial t = \Phi_i$ in nmol s^{-1}), the individual flux components of the dynamic plant chamber system are defined as follows:

- $\Phi_{\text{in},i}$ = molar mass flux of trace gas i entering the plant chamber
- $\Phi_{\text{out},i}$ = molar mass flux of trace gas i leaving the plant chamber

AMTD
4, 5183–5274, 2011

- $\Phi_{\mathrm{wall},i}$ = molar mass flux of trace gas i to the inner wall of the plant chamber (due to ad-/absorption of trace gas i)
- $\Phi_{\mathrm{em},i}$ = molar mass flux of trace gas i caused by (biogenic) emission from the leaves
- $\Phi_{\mathrm{dep},i}$ = molar mass flux of trace gas i caused by uptake to the leaves (e.g. cuticular, stomatal, and/or mesophyllic uptake)
- $\Phi_{\mathrm{prod},i}$ = molar mass flux of trace gas i into the plant chamber's volume caused by gas phase production, i.e. from photochemical decay or fast chemical reaction of other trace gas(es)
- $\Phi_{\mathrm{dest},i}$ = molar mass flux of trace gas i out of the plant chamber's volume caused by gas-phase destruction, i.e. by photochemical decay of trace gas i or by fast chemical reaction with other trace gas(es).

Under steady-state conditions (i.e. concentrations of trace gas i are constant (have reached equilibrium)) and considering the convention, that mass fluxes into (out) of the plant chamber's volume are counted positive (negative), the molar mass flux balance of the trace gas i is given by

$$+\Phi_{\mathrm{in},i} - \Phi_{\mathrm{out},i} - \Phi_{\mathrm{wall},i} + \Phi_{\mathrm{em},i} - \Phi_{\mathrm{dep},i} + \Phi_{\mathrm{prod},i} - \Phi_{\mathrm{dest},i} = 0 \tag{A1}$$

While the first three and the last two left-hand terms of Eq. (A1) may be known and/or are determined by laboratory or in-situ measurements, $\Phi_{\mathrm{em},i}$ and $\Phi_{\mathrm{dep},i}$ are the unknown fluxes of trace gas i. We combine these two fluxes to the bi-directional "exchange flux" $\Phi_{\mathrm{ex},i}$

$$\Phi_{\mathrm{ex},i} = +\Phi_{\mathrm{em},i} - \Phi_{\mathrm{dep},i} \qquad i = \mathrm{NO_2, NO, O_3} \tag{A2}$$

Considering the purging rate Q ($\mathrm{m^3\,s^{-1}}$) and the molar concentration $m_{\mathrm{a},i}$ ($\mathrm{nmol\,m^{-3}}$) of trace gas i in ambient air, the ingoing flux is

$$\Phi_{\mathrm{in},i} = Q \cdot m_{a,i} \qquad i = \mathrm{NO_2, NO, O_3} \tag{A3}$$

AMTD
4, 5183–5274, 2011

The molar concentration at the outlet of the plant chamber is equivalent to the molar concentration within the plant chamber ($m_{s,i}$ in nmol m^{-3}), provided the plant chamber's volume is well mixed by one (or more) appropriate fan(s) (see Meixner et al., 1997; Pape et al., 2009). Then, the flux leaving the chamber is defined by

$$\Phi_{\text{out},i} = Q \cdot m_{s,i} \qquad i = NO_2, NO, O_3 \tag{A4}$$

The flux to the inner walls can be easily determined by corresponding laboratory experiments (e.g. Ludwig, 1994; Meixner et al., 1997). If the material of the plant chamber is consisting of chemically inert material, the flux $\Phi_{\text{wall},i}$ can usually be neglected. In case of the NO-NO_2-O_3 triad, the relevant photochemical reactions controlling the gas-phase production and destruction of the respective trace gas are

$$NO + O_3 = NO_2 + O_2, \qquad k_{R1} = k = 1.4 \times 10^{-12} \times e^{(-1310/T)} \tag{R1}$$

$$NO_2 + h\nu = NO + O, \qquad k_{R2} = j(NO_2), \qquad \lambda \le 420\,\text{nm} \tag{R2}$$

Applying simple reaction kinetics, the corresponding fluxes $\Phi_{\text{prod},i}$ and $\Phi_{\text{dest},i}$ are given by

$$\Phi_{\text{prod},NO_2} = \Phi_{\text{dest},NO} = \Phi_{\text{dest},O_3} = V \cdot k \cdot m_{s,NO} \cdot m_{s,O_3} \tag{A5}$$

and

$$\Phi_{\text{dest},NO_2} = \Phi_{\text{prod},NO} = \Phi_{\text{prod},O_3} = V \cdot j(NO_2) \cdot m_{s,NO_2} \tag{A6}$$

Where V is the plant chamber's volume (m^3), k is the (temperature-dependent) reaction coefficient of the NO + O_3 reaction (m^3 nmol^{-1} s^{-1}) (Atkinson et al., 2004), and $j(NO_2)$ (s^{-1}) is the photolysis rate of Reaction (R2), which can be measured in-situ (or parameterized from data of global radiation; see Trebs et al., 2009).

Considering Eqs. (A1)–(A6), the molar mass flux balances of the trace gas triad NO-NO_2-O_3 (under steady state conditions) can be formulated as follows:

$$\Phi_{\text{ex},NO_2} = Q \cdot m_{s,NO_2} - Q \cdot m_{a,NO_2} - V \cdot k \cdot m_{s,NO} \cdot m_{s,O_3} + V \cdot j(NO_2) \cdot m_{s,NO_2} \tag{A7.1}$$

AMTD
4, 5183–5274, 2011

$$\Phi_{ex,NO} = Q \cdot m_{s,NO} - Q \cdot m_{a,NO} + V \cdot k \cdot m_{s,NO} \cdot m_{s,O_3} - V \cdot j(NO_2) \cdot m_{s,NO_2} \quad (A7.2)$$

$$\Phi_{ex,O_3} = Q \cdot m_{s,O_3} - Q \cdot m_{a,O_3} + V \cdot k \cdot m_{s,NO} \cdot m_{s,O_3} - V \cdot j(NO_2) \cdot m_{s,NO_2} \quad (A7.3)$$

Equations (A7.1)–(A7.3) explicitly define the molar mass fluxes (in nmol s^{-1}) of the NO_2, NO, and O_3 surface exchange between the plant chamber's atmosphere and the enclosed leaves in terms of measured and/or a priori known quantities only.

Appendix B

Bi-variate weighted linear least-squares fitting regression analysis

Field data of concentrations in particular, have usually not all the same uncertainty. All kinds of linear least square fitting methods (considering errors in y and x) account for the fact, that data with the least uncertainty should have the greatest influence on the intercept n and the slope b of the fitted line. This is achieved by weighting each of the data points ($m_{a,i}$, $m_{s,i}$) with a factor ω_i, which is usually set to the inverse of the square of standard errors (standard deviations) of x and y-values (here: $s^{-2}_{ma,i}$ and $s^{-2}_{ms,i}$).

York et al. (2004) have provided a very detailed description of the bi-variate weighted linear least-squares fitting method. Here, only those equations are presented which are necessary to calculate the intersect n and the slope b of the best straight line (and related standard errors, s_n and s_b). For the sake of comparability with York et al. (2004), we set $m_{a,i} = X_i$ and $m_{s,i} = Y_i$, $s^{-2}_{ma,i} = \omega X_i$, and $s^{-2}_{ms,i} = \omega Y_i$. The method of York et al. (2004) to calculate the intercept n (s_n) and the slope b (s_b) comprises the following set of four equations:

$$n = \bar{Y} - b\bar{X}; \qquad i = 1, 2, \ldots, N \quad (B1.1)$$

$$b = \frac{\sum W_i \beta_i (Y_i - \bar{Y})}{\sum W_i (X_i - \bar{X})} \quad (B1.2)$$

AMTD
4, 5183–5274, 2011

The dynamic chamber method

C. Breuninger et al.

$$s_n^2 = \frac{1}{\sum W_i} + \bar{x}^2 s_b^2 \quad \text{(B1.3)}$$

$$s_b^2 = \frac{1}{\sum W_i (x_i - \bar{x})_i^2} \quad \text{(B1.4)}$$

where,

$$x_i = \bar{X} + \beta_i; \quad y_i = \bar{Y} + \beta_i;$$

$$\bar{X} = \frac{\sum W_i X_i}{W_i}; \quad \bar{Y} = \frac{\sum W_i Y_i}{W_i}; \quad \bar{x} = \frac{\sum W_i x_i}{W_i}; \quad \bar{y} = \frac{\sum W_i y_i}{W_i}$$

$$W_i = \frac{\omega(X_i)\,\omega(Y_i)}{\omega(X_i) + b^2 \omega(Y_i)}; \quad \omega(X_i) = s_{X,i}^{-2}; \quad \omega(Y_i) = s_{Y,i}^{-2}$$

$$\beta_i = W_i \left(\frac{X_i - \bar{X}}{\omega(Y_i)} + \frac{b\,(Y_i - \bar{Y})}{\omega(X_i)} \right); \quad \text{(B1.5)}$$

The original set of equations presented by York et al. (2004) contain additional terms in the equations for W_i and β_i for consideration of potential correlations between $s_{X,i}$ and $s_{Y,i}$, which are set to zero here (i.e. $s_{\mathrm{ma},i}$ and $s_{\mathrm{ms},i}$ are assumed to be uncorrelated). Since the equation for the slope b (Eq. B1.2) contains the variables W_i and β_i, which are in turn functions of b (see Eq. (B1.5)), Eq. (B1.2) has to be solved iteratively.

Appendix C

Calculation of standard errors of $F_{\mathrm{ex},i}$, $v_{\mathrm{dep},i}$, and $m_{\mathrm{comp},i}$

Standard errors of $F_{\mathrm{ex},i}$, $v_{\mathrm{dep},i}$, and $m_{\mathrm{comp},i}$ have been calculated by application of the general Gaussian error propagation according to Eq. (11). During field experiments,

AMTD
4, 5183–5274, 2011

all $m_{a,i}$ and $m_{s,i}$ of the NO-NO_2-O_3 triad have been measured in cycles of 4 minutes. During this time period, it has been shown, that the error of the purging rate Q is negligible. The volume V of the chambers is a-priori known, its error is considered to be zero. Standard errors of $m_{a,i}$ and $m_{s,i}$ are known for each data pair of measurements. Averages and standard errors of A_{leaf}, $j(NO_2)$, k and conjugated concentrations $m_{s,j}$ ($j \neq i$) have to be calculated individually from each data set which is used for the determination of $F_{ex,i}$, $v_{dep,i}$, and $m_{comp,i}$.

Therefore, according to Eq. (1.1), the mass exchange flux density F_{exNO_2} is a function of 7 error-prone variables, namely $x_1 = m_{a,NO_2}$, $x_2 = m_{s,NO_2}$, $x_3 = j(NO_2)$, $x_4 = k$, $x_5 = m_{s,NO}$, $x_6 = m_{s,O_3}$, and $x_7 = A_{leaf}$. Analogously to F_{ex,NO_2}, the 7 variables for $F_{ex,NO}$ (F_{ex,O_3}) in Eq. (1.2) (Eq. 1.3) are $x_1 = m_{a,NO}$ (m_{a,O_3}), $x_2 = m_{s,NO}(m_{s,O_3})$, $x_3 = j(NO_2)$, $x_4 = k$, $x_5 = m_{s,NO_2}$, $x_6 = m_{s,O_3}(m_{s,NO})$, and $x_7 = A_{leaf}$. Considering Eq. (6.1), the deposition velocity v_{dep,NO_2} is a function of 3 error-prone variables, $x_1 = m_1$, $x_2 = j(NO_2)$, and $x_3 = A_{leaf}$, while the deposition velocity $v_{dep,NO}$ (v_{dep,O_3}) depends on 4 error-prone variables, namely $x_1 = b_2$ (b_3), $x_2 = k$, $x_3 = m_{s,O_3}$ ($m_{s,NO}$), and $x_4 = A_{leaf}$. The compensation point concentrations m_{comp,NO_2} ($m_{comp,NO}$,m_{comp,O_3}) are each functions of 6 error-prone variables (see Eqs. (7.1)–(7.3)). These are $x_1 = n_1$ (n_2, n_3), $x_2 = b_1$ (b_2, b_3), $x_3 = j(NO_2)$, $x_4 = k$, $x_5 = m_{s,NO}$ (m_{s,NO_2}, m_{s,NO_2}), and $x_6 = m_{s,O_3}$ (m_{s,O_3}, $m_{s,NO}$). Bi-variate weighted linear least-squares fitting regression analysis of measured $m_{s,i}$ versus $m_{a,i}$ (which considers both, $s_{ma,i}$ and $s_{ms,i}$) delivers the quantities n_1, n_2, n_3 and b_1, b_2, b_3 as well as their standard errors s_{n1}, s_{n2}, s_{n3}, and s_{b1}, s_{b2}, s_{b3}. To calculate the standard errors s_{Fex,NO_2}, $s_{Fex,NO}$, s_{Fex,O_3}, s_{v,dep_NO_2}, s_{v,dep_NO}, s_{v,dep_O_3}, $s_{m,comp\_NO_2}$, $s_{m,comp\_NO}$, and $s_{m,comp\_O_3}$ by application of the general Gaussian error propagation (Eq. (11)), one have to calculate all the derivatives of $y_i = F_{ex,i}$, $y_i = v_{dep,i}$, and $y_i = m_{comp,i}$, ($i = NO_2$, NO, O_3) with respect to the corresponding variables x_1, x_2, $\ldots$, x_n mentioned above.

AMTD
4, 5183–5274, 2011

The dynamic chamber method

C. Breuninger et al.

Appendix D

List of symbols and abbreviations

A_{leaf}	leaf area	m^2
b_i	slope of regression analysis of gas i	$nmol\,m^{-3}$
$F_{ex,i}$	exchange flux density of gas i	$nmol\,m^{-2}\,s^{-1}$
$j(NO_2)$	photolysis rate of NO_2 ($\lambda \leq 420\,nm$)	s^{-1}
k	rate constant for chemical reactions	$cm^3\,molecule^{-1}\,s^{-1}$
$m_{a,i}$	molar concentration in ambient air of gas i	$nmol\,m^{-3}$, ppb
$m_{s,i}$	molar concentration within plant chamber of gas i	$nmol\,m^{-3}$, ppb
$m_{comp,i}$	compensation point concentration of gas i	$nmol\,m^{-3}$ or ppb
M_i	molar mass of gas i	$nmol\,s^{-1}$
n_i	intercept of regression analysis of gas i	$nmol\,m^{-3}$
N	number of samples	–
PAR	Photosynthetically Active Radiation	$\mu mol\,m^{-2}\,s^{-1}$
Q	purging rate	$m^3\,s^{-1}$
R^2	regression coefficient	–
s	standard error	
s	standard error	
σ	standard deviation	
T	temperature	°C or K
τ	characteristic time scale	s
V	chamber volume	m^3
$v_{dep,i}$	deposition velocity of gas i	$m\,s^{-1}$

The service charges for this open access publication have been covered by the Max Planck Society.

AMTD
4, 5183–5274, 2011

Acknowledgements. The authors gratefully acknowledge financial support by the German Research Foundation (DFG project EGER, ME 2100/4-1) and the Max Planck Society. We also thank the University of Bayreuth for fruitful cooperation. The nutrient content of the needles were analyzed through Bayreuth Center of Ecology and Environmental Research (BayCEER). We are grateful to Michael Welling and Eva Falge for help and support during the EGER experiment and Eva Falge also for many helpful discussions concerning the statistical treatment of our data. We thank Terry Dillon for improving the language of this paper.

References

Alsheimer, M.: Charakterisierung räumlicher und zeitlicher Heterogenität der Transpiration unterschiedlicher montaner Fichtenbestände durch Xylemflussmessungen, Bayreuther Forum Ökologie, 49, 1–143, 1997.

Atkinson, R., Baulch, D. L., Cox, R. A., Crowley, J. N., Hampson, R. F., Hynes, R. G., Jenkin, M. E., Rossi, M. J., and Troe, J.: Evaluated kinetic and photochemical data for atmospheric chemistry: Volume I – gas phase reactions of O_x, HO_x, NO_x and SO_x species, Atmos. Chem. Phys., 4, 1461–1738, doi:10.5194/acp-4-1461-2004, 2004.

Beier, N. and Schneewind, R.: Chemical reactions of gases in tubes of probing systems and their influence on measured concentrations, Ann. Geophysicae, 9, 703–707, 1991.

Cantrell, C. A.: Technical Note: Review of methods for linear least-squares fitting of data and application to atmospheric chemistry problems, Atmos. Chem. Phys., 8, 5477–5487, doi:10.5194/acp-8-5477-2008, 2008.

Chaparro-Suarez I. G., Meixner, F. X., and Kesselmeier, J.: Nitrogen dioxide (NO_2) uptake by vegetation controlled by atmospheric concentrations and plant stomatal aperture, Atmos. Environ., in press, doi:10.1016/j.atmosenv.2011.07.021, 2011.

Conrad, R.: Compensation concentration as critical variable for regulating the flux of trace gases between soil and atmosphere, Biogeochemistry, 27, 155–170, 1994.

Cox, R. A., Jones, B. M. J., Penkett, S. A., and Sheppard, D. A.: Mechanism of photochemical and free radial oxidation of sulfur compounds in the gas phase, paper presented at the 5th International Conference of the Commission on Atmospheric Chemistry and Global Pollution, Oxford, England, Aug 28 to Sept 3, 1983.

Crutzen, P. J.: The role of NO and NO_2 in the chemistry of the troposphere and stratosphere, Annu. Rev. Earth Pl. Sc., 7, 443–472, 1979.
Drummond, J. W., Castledine, C., Green, J., Denno, R., Mackay, G. I., and Schiff, H. I.: New technologies for use in acid deposition networks. In Monitoring Methods for Toxics in the Atmosphere. ASTM Special Technical Publication No. 1052, Philadelphia, 1989.
Fehsenfeld, F. C., Dickerson, R. R., Hübler, G., Luke, W. T., Nunnermacker, L. J., Williams, E. J., Roberts, J. M., Calvert, J. G., Curran, C. M., Delany, A. C., Eubank, C. S., Fahey, D. W., Fried, A., Gandrud, B.W., Langford, A. O., Murphy, P. C., Norton, R. B., Pickering, K. E., and Ridley, B. A.: A Ground-Based Intercomparison of NO, NO_x and NO_y Measurement Techniques, J. Geophys. Res., 92(D12), 14710–14722, 1987.
Fehsenfeld, F. C., Drummond, J. W., Roychowdhury, U. K., Galvin, P. J., Williams, E. J., Buhr, M. P., Parrish, D. D., Hübler, G., Langford, A. O., Calvert, J. G., Ridley, B. A., Grahek, F., Heikes, B. G., Kok, G. L., Shetter, J. D., Walega, J. G., Elsworth, C. M., Norton, R. B., Fahey, D. W., Murphy, P. C., Hovermale, C., Mohnen, V. A., Demerjian, K. L., Mackay, G. I., and Schiff, H. I.: Intercomparison of NO_2 measurement techniques, J. Geophys. Res., 95, 3579–3597, 1990.
Gehrig, R. and Baumann, R.: Comparison of 4 different types of commercially available monitors for nitrogen oxides with test gas mixtures of NH_3, HNO_3, PAN and VOC and in ambient air, paper presented at EMEP Workshop on Measurements of Nitrogen-Containing Compounds, EMEP/CCC Report 1/93, Les Diablerets, Switzerland, 1993.
Geßler, A., Rienks, M., and Rennenberg, H.: NH_3 and NO_2 fluxes between beech trees and the atmosphere - correlation with climatic and physiological parameters, New Phytol, 147, 539–560, 2000.
Geßler, A., Rienks, M., and Rennenberg, H.: Stomatal uptake and cuticular adsorption contribute to dry deposition of NH_3 and NO_2 to needles of adult spruce (Picea abies) trees, New Phytol 156, 179–194, 2002.
Grosjean, D. and Harrison, J.: Response of chemiluminescence NO_x analyzers and ultraviolet ozone analyzers to organic air pollutants, Environ. Sci. Technol., 19, 862–865, 1985.
Gut, A., Scheibe, M., Rottenberger, S., Rummel, U., Welling, M., Ammann, C., Kirkman, G. A., Kuhn, U., Meixner, F. X., Kesselmeier, J., Lehmann, B. E., Schmidt, W., Müller, E., and Piedade, M. T. F.: Exchange fluxes of NO_2 and O_3 at soil and leaf surfaces in an Amazonian rain forest, J. Geophys. Res., 107(D20), 8060, doi:10.1029/2001JD000654, 2002.
Hanson, P. J., Rott, K., Taylor Jr., G. E., Gunderson, C. A., Lindberg, S. E., and Ross-Todd, B.

M.: NO_2 deposition to elements representative of a forest landscape, Atmos. Environ., 23(8), 1783–1794, 1989.
Hereid, D. P. and Monson, R. K.: Nitrogen oxide fluxes between corn (Zea mays L.) leaves and the atmosphere, Atmos. Environ., 35, 975–983, 2001.
Hicks, B. B., Baldocchi, D. D., Meyers, T. P., Hosker, R. P., and Matt, D. R.: A preliminary multiple resistance routine for deriving dry deposition velocities from measured quantities, Water Air. Soil. Poll., 36, 311–330, 1987.
Hosaynali Beygi, Z., Fischer, H., Harder, H. D., Martinez, M., Sander, R., Williams, J., Brookes, D. M., Monks, P. S., and Lelieveld, J.: Oxidation photochemistry in the Southern Atlantic boundary layer: Unexpected deviations of photochemical steady state, Atmos. Chem. Phys. Discuss., 11, 7045–7093, doi:10.5194/acpd-11-7045-2011, 2011.
Jacob, D. J. and Wofsy, S. C.: Budgets of Reactive Nitrogen, Hydrocarbons, and Ozone over the Amazon Forest during the Wet Season, J. Geophys. Res., 95(D10), 16737–16754, 1990.
Kelly, T. J., Stedman, D. H., Ritter, J. A., and Harvey, R. B.: Measurements of Oxides of Nitrogen and Nitric Acid in Clean Air, J. Geophys. Res., 85, C12, 7417–7425, 1980.
Kelly, T. J., Spicer, C. W., and Ward, G. F.: An assessment of the luminol chemiluminescence technique for measurement of NO_2 in ambient air, Atmos. Environ., 24A, 2397–2403, 1990.
Kesselmeier, J., Meixner, F. X., Hofmann, U., Ajavon, A., Leimbach, S., and Andreae, M. O.: Reduced sulfur compound exchange between the atmosphere and tropical tree species in southern Cameroon, Biogeochemistry, 23, 23–45, 1993.
Kesselmeier, J., Schäfer, L., Ciccioli, P., Branceleoni, E., Cecinato, A., Frattoni, M., Foster, P., Jacob, V., Denis, J., Fugit, J. L., Dutaur, L., and Torres, L.: Emission of monoterpenes and isoprene from a Mediterranean oak species Quercus ilex L. measured within the BEMA (Biogenic Emissions in the Mediterranean Area) project, Atmos. Environ., 30, 1841–1850, 1996.
Kesselmeier, J., Bode, K., Hofmann, U., Mueller, H., Schaefer, L., Wolf, A., Ciccioli, P., Brancaleoni, E., Cecinato, A., Frattoni, M., Foster, P., Ferrari, C., Jacob, V., Fugit, J. L., Dutaur, L., Simon, V., and Torres, L.: Emission of short chained organic acids, aldehydes and monoterpenes from Quercus ilex L. and Pinus pinea L. in relation to physiological activities, carbon budget and emission algorithms, Atmos. Environ., 31(SI), 119–134, 1997.
Kesselmeier, J., Bode, K., Gerlach, C., and Jork, E. M.: Exchange of atmospheric formic and acetic acids with trees and crop plants under controlled chamber and purified air conditions, Atmos. Environ., 32, 1765–1775, 1998.

AMTD
4, 5183–5274, 2011

Kuhn, U., Wolf, A., Gries, C., Nash, T. H., and Kesselmeier, J.: Field measurements on the exchange of carbonyl sulfide between lichens and the atmosphere, Atmos. Environ., 34, 4867–4878, 2000.
Kuhn, U., Rottenberger, S., Biesenthal, T., Wolf, A., Schebeske, G., Ciccioli, P., Brancaleoni, E., Frattoni, M., Tavares, T. M., and Kesselmeier, J.: Isoprene and monoterpene emissions of Amazonian tree species during the wet season: Direct and indirect investigations on controlling environmental functions, J. Geophys. Res., 107(D20), 8071, doi:10.1029/2001JD000978, 2002.
Kurtenbach, R., Becker, K. H., Gomes, J. A. G., Kleffmann, J., Lörzer, J. C., Sittler, M., Wiesen, P., Ackermann, R., Geyer, A., and Platt, U.: Investigations of emissions and heterogeneous formation of HONO in a road traffic tunnel, Atmos. Environ., 35, 3385–3394, 2001.
Lerdau, M. T., Munger, J. W., and Jacob, D. J.: The NO_2 Flux Conundrum, Science, 289(5488), 2291–2293, 2000.
Ludwig, J.: Untersuchungen zum Austausch von NO und NO_2 zwischen Atmosphäre und Biosphäre, PhD Thesis, University of Bayreuth, Bayreuth, Germany, 251 pp., 1994.
MacDougall, D. and Crummett, W. B.: Guidelines for Data Acquisition and Data Quality Evaluation in environmental chemistry, Anal. Chem., 52, 2242–2249, doi:10.1021/ac5064a004, 1980.
Matthews, R. D., Sawyer R. F., and Schefer R. W. Interferences in Chemiluminescent Measurement of NO and NO_2 Emissions from Combustion Systems, Environ. Sci. Technol., 11, 1092–1096, 1977.
Maeda, Y. K., Aoki, K., and Munemori, M.: Chemiluminescence method for the determination of nitrogen dioxide, Anal. Chem., 52, 307–311, 1980.
Meixner, F. X.: Surface exchange of odd nitrogen oxides, Nova Acta Leopoldina NF 70, Nr. 288, 299–348, 1994.
Meixner, F. X., Fickinger, Th., Marufu, L., Serca, D., Nathaus, F. J., Makina, E., Mukurumbira, L., and Andreae, M. O.: Preliminary results on nitric oxide emission from a southern African savanna ecosystem, Nutrient Cycling in Agroecosystems, 48, 123–138, 1997.
Neubert, A., Kley, D., and Wildt, J.: Uptake of NO, NO_2 and O_3 by sunflower (Helianthus annuus L.) and Tobacco plants (Nicotiana tabacum L.): dependence on stomatal conductivity, Atmos. Environ., 27A(14), 2137–2145, 1993.
Pape, L., Ammann, C., Nyfeler-Brunner, A., Spirig, C., Hens, K., and Meixner, F. X.: An automated dynamic chamber system for surface exchange measurement of non-reactive and

reactive trace gases of grassland ecosystems, Biogeosciences, 6, 405–429, doi:10.5194/bg-6-405-2009, 2009.
Phillips, N., Bond, B. J., McDowell, N. G., and Ryan, M. G.: Canopy and hydraulic conductance in young, mature and old Douglas-fir trees, Tree Physiol., 22, 205–211, 2002.
Plake, D.: Vertikale Konzentrationsprofile und Flüsse von reaktiven und nicht reaktiven Spurengasen im Fichtelgebirge, Diplomarbeit Thesis, Universität Münster, Münster, Germany, 144 pp., 2009.
Raivonen, M., Vesala, T., Pirjola, L., Altimir, N., Keronen, P., Kulmala, M., and Hari, P.: Compensation point of NO_x exchange: Net result of NO_x consumption and production, Agr. Forest Meteorol., 149, 1073–1081, 2009
Rennenberg, H., Kreutzer, K., Papen, H., and Weber, P.: Consequences of high loads of nitrogen for spruce (Picea abies L.) and beech (Fagus sylvatica L.) forests, New Phytol., 139, 71–86, 1998.
Ridley, B. A., Carroll, M. A., Torres, A. L., Condon, E. P., Sachse, G. W., Hill, G. F., and Gregory, G. L.: An intercomparison of results from ferrous sulphate and photolytic converter techniques for measurements of NO_x made during the NASA GTE/CITE 1 aircraft program, J. Geophys. Res., 93(D12), 15803–15811, 1988.
Riederer, M., Kurbasik, K., Steinbrecher, R., and Voss, A.: Surface areas, lengths and volumes of Picea abies (L.) Karst. Needles: determination, biological variability and effect of environmental factors, Trees 2, 165–172, 1988.
Rondón, A. and Granat, L.: Studies on the dry deposition of NO_2 to coniferous species at low NO_2 concentrations, Tellus, 46B, 339–352, 1994.
Rondón, A., Johansson, C., and Granat, L.: Dry deposition of nitrogen dioxide and ozone to coniferous forest, J. Geophys. Res., 98, 5159–5172, 1993.
Ryerson, T. B., Williams, E. J., and Fehsenfeld, F. C.: An efficient photolysis system for fast-response NO_2 measurements, J. Geophys. Res., 105(D21), 26447–26461, 2000.
Schäfer, L., Kesselmeier, J., and Helas, G.: Formic and Acetic acid emission from conifers measured with a “cuvette” technic, in CeC Air Pollution Research 39: Field Measurements and Interpretation of Species Related to Photooxidants and Acid Deposition, edited by: Angeletti, G., Beilke, S., and Slanina, J., 319–323, Eur. Comm., Brussels, 1992.
Schiff, H. I., Mackay, G. I., Castledine, C., Harris, G. W., and Tran, Q.: Atmospheric measurements of nitrogen dioxide with a sensitive luminol instrument, Water Air Soil Poll., 30, 105–114, 1986.

AMTD
4, 5183–5274, 2011

Seinfeld, J. H. and Pandis, S. N.: Atmospheric Chemistry and Physics: From Air Pollution to Climate Change, 2nd ed., John Wiley & Sons, Inc., Hoboken, New Jersey, 2006.
Serafimovich, A., Siebicke, L., Staudt, K., Lüers, J., Hunner, M., Gerken, T., Schier, S., Biermann, T., Rtz, F., von Buttlar, J., Riederer, M., Falge, E., Mayer, J.-C., Foken, T.: ExchanGE processes in mountainous Regions (EGER) - Documentation of the Intensive Observation Period (IOP2) June, 1st to July, 15th 2008, Arbeitsergebnisse. 37, Universität Bayreuth, Abteilung Mikrometeorologie ISSN 1614-8916, Bayreuth, 147 pp., 2008.
Sparks, J. P., Monson, R. K., Sparks, K. L., and Lerdau, M.: Leaf uptake of nitrogen dioxide (NO_2) in a tropical wet forest: implications for tropospheric chemistry, Oecologia, 127, 214–221, 2001.
Steinbacher, M., Zellweger, C., Schwarzenbacher, B., Bugmann, S., Buchmann, B., Ordóñez, C., Prevot, A. S. H., and Hueglin C.: Nitrogen oxide measurements at rural sites in Switzerland: Bias of conventional measurement techniques, J. Geophys. Res., 112, D11307, doi:10.1029/2006JD007971, 2007.
Stulen, I., Perez-Soba, M., De Kok, L. J., and Van der Eerden, L.: Impact of gaseous nitrogen deposition on plant functioning, New Phytol., 139, 61–70, 1998.
Taylor, J. R.: An introduction to error analysis: The study of uncertainties in physical measurements, Oxford University Press, Mill Valley, CA, p. 270, 1982.
Teklemariam, T. A. and Sparks, J. P.: Leaf fluxes of NO and NO_2 in four herbaceous plant species: the role of ascorbic acid, Atmos. Environ., 40, 2235–2244, 2006.
Thoene, B., Schröder, P., Papen, H., Egger, A., and Rennenberg, H.: Absorption of atmospheric NO_2 by spruce (Picea abies L. Karst.) trees: I. NO_2 influx and its correlation with nitrate reduction, New Phytol., 117, 575–585, 1991.
Thoene, B., Rennenberg, H., and Weber, P.: Absorption of atmospheric NO_2 by spruce (Picea abies) trees: II. Parameterization of NO_2 fluxes by controlled dynamic chamber experiments, New Phytol., 134, 257–266, 1996.
Thomas, C. and Foken, T.: Flux contribution of coherent structures and its implications for the exchange of energy and matter in a tall spruce canopy, Bound-Lay. Meteorol., 123, 317–337, 2007.
Trebs, I., Bohn, B., Ammann, C., Rummel, U., Blumthaler, M., Königstedt, R., Meixner, F. X., Fan, S., and Andreae, M. O.: Relationship between the NO_2 photolysis frequency and the solar global irradiance, Atmos. Meas. Tech., 2, 725–739, doi:10.5194/amt-2-725-2009, 2009.

Wang, Y., Jacob, D. J., and Logan, A.: Global simulation of troposheric O_3-NO_x-hydrocarbon chemistry 1. Model formulation, J. Geophys. Res., 103(D9), 10713–10725, 1998.

Weber, P. and Rennenberg, H.: Dependency of nitrogen dioxide (NO_2) fluxes to wheat (Triticum aestivum L.) leaves from NO_2 concentration, light intensity, temperature and relative humidity determined from controlled dynamic chamber experiments, Atmos. Environ., 30(17), 3001–3009, 1996a.

Weber, P. and Rennenberg, H.: Exchange of NO and NO_2 between wheat canopy monoliths and the atmosphere, Plant Soil, 180, 197–208, 1996b.

Wendel, A., Stedman, D. H., Cantrell, C. A., and Damrauer, L. D.: Luminol-based nitrogen oxide detector, Anal. Chem., 55, 937–940, 1983.

Winer, A. M., Peters, J. W., Smith, J. P., and Pitts, J. N.: Response of Commercial Chemiluminescent NO-NO_2 Analyzers to other Nitrogen-Containing Compounds, Environ. Sci. Technol., 8, 1118–1121, 1974.

Yienger, J. J. and Levy II, H.: Empirical model of global soil-biogenic NO_x emissions, J. Geophys. Res., 100(D6), 11447–11464, 1995.

York, D., Evensen, M., Lopez Martinez, M., and De Basabe Delgado, J.: Unified equations for the slope, intercept, and standard errors of the best straight line, Am. J. Phys., 72(3), 367–375, 2004.

Table 1. Interferences of chemiluminescence NO-NO_2-NO_x analyzers using different NO_2 converters.

NO_2 converter	conversion principle	compound	Response %of concn	author
luminol	NO_2 reacts with luminol solution	PAN	25 %	Drummond et al. (1989)
		O_3	0.0033 ppb NO_2 (per ppb O_3)	Kelly et al., 1990
molybdenum (Mo)	heated ~ 400 °C surface oxidation	PAN	92 %	Winer et al. (1974)
		ethyl nitrate	103 %	
		ethyl nitrite	92 %	
		HNO_3	not quantified	
		HNO_3	≥98 %	Grosjean & Harrison (1985)
		PAN	≥98 %	
		methyl nitrate	≥98 %	
		n-propyl nitrate	≥98 %	
		n-butyl nitrate	≥98 %	
		hydrocarbons	negative interferences	Kurtenbach et al. (2001)
ferrous sulfate ($FeSO_4$)	surface oxidation	PAN	20 %	Kelly et al. (1980)
		HONO	100 %	Cox et al. (1983)
		n-propyl nitrate	32 %	Fehsenfeld et al. (1987)
		PAN	35–45 %	
photolytic	ultraviolet light (320–500 nm)	none		Fehsenfeld et al. (1990)
photolytic	ultraviolet light (>350 nm)	HONO	37 %	Ryerson et al. (2000)
		$BrONO_2$	5 %	
		NO_3	10 %	
		N_2O_5	3 %	
		HO_2NO_2	12 %	

AMTD
4, 5183–5274, 2011

Table 2. Measured parameters and instrument specifications. Limit of detection (LOD(m_i), 3σ-definition) for the gas concentrations were determined under field and laboratory conditions.

parameter	symbol	unit	LOD(m_i) lab	LOD(m_i) field	instrument (model)
nitric oxide	NO	ppb	0.23 ppb	0.10 ppb	ThermoElectron, 42C
nitrogen dioxide	NO_2	ppb	1.01 ppb	0.31 ppb	ThermoElectron, 42C
ozone	O_3	ppb	0.8 ppb	0.98 ppb	ThermoElectron, 49C
carbon dioxide	CO_2	ppm	1.2 ppm	1.5 ppm	LiCor, LI-6262/LI-7000
water vapour	H_2O	ppth	0.3 ppth	0.2 ppth	LiCor, LI-6262/LI-7000
air temperature	T	°C			thermocouple
relative humidity	rH	%			Rotronic, MP100A
photosynthetic active radiation	PAR	$\mu mol\ m^{-2}\ s^{-1}$			LiCor, LI-190SA
photolysis rate	$j(NO_2)$	s^{-1}			filter radiometer
air pressure	P	hPa			Ammonit

Table 3. Manufacturer details for parts of the dynamic chamber system.

	part	manufacturer	specifications
(1) + (2)	chamber frame and lid	MPI workshop, Germany	PVC, acrylic glass
(3)	inner chamber wall	Saint Gobain, Germany	FEP (fluorinated ethylene propylene) film, thickness 0.05 mm, chemically inert, transparent for visible and UV light
(4)	clamps	Holex, Germany	parallel clamp, typ 25
(5)	silicon straps	Dichtungstechnik Bensheim GmbH, Germany	transparent MVQ-silicone cord, diameter 5 mm
(6)	inlet fan	Micronel, Switzerland	axial fan, model D344T012GK-2
(7)	air mass flow sensor	Honeywell International Inc., USA	model AWM 700
(8)	propeller	APC Propellers, USA	Sport Prop, 10 × 7, Teflon® coating by MPI workshop
(9)	mixing fan	Micronel, Switzerland	ultra slim fan, model F62MM012GK-9, Teflon® coating by MPI workshop
(10)	tubing	diverse	1/4” PFA tubing
(11)	in-line filter case	Entegris Inc., USA	Galtek® Integral Ferrule in-line filters
	particulate membrane filter	Pall Corporation, USA	Zefluor^{TM} membrane disc filters, model P5PJ047, pore size 2 µm, diameter 47 mm
	solenoid valves	Entegris Inc., USA	Galtek® diaphragm valves, 3-way, 1/4”orifice
	sample pump	Vakuubrand, Germany	diaphragm pump, model MZ4C, chemical resistant
	heating tape	EHT Haustechnik AEG, Germany	typ HT SLH 15/L300, self limiting, max. holding temperature 60 °C, heat output 15 W m^{-1}

AMTD
4, 5183–5274, 2011
The dynamic chamber method
C. Breuninger et al.

AMTD
4, 5183–5274, 2011

Table 4. Results of the temperature dependence tests of the analyzers used in this work. Stated temperatures are internal temperatures of the analyzers. The drift specifies the signal change over the whole temperature range. The signal noise is the maximum noise (3σ) detected with zero air during the test.

analyzer	trace gas	temperature range	drift	signal noise (3σ)
LI-7000	CO_2	22–44 °C	+0.97 ppm	0.25 ppm
LI-6262	CO_2	22–44 °C	−3.5 ppm	0.23 ppm
TEI 49C	O_3	21–46 °C	+0.4 ppb	0.7 ppb
TEI 42C	NO	18–46 °C	−1.9 ppb	0.2 ppb
TEI 42C/BLC	NO_2	18–46 °C	−10.4 %	0.5 ppb

Table 5. Parameters of sorption effects to the inner chamber walls determined by laboratory experiments. q_{10} and q_{90} denote the 10 % and 90 % quantiles of the entire blank flux density $F_{\mathrm{wall},i}$ data, concentration ranges represent applied fumigation concentrations during the experiment, Δc_{mean} denotes the mean concentration difference of incoming and outgoing chamber air in % (range of differences in %).

	$F_{\mathrm{wall},i}$, pmol m^{-2} s^{-1}			concentrations	
gas	mean ($\pm\sigma$)	$q_{10}\ldots q_{90}$	$v_{\mathrm{dep\_wall},i}$, m s^{-1}	range, ppb	Δc_{mean}
NO	−4.47 (± 3.52)	−7.95 ... −1.13	-2.12×10^{-6}	10–62	0.8 % (0.3–1.6)
NO_2	−4.43 (± 3.11)	−9.11 ... −1.51	-2.92×10^{-6}	6–47	1.8 % (0.4–3.4)
O_3	−4.88 (± 2.47)	−7.05 ... −2.05	-1.94×10^{-6}	7–45	1.6 % (0.5–3.7)

AMTD
4, 5183–5274, 2011

Table 6. Parameters of NO_2 laboratory measurements of simple (no errors considered), simple (standard error of $m_{\mathrm{s,NO_2}}$ considered) and bi-variate weighted (standard error of $m_{\mathrm{s,NO_2}}$ and $m_{\mathrm{a,NO_2}}$ considered) linear least-squares fitting regression analysis. Data were separated for all data of $\Delta m_{\mathrm{NO_2}} = (m_{\mathrm{a,NO_2}} - m_{\mathrm{s,NO_2}})$ and for only significant data of $\Delta m_{\mathrm{NO_2}}$. Limit of detection (LOD) of 2σ, 1σ and no LOD was applied to the data.

			all ($m_{\mathrm{a,NO_2}} - m_{\mathrm{s,NO_2}}$) data			only significant ($m_{\mathrm{a,NO_2}} - m_{\mathrm{s,NO_2}}$) data		
			linear least-squares fitting algorithm			linear least-squares fitting algorithm		
LOD($m_{\mathrm{NO_2}}$) definition	statistical quantity	unit	simple, no errors considered	simple, only $s_{\mathrm{m\_s,NO_2}}$ considered	bi-variate & weighted, $s_{\mathrm{m,a,NO_2}}$ & $s_{\mathrm{m,s,NO_2}}$ considered	simple, no errors considered	simple, only $s_{\mathrm{m\_s,NO_2}}$ considered	bi-variate & weighted, $s_{\mathrm{m,a,NO_2}}$ & $s_{\mathrm{m,s,NO_2}}$ considered
LOD($m_{\mathrm{NO_2}}$) $2\times\sigma_{\mathrm{m\_NO_2,0}}$ definition	N	[1]	17	17	17	14	14	14
	$R^2(m_{\mathrm{a,NO_2}}, m_{\mathrm{s,NO_2}})$	[1]	0.9692	0.9716	0.9610	0.9794	0.9778	0.9706
	$m_{\mathrm{comp,NO_2}}$	nmol m^{-3}	16.5 ± 1.81	14.2 ± 12.15	17.3 ± 7.29	6.8 ± 2.22	2.2 ± 16.76	5.9 ± 9.13
	$m_{\mathrm{comp,NO_2}} \neq 0$?	%	99.99 (HS)	99.99 (HS)	99.99 (HS)	99.99 (HS)	37.1 (UL)	96.6 (L)
	$v_{\mathrm{dep,NO_2}}$	mm s^{-1}	0.27 ± 0.007	0.24 ± 0.016	0.26 ± 0.014	0.21 ± 0.006	0.20 ± 0.015	0.22 ± 0.013
LOD($m_{\mathrm{NO_2}}$) $1\times\sigma_{\mathrm{m\_NO_2,0}}$ definition	N	[1]	45	45	45	33	33	33
	$R^2(m_{\mathrm{a,NO_2}}, m_{\mathrm{s,NO_2}})$	[1]	0.9695	0.9754	0.9605	0.9847	0.9851	0.9782
	$m_{\mathrm{comp,NO_2}}$	nmol m^{-3}	6.8 ± 0.52	7.3 ± 5.95	8.1 ± 3.46	−1.8 ± 0.63	−0.7 ± 7.82	0.6 ± 3.67
	$m_{\mathrm{comp,NO_2}} \neq 0$?	%	99.99 (HS)	99.99 (HS)	99.99 (HS)	99.99 (HS)	39.5 (UL)	61.8 (UL)
	$v_{\mathrm{dep,NO_2}}$	mm s^{-1}	0.21 ± 0.004	0.22 ± 0.012	0.22 ± 0.010	0.19 ± 0.003	0.20 ± 0.012	0.20 ± 0.009
LOD($m_{\mathrm{NO_2}}$) not considered	N	[1]	51	51	51	36	36	36
	$R^2(m_{\mathrm{a,NO_2}}, m_{\mathrm{s,NO_2}})$	[1]	0.9682	0.9728	0.9575	0.9819	0.9815	0.9719
	$m_{\mathrm{comp,NO_2}}$	nmol m^{-3}	7.1 ± 0.44	6.8 ± 4.72	7.6 ± 3.07	−1.6 ± 0.60	−0.4 ± 6.22	±
	$m_{\mathrm{comp,NO_2}} \neq 0$?	%	99.99 (HS)	99.99 (HS)	99.99 (HS)	99.99 (HS)	27.6 (UL)	60.4 (UL)
	$v_{\mathrm{dep,NO_2}}$	mm s^{-1}	0.22 ± 0.004	0.22 ± 0.012	0.22 ± 0.010	0.19 ± 0.003	0.20 ± 0.011	0.20 ± 0.010

AMTD
4, 5183–5274, 2011

Title Page
Abstract | Introduction
Conclusions | References
Tables | Figures
◂◂ | ▸▸
◂ | ▸
Back | Close
Full Screen / Esc
Printer-friendly Version
Interactive Discussion

Table 7. Percentage of data m_i (i = NO, NO_2, O_3) above limit of detection (LOD(m_i), 3σ-definition) and significant differences $\Delta m_i = (m_{a,NO_2} - m_{s,NO_2})$ of tree 1 and 2 for field measurements.

	tree 1 m_i > LOD + significant Δm_i % of total (number of total)			tree 2 m_i > LOD + significant Δm_i % of total (number of total)		
	all (2988)	day (1885)	night (1103)	all (2993)	day (1887)	night (1106)
NO	24	33	7	24	33	8
NO_2	57	62	48	67	69	63
O_3	96	98	93	98	99	97

AMTD
4, 5183–5274, 2011

Table 8. Parameters of bi-variate weighted linear least-squares fitting regression analysis for field measurements. NO_2 data were separated for all data of $\Delta m_{NO_2} = (m_{a,NO_2} - m_{s,NO_2})$ and for only significant data of Δm_{NO_2}. Data of O_3 were almost significant for $\Delta m_{O_3} = (m_{a,O_3} - m_{s,O_3})$. 3σ detection limit was applied to the data.

statistical quantity	unit	all $(m_{a,NO_2} - m_{s,NO_2})$ data NO_2	only significant $(m_{a,NO_2} - m_{s,NO_2})$ data NO_2	only significant $(m_{a,O_3} - m_{s,O_3})$ data O_3
N	[1]	154	123	155
$R^2(m_{a,i}, m_{s,i})$	[1]	0.9404	0.9480	0.9847
$m_{comp,i}$	$nmol\,m^{-3}$	-18.2 ± 17.57	-9.5 ± 14.75	0*
$m_{comp,i} \neq 0$?	%	99.99 (HS)	99.99 (HS)	–
$v_{dep,i}$	$mm\,s^{-1}$	0.14 ± 0.031	0.18 ± 0.034	0.32 ± 0.018

* assumption for O_3: $m_{comp,O_3} = 0$.

AMTD
4, 5183–5274, 2011

The dynamic chamber method

C. Breuninger et al.

Table 9. Overview of studies which have performed dynamic chamber NO_2 flux measurements on different plant species.

author	plant species	measured gases	location	wall material[1]	purging air[2]	NO_2 concentration in purging air, ppb	chamber volume, L	NO_2 converter[3]	analyzer	LOD[4], ppb 3σ-definition
Hanson et al. (1989)	deciduous, coniferous	NO_2	lab	glass	pure air^w + CO_2 + NO_2	60–70	22.7	Luminol	LMA-3, Luminox	n.s.
Thoene et al. (1991, 1996)	spruce	NO_2	lab	glass	zero air^w + NO_2	1.6–125	3	Mo	Thermo Electron, 14B/E	NO_2: 1.0*
Neubert et al. (1993)	sunflower, tobacco	NO, NO_2, O_3	lab	PTFE	zero air^w + NO/NO_2/O_3	< 100	160	PLC	Tecan, CLD 770 AL ppt	NO: 0.02; NO_2: 0.1*
Rondón et al. (1993)	pine, spruce	NO, NO_2, O_3	field	FEP	ambient air, O_3 free + NO_2	0.25–120	10	$FeSO_4$	Teco, 14D	NO: 0.3*
					ambient air + NO_2			Mo	Tecan, CLD 770 AL ppt	NO: 0.06*
Rondón & Granat (1994)	pine, spruce	NO, NO_2, O_3	lab	FEP	zero air^w + CO_2 + NO_2 + O_3	0.2–25	12.6	$FeSO_4$/PLC	Tecan, CLD 770 AL ppt	NO: 0.075; NO_2: 0.3
Weber & Rennenberg (1996a, b)	wheat	NO, NO_2	lab	PMMA	zero air^w + NO_2	0–90	18–124	PLC	Tecan, CLD 770 AL ppt	NO: 0.075**
Geßler et al. (2000, 2002)	beech, spruce	NO_2, NH_3	field, lab	BG	zero air^w + NO_2/NH_3	0.2–37	3	PLC	Tecan, CLD 770 AL ppt	NO_2: <0.1*
Sparks et al. (2001)	tropical trees	NO_2	field	n.s. (L)	pure air^w + CO_2 + NO_2	0.1–13	n.s.	Luminol	LMA-3, Luminox	NO_2: 0.005*
Hereid & Monson (2001)	corn	NO, NO_2	field	n.s. (L)	pure air^w + CO_2 +NO/NO_2	0.1– > 10	n.s.	Luminol	LMA-3, Luminox	NO_2: 0.005*
Gut et al. (2002)	tropical trees	NO, NO_2, O_3	lab	FEP	ambient air	5–18	75	PLC	Eco-Physics, CLD 780 TR	NO: 0.052*
Teklemariam & Sparks (2006)	corn, sunflower, wheat	NO, NO_2	lab	n.s. (L)	pure air^w + CO_2 +NO/NO_2	1–5	n.s.	Mo	TEI 42	NO_2: 0.5*
Raivonen et al. (2009)	Scots pine	NO, NO_2	field	FEP, QG	ambient air	< 1	1	Mo	TEI 42S	n.s.
Chaparro-Suarez et al. (2011)	deciduous, coniferous	NO, NO_2, O_3	lab	FEP	zero air^w + NO_2	0–5	7.3	PLC	Eco-Physics, CLD 780 TR	NO: 0.06
this study	spruce	NO, NO_2, O_3	field	FEP	ambient air	0.4–21	75	BLC	TEI 42C	NO: 0.1; NO_2:0.31
			lab	zero air^w + NO_2	0.3–4	60			NO: 0.2; NO_2:1.0	

n.s. = not specified.

[1] QG = quartz glass; BG = borosilicate glass; FEP, PFA, PTFE = Teflon materials; PMMA = polymethylmethacrylate (Plexiglas); L = dynamic leaf chamber of gas exchange system Model LI-6400, LiCor, Lincoln, Nebraska, USA.

[2] ^{w} air humidified; pure air = air from a pure air generator; zero air = reactive trace gases removed with filters (NO_x, NH_3, H_2S, SO_2, O_3).

[3] Mo = molybdenum converter; PLC = photolytic converter; $FeSO_4$ = ferrous sulphate converter; BLC = blue light converter.

[4] * LOD definition unknown; ** manufacturer's data.

AMTD
4, 5183–5274, 2011

The dynamic chamber method

C. Breuninger et al.

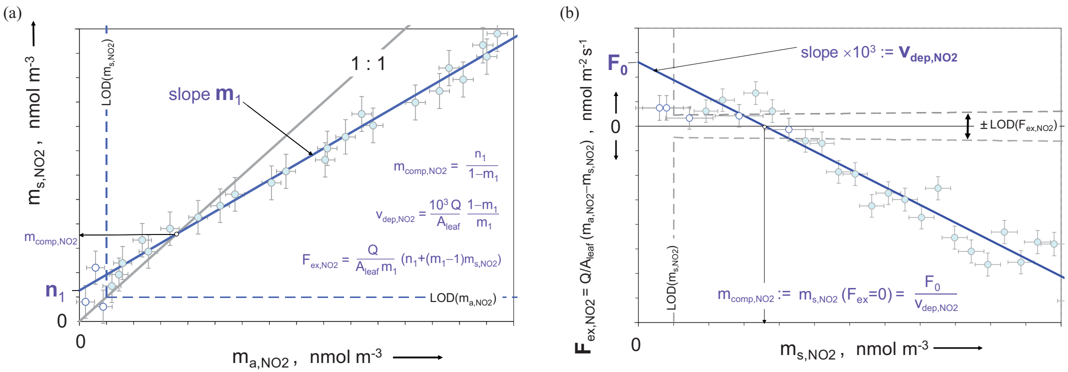

Fig. 1. Schematic representation of the determination of bi-directional NO_2 exchange flux density (F_{ex,NO_2}), NO_2 deposition velocity (v_{dep,NO_2}), and NO_2 compensation point concentration (m_{comp,NO_2}) from measurements of NO_2 concentrations at the plant chamber inlet (m_{a,NO_2}) and outlet (m_{s,NO_2}) under laboratory conditions ($m_{a,NO} = m_{a,O_3} = j(NO_2) \approx 0$). **(a)**: by linear regression of m_{s,NO_2} with m_{a,NO_2}. **(b)**: by plotting F_{ex,NO_2} vs. m_{s,NO_2}. Dashed lines represent the limits of detection (3σ-definition) for NO_2 concentration measurements (**(a)** and **(b)** panel) and the determination of the NO_2 exchange flux density (b panel), which are both defined by the sensitivity of the applied NO_2 analyzer (note: LOD(m_{a,NO_2}) = LOD(m_{s,NO_2})). Data points and error bars of NO_2 concentrations have been simulated to match $R^2(m_{a,NO_2}, m_{s,NO_2}) = 0.9925$, error bars of NO_2 exchange flux have been calculated by Gaussian error propagation (c.f. Eq. (1.4)). Filled circles identify data points > LODs, hollow circles those ≤ LODs.

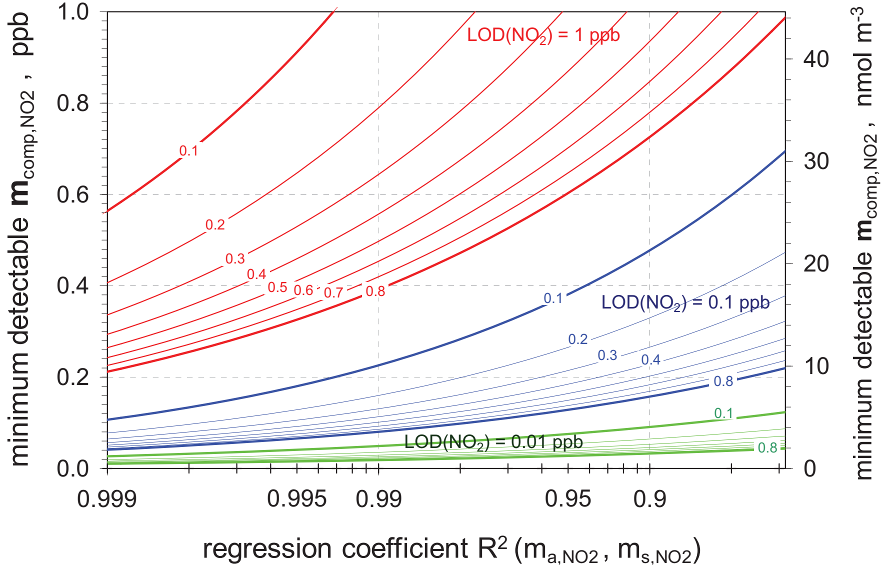

Fig. 2. The dynamic plant chamber at well defined (laboratory) conditions: minimum detectable NO_2 compensation point concentrations (m_{comp,NO_2} at $P \geq 0.999$, i.e. "highly significant") as function of NO_2 deposition velocity (v_{dep,NO_2}; per leaf area) and the goodness (R^2) of the ambient vs. sample NO_2 concentration measurements (standard errors of NO_2 concentration measurements considered). Results are from data simulation (random number application) matching pre-scribed $R^2(m_{a,NO_2}, m_{s,NO_2})$ and prescribed $v_{dep,NO_2}(0.999 \leq R^2 \leq 0.6$ and $v_{dep,NO_2} = 0.1, 0.2, \ldots, 0.8\,\mathrm{mm\,s^{-1}})$. The greenish range represents simulated data of a NO_2 analyzer with LOD(m_{NO_2}) = 0.4 nmol m^{-3} (0.01 ppb), the bluish range for LOD(m_{NO_2}) = 4.5 nmol m^{-3} (0.1 ppb), the reddish range for LOD(m_{NO_2}) = 44.6 nmol m^{-3} (1.0 ppb).

AMTD
4, 5183–5274, 2011

The dynamic chamber method

C. Breuninger et al.

Title Page
Abstract | Introduction
Conclusions | References
Tables | Figures
◀ | ▶
Back | Close
Full Screen / Esc
Printer-friendly Version
Interactive Discussion

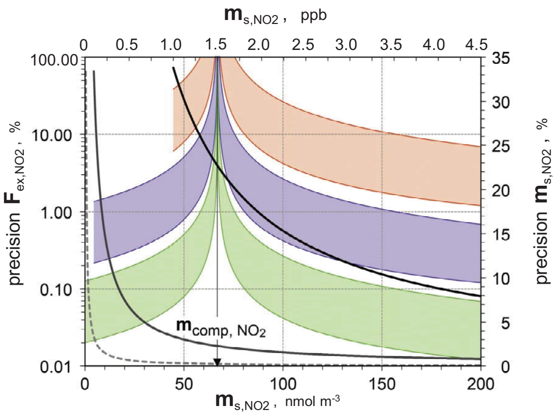

Fig. 3. The dynamic plant chamber at well defined (laboratory) conditions: precision of NO_2 concentration measurements (= $s_{m,s\_NO_2}/m_{s,NO_2}$; right axis) and precision of derived NO_2 exchange flux densities (= $s_{Fex\_NO_2}/F_{ex,NO_2}$, left axis) as function of the NO_2 concentration measured at the outlet of the dynamic chamber (precision m_{s,NO_2}, right axis). Results are from data simulation (random number application), which considers standard errors of NO_2 concentration measurements, and which matches pre-scribed $R^2(m_{a,NO_2}, m_{s,NO_2})$ and pre-scribed $m_{comp,NO_2} = 67\,\text{nmol m}^{-3}$ (1.5 ppb). Dark purple, purple, and pink lines (= precision of m_{s,NO_2}) represent data for a NO_2 analyzer characterized by LOD(m_{s,NO_2}) = 44.6 nmol m^{-3} (1.0 ppb), LOD(m_{s,NO_2}) = 4.5 nmol m^{-3} (0.1 ppb), and LOD(m_{s,NO_2}) = 0.4 nmol m^{-3} (0.01 ppb), respectively. Ranges of the precision of derived NO_2 exchange flux densities are identified by reddish, bluish, and greenish areas for LOD(m_{s,NO_2}) = 44.6 nmol m^{-3} (1.0 ppb), LOD(m_{s,NO_2}) = 4.5 nmol m^{-3} (0.1 ppb), and LOD(m_{s,NO_2}) = 0.4 nmol m^{-3} (0.01 ppb). The width of the colored areas stands for all considered combinations of R^2 and v_{dep,NO_2} ($0.99 \le R^2 \le 0.9$ and $0.3 \le v_{dep,NO_2} \le 0.6\,\text{mm s}^{-1}$). The respective upper boundary of each colored area represents the combination $v_{dep,NO_2} = 0.3\,\text{mm s}^{-1}$ and $R^2 = 0.9$, while the lower boundary represents $v_{dep,NO_2} = 0.6\,\text{mm s}^{-1}$ and $R^2 = 0.99$.

AMTD
4, 5183–5274, 2011

The dynamic chamber method

C. Breuninger et al.

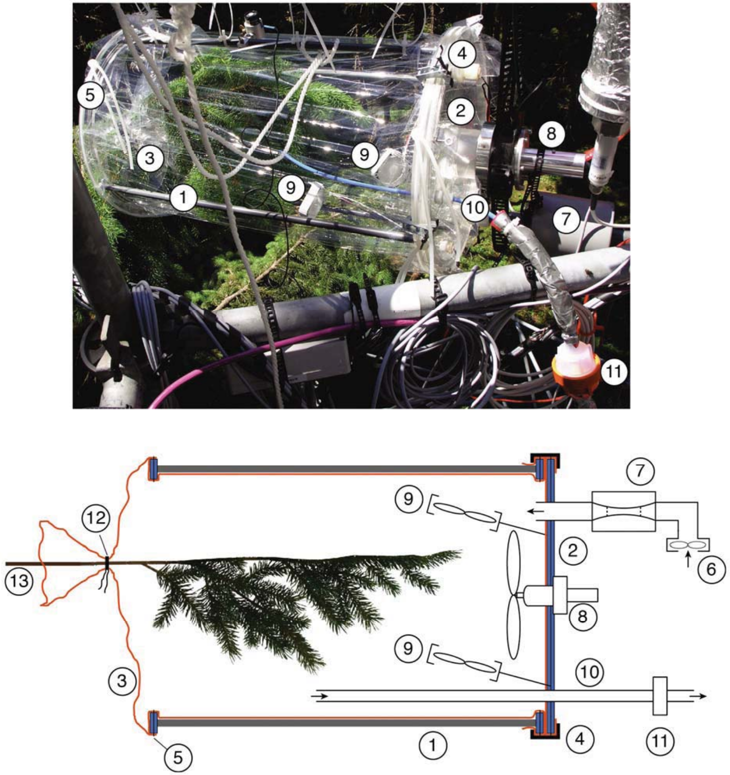

Fig. 4. Photograph and schematic drawing of a dynamic chamber consisting of: (1) PVC (grey parts) frame, (2) acrylic glass (blue parts)n lid, (3) FEP film (red parts in the scheme), (4) clamp to attach lid to frame, (5) silicon straps, (6) inlet fan, (7) air mass flow sensor, (8) Teflon propeller, (9) mixing fan, (10) sample tube for chamber air, (11) filter, (12) closure, (13) plant material.

AMTD

4, 5183–5274, 2011

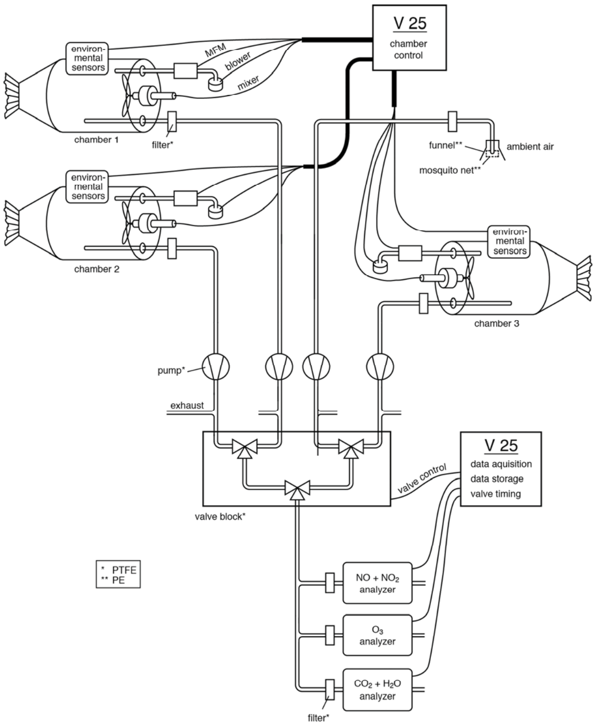

Fig. 5. Schematic set-up of the system with three dynamic chambers. Open lines are PFA sampling tubes, black lines are cables for data acquisition and control.

AMTD
4, 5183–5274, 2011

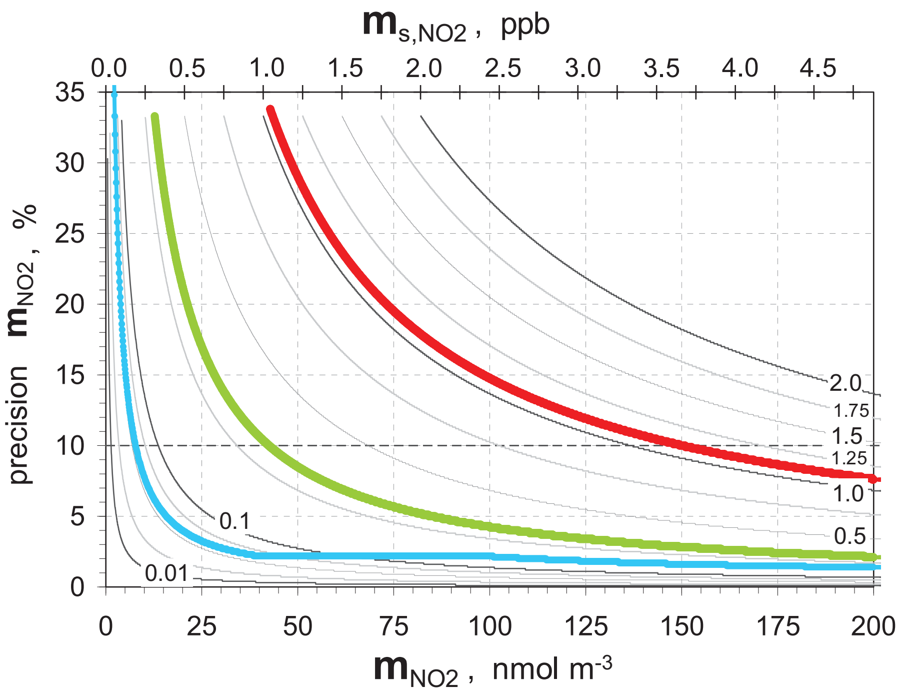

Fig. 6. Precision ($s_{m,NO_2}/m_{NO_2}$) of the applied NO/NO_2 analyzer during laboratory (red curve) and field experiments (green curve). For comparison, curves for precisions of hypothetical analyzers with $0.01 \leq \mathrm{LOD}(m_{NO_2}) \leq 2$ ppb are also shown (numbers on black and grey curves). The blue curve is the precision of the blended NO_2 concentration used for fumigation of the young spruce trees in the laboratory.

AMTD
4, 5183–5274, 2011

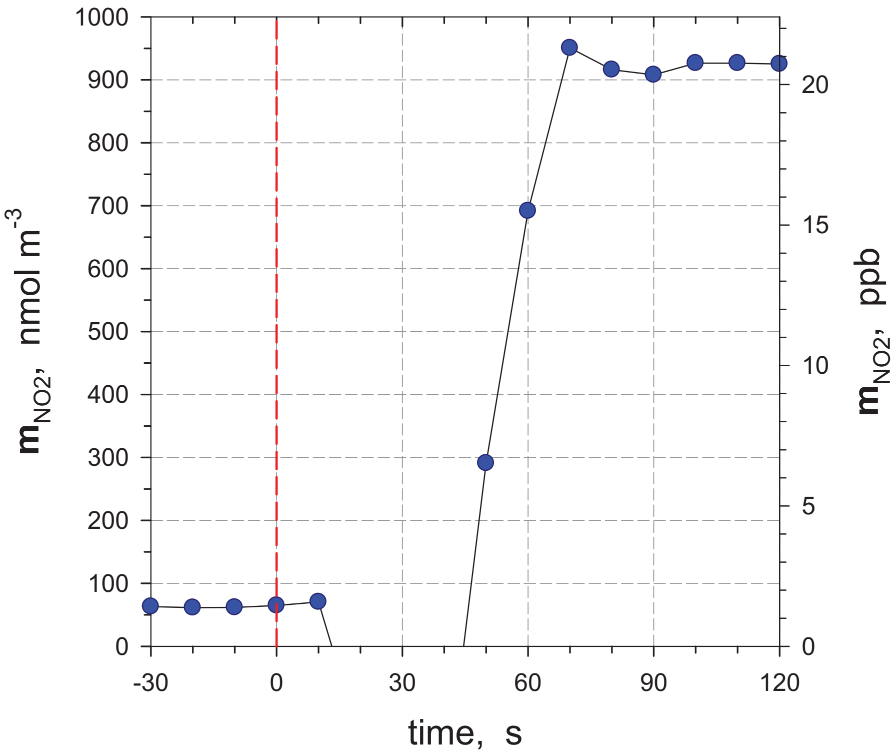

Fig. 7. Response test for step changes between two different NO_2 concentrations (m_{NO_2}). The red dashed line marks the switching point.

AMTD
4, 5183–5274, 2011

The dynamic chamber method

C. Breuninger et al.

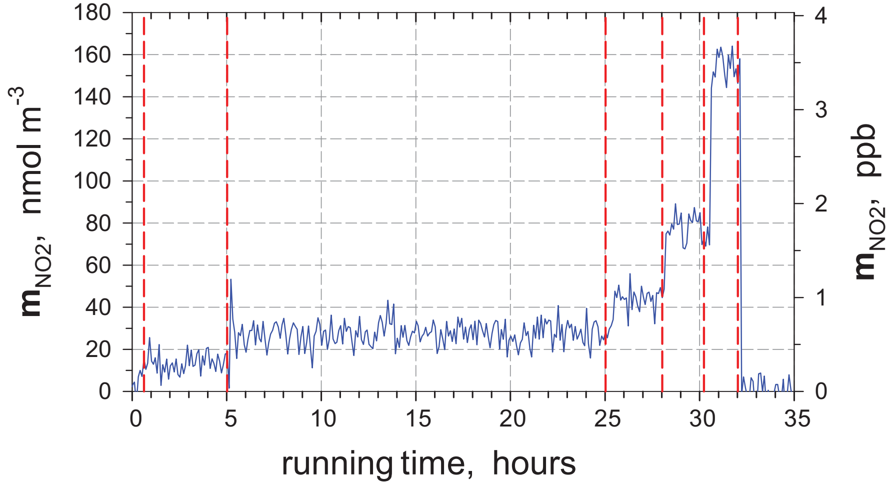

Fig. 8. Temporal course of blended NO_2 concentrations (12.3, 24.6, 41.0, 73.8, and 139.4 nmol m^{-3} (0.3, 0.6, 1.0, 1.8, 3.4 ppb)) used for fumigation of young spruce trees during the laboratory experiments. NO_2 concentrations were provided by diluting a NO_2 standard into purified air. Red dashed lines indicate times where blending was changed to obtain the next NO_2 concentration.

AMTD
4, 5183–5274, 2011

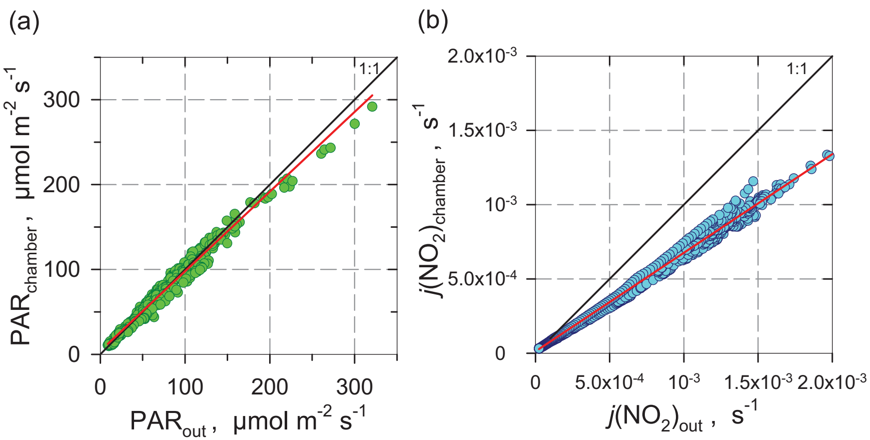

Fig. 9. Simultaneous measurements of radiation in and outside a chamber. **(a)** Photosynthetically active radiation PAR (slope = 0.94, R^2 = 0.98, N = 456), **(b)** photolysis rate $j(NO_2)$ (slope = 0.66, R^2 = 0.99, N = 1440). The black line indicates the 1:1 line and the red line represents the linear fit on the data points.

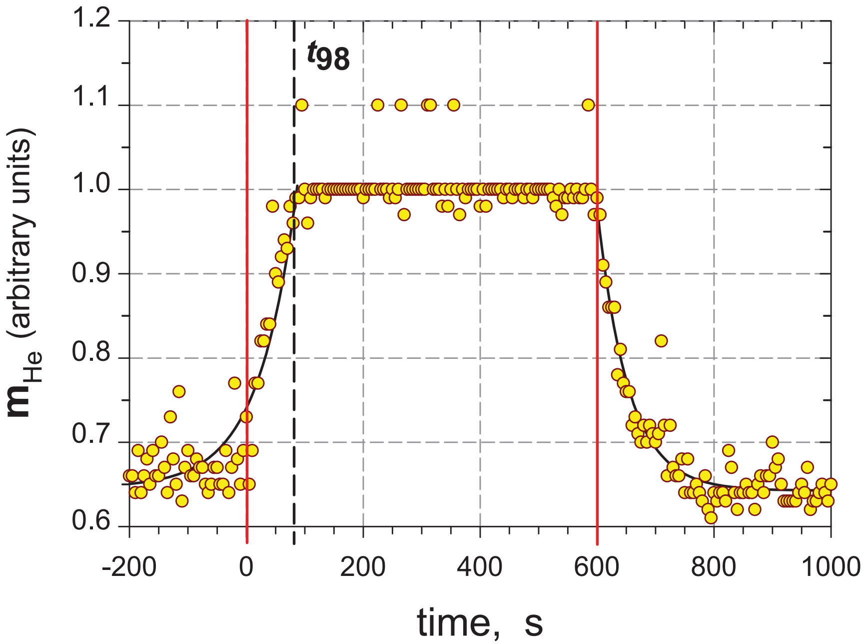

Fig. 10. Results of the response time test with helium. The chamber ($V = 0.079\,m^3$) was operated with purging air flow rate $Q = 60\,L\,min^{-1}$. The red lines represent start and end of the helium addition, the black dashed line marks the end of equilibration. For a reasonable approximation of a complete gas exchange of the chamber volume we used the time interval for 98 % approximation (t_{98}).

AMTD
4, 5183–5274, 2011

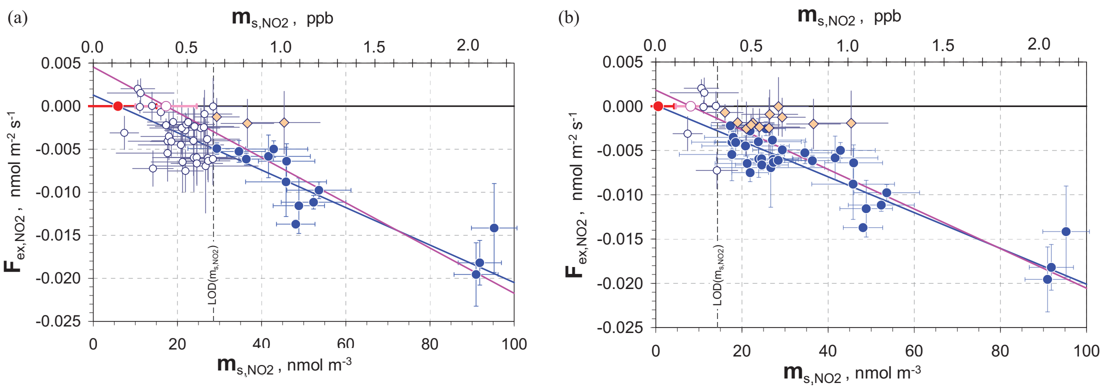

Fig. 11. Laboratory NO_2 fumigation of 3–4 yr old Norway Spruce trees (*Picea abies* L.) under controlled conditions (25 °C, 60 %, 450 µmol photons m^{-2} s^{-1}): NO_2 exchange flux density (F_{ex,NO_2}) vs. NO_2 concentration measured at the outlet of the dynamic plant chamber (m_{s,NO_2}) for application of 2σ-LOD(m_{s,NO_2})-definition (**(a)** panel) and 1σ-LOD(m_{s,NO_2})-definition (**(b)** panel). F_{ex,NO_2} data were calculated according Eq. (1.4), their standard errors according to Eq. (11). Blue circles identify F_{ex,NO_2} where $m_{s,NO_2} > \mathrm{LOD}(m_{s,NO_2})$, white circles stand for F_{ex,NO_2} where $m_{s,NO_2} \leq \mathrm{LOD}(m_{s,NO_2})$, and reddish diamonds for those F_{ex,NO_2} data, which have to be rejected for non-significance of $\Delta m_{NO_2} = (m_{a,NO_2} - m_{s,NO_2})$. Blue line (considering blue circle data) and pink line (considering blue circle and reddish diamond data) were calculated according to Eq. (8.1.1). NO_2 compensation point concentration m_{comp,NO_2} was calculated according to Eq. (8.3.1) and is represented by red filled circles (considering blue circle data) and pink hollow circles (considering blue circle and reddish diamond data). More details of statistical evaluation are listed in Table 6.

AMTD
4, 5183–5274, 2011

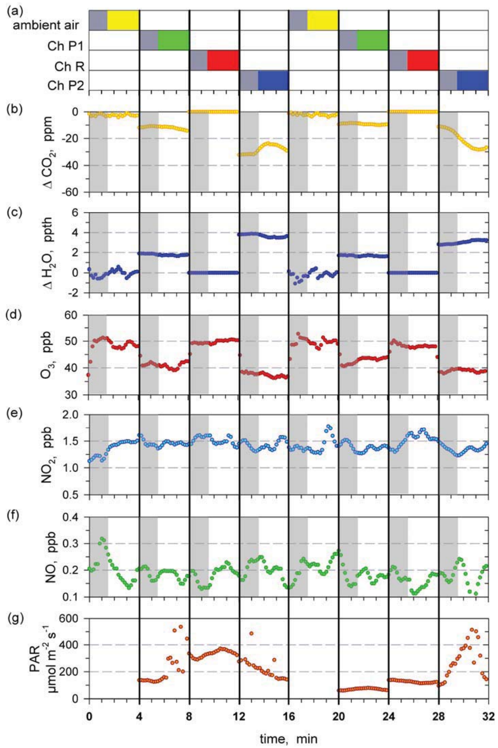

Fig. 12. Switching scheme and time series of trace gas mixing ratios over two full measurement cycles during EGER field experiment. Data were corrected for calibration factors, temperature dependency and offset of analyzers. **(a)** Control scheme indicating periods of skipped data (first 90 s) for data processing (grey bars), sampling/analysis of ambient air (yellow bars), sampling/analysis of plant chamber 1 (green bars), sampling/analysis of reference chamber (red bars) and sampling/analysis of plant chamber 2 (blue bars). **(b–c)** Time series of CO_2 and H_2O mixing ratios measured as difference between reference chamber and respectively switched intake. **(d–f)** Time series of O_3, NO_2, and NO mixing ratios. **(g)** Photosynthetic active radiation (PAR).

AMTD
4, 5183–5274, 2011

The dynamic chamber method

C. Breuninger et al.

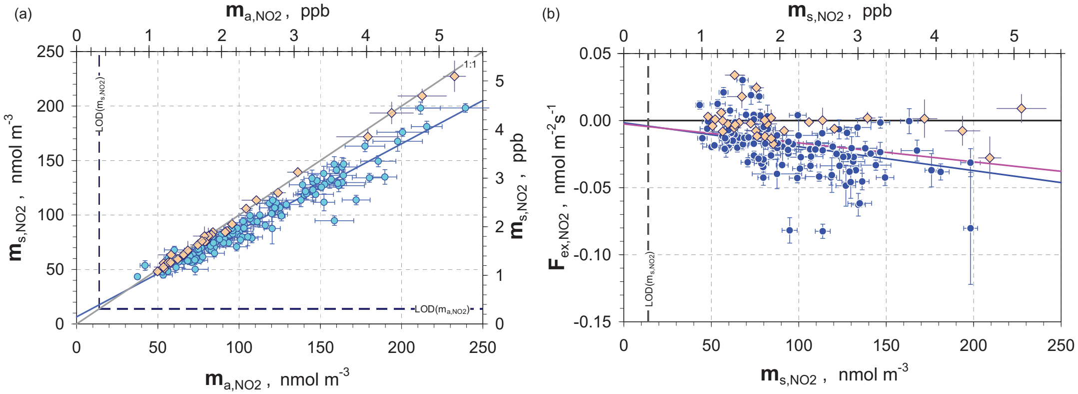

Fig. 13. Field measurements: **(a)** NO_2 concentration measured at the outlet of the dynamic plant chamber (m_{s,NO_2}) vs. NO_2 concentration measured at the inlet of the dynamic plant chamber (m_{a,NO_2}). Light blue circles identify data pairs for significance of $\Delta m_{NO_2} = (m_{a,NO_2} - m_{s,NO_2})$ and reddish diamonds for those data pairs, which have to be rejected for non-significance of $\Delta m_{NO_2} = (m_{a,NO_2} - m_{s,NO_2})$. Blue line (considering blue circle data) was calculated according to bi-variate weighted linear least-squares fitting regression analysis (see Sect. 3.4.6). **(b)** NO_2 exchange flux density (F_{ex,NO_2}) vs. NO_2 concentration measured at the outlet of the dynamic plant chamber (m_{s,NO_2}). F_{ex,NO_2} data were calculated according Eq. (1.4), their standard errors according to Eq. (11). Reddish diamonds stand for those F_{ex,NO_2} data, which have to be rejected for non-significance of $\Delta m_{NO_2} = (m_{a,NO_2} - m_{s,NO_2})$. Blue line (considering blue circle data) and pink line (considering blue circle and reddish diamond data) were calculated according to Eq. (8.1.1)

AMTD
4, 5183–5274, 2011

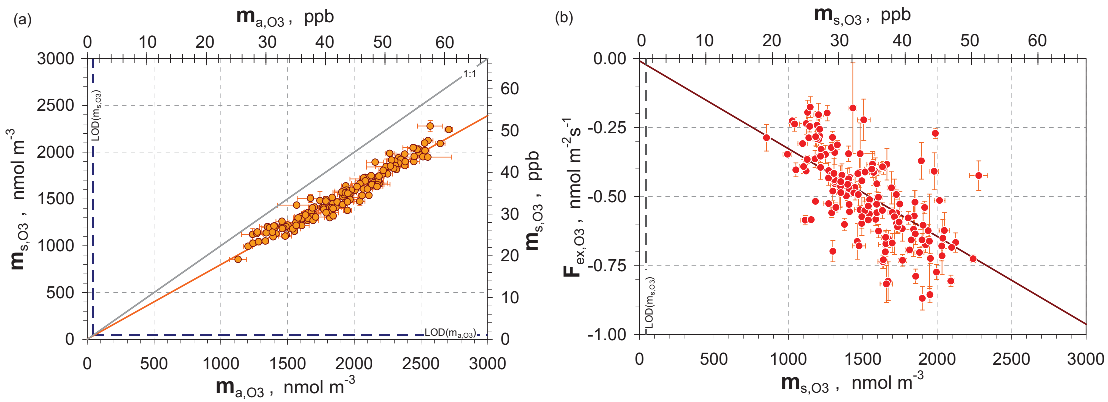

Fig. 14. Field measurements: **(a)** O_3 concentration measured at the outlet of the dynamic plant chamber (m_{s,O_3}) vs. O_3 concentration measured at the inlet of the dynamic plant chamber (m_{a,O_3}). Orange circles identify data pairs for significance of $\Delta m_{O_3} = (m_{a,O_3} - m_{s,O_3})$. Orange line was calculated according to bi-variate weighted linear least-squares fitting regression analysis (see Sect. 3.4.6). **(b)** O_3 exchange flux density (F_{ex,O_3}) vs. O_3 concentration measured at the outlet of the dynamic plant chamber (m_{s,O_3}). F_{ex,O_3} data were calculated according Eq. (1.4), their standard errors according to Eq. (11). Dark red line was calculated according to Eq. (8.1.1).

AMTD
4, 5183–5274, 2011

The dynamic chamber method

C. Breuninger et al.

Title Page
Abstract | Introduction
Conclusions | References
Tables | Figures
◄ | ►
Back | Close
Full Screen / Esc
Printer-friendly Version
Interactive Discussion

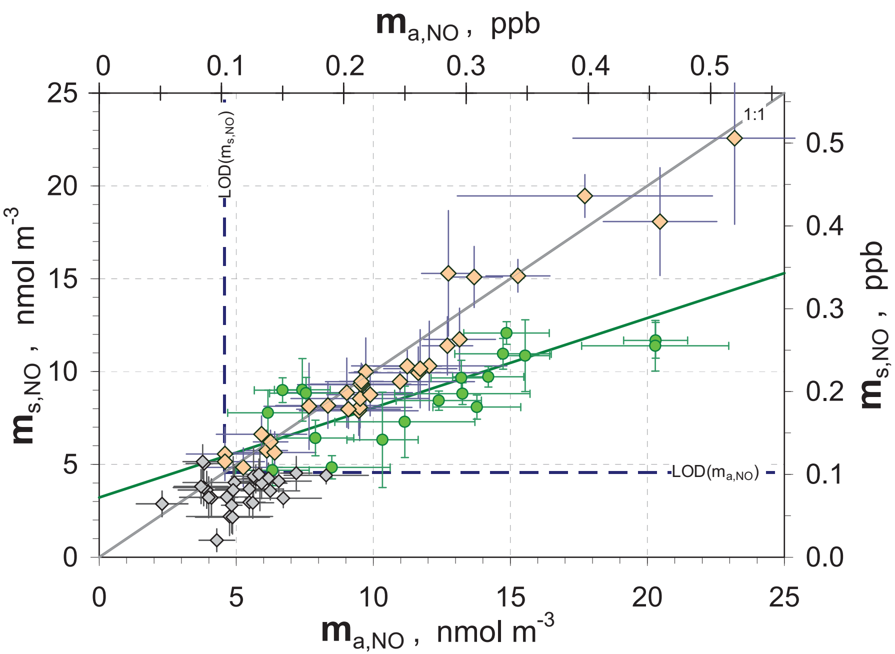

Fig. 15. Field measurements: NO concentration measured at the outlet of the dynamic plant chamber ($m_{s,NO}$) vs. NO concentration measured at the inlet of the dynamic plant chamber ($m_{a,NO}$). Light green circles identify data pairs for significance of $\Delta m_{NO=} = (m_{a,NO} - m_{s,NO})$, reddish diamonds stand for those data pairs, which have to be rejected for non-significance of Δm_{O_3} and grey diamonds for data pairs where $m_{NO} \leq \mathrm{LOD}(m_{NO})$. Green line (considering green circle data) was calculated according to bi-variate weighted linear least-squares fitting regression analysis (see Sect. 3.4.6).

AMTD
4, 5183–5274, 2011

The dynamic chamber method

C. Breuninger et al.

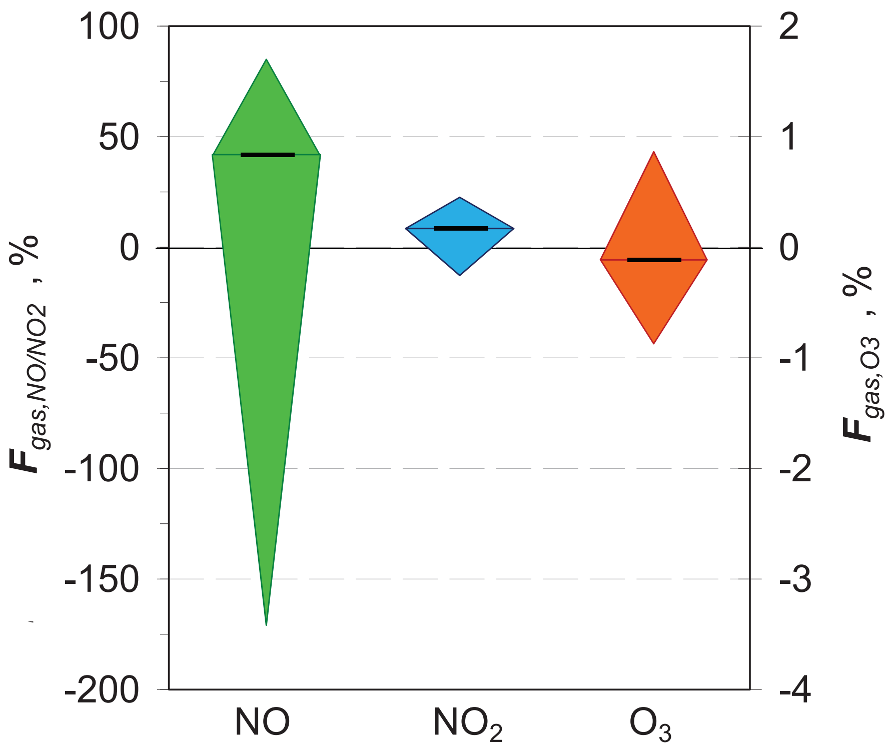

Fig. 16. Percentage of gas-phase flux densities $F_{\mathrm{gas},i}$ at the exchange flux densities $F_{\mathrm{ex},i}$ for NO (green diamond), NO_2 (blue diamond) and O_3 (orange diamond). Results are from the field experiment, restricted to one selected data category (see Sect. 4.4.2). The apexes of the diamonds represented the upper (75 %) and the lower (25 %) quantile and the black dash in the middle of the diamonds the median. $F_{\mathrm{gas,NO}}$ and $F_{\mathrm{gas,NO_2}}$ were applied to the left y-axis and $F_{\mathrm{gas,O_3}}$ to the right y-axis.

AMTD
4, 5183–5274, 2011